Chloroplast RNA Metabolism:

Global Players and Site Specific Factors

Dissertation

zur Erlangung des Doktorgrades der Naturwissenschaften

Fakultät für Biologie

Ludwig-Maximilians-Universität München

Rhea Stoppel

München, November 2011

1. Gutachter: PD Dr. Jörg Meurer

2. Gutachter: Prof. Dr. Jörg Nickelsen

Tag der mündlichen Prüfung: 13. 01. 2012

CONTENTS

1 INTRODUCTION

1.1 Origin and Function of Higher Plant Chloroplasts

The chloroplast evolved as a result of an endosymbiotic event in which a cyanobacterial ancestor was taken over by a eukaryotic cell (Figure 1). Though main parts of the originally plastid genes were transferred into the nucleus, chloroplasts still have retained their own independent genome of less than 100 protein-coding genes mainly involved in photosynthesis, as well as several genes for tRNAs and rRNAs. These genes are embedded in the regulatory network of the cell enabling an adaptive and developmentally regulated chloroplast biogenesis, which is mainly controlled by nuclear factors (Stern *et al.*, 2010).
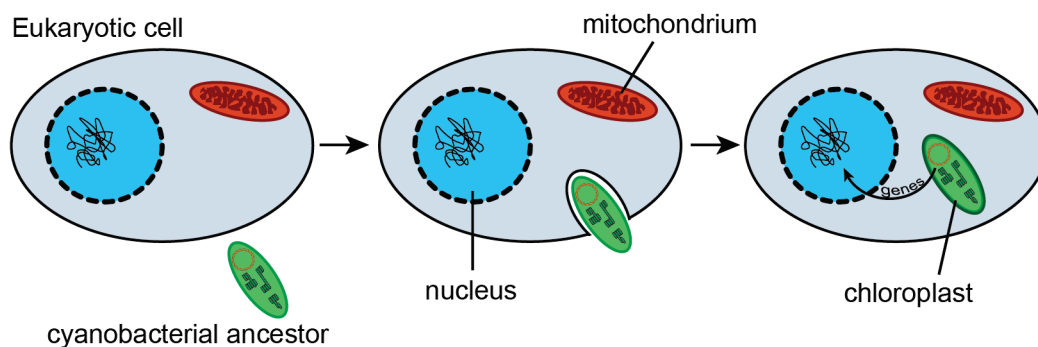
Figure 1. Primary Endosymbiosis and Endosymbiotic Gene Transfer.

In the course of endosymbiosis a cyanobacterial ancestor was ingested by a eukaryotic cell. Subsequently many originally plastid genes were transferred into the nucleus (depicted by an arrow).

Chloroplasts and related plastidic forms are the characteristic organelles of photoautotrophic eukaryotes bearing important roles in nitrogen, sulphur, and lipid metabolism and catalyzing the transformation of light energy into chemical energy. This step results in production of sugar and molecular oxygen, prerequisite for life on Earth.

1.2 Photosynthetic Complexes of the Thylakoid Membrane

A chloroplast is one of several differentiated types of plastids all originating from a so-called proplastid which is present in meristematic regions of the plant. In the presence of light the so far unstructured proplastid differentiates into a chloroplast and develops the highly structured thylakoid membrane. This complex membrane system consists of membrane stacks (grana)

interconnected with single membranes (stroma lamellae). In the course of the endosymbiotic gene transfer many originally plastid genes were transferred to the nucleus, making the thylakoid membrane a mosaic of nuclear- and plastid-encoded proteins (Figure 2). The expression of plastid-encoded subunits is predominantly controlled by nuclear-encoded factors on the level of RNA metabolism, translation, and assembly (Race *et al.*, 1999).
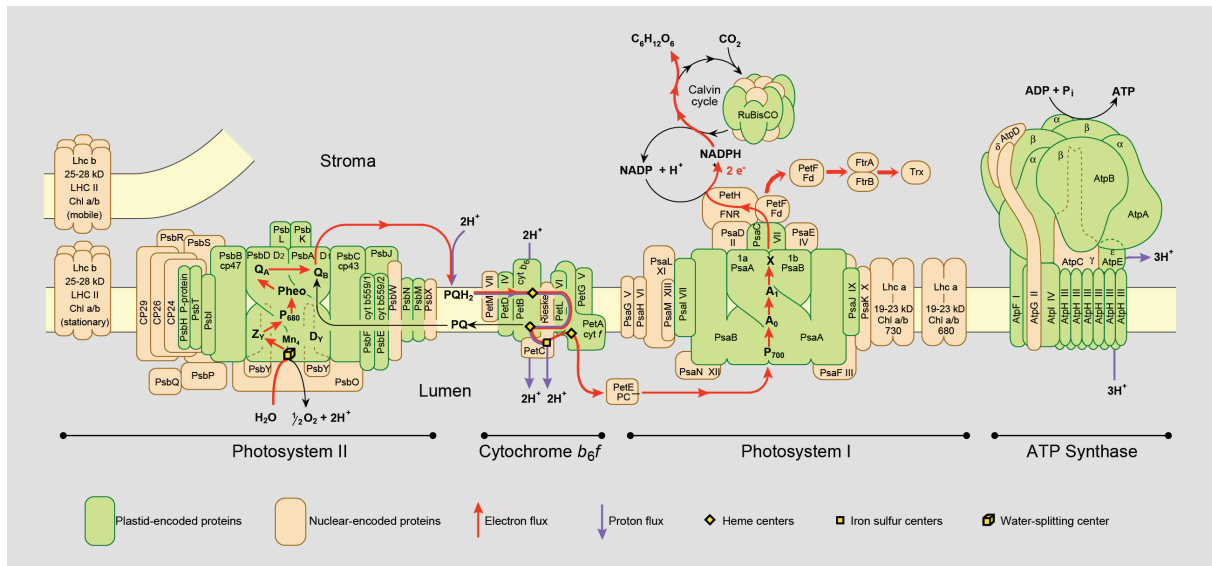
Figure 2. The Thylakoid Membrane of Vascular Plant Chloroplasts.
A schematic view of the thylakoid membrane demonstrates the arrangement of components of the photosynthetic machinery in *Arabidopsis thaliana* chloroplasts (modified from Race *et al.*, 1999). Each of the four major complexes consists of various nucleus- and plastid-encoded proteins colored in orange and green, respectively. A fifth complex, the NADPH-dehydrogenase is not shown.

The photosynthetic machinery mainly consists of four multiprotein complexes embedded in the thylakoid membrane, namely the photosystem II (PSII), the cytochrome b_6f complex, the photosystem I (PSI) and the ATP synthase (Rochaix, 2011a). Both photosystems 'collect' light by use of the light harvesting complexes (LHCI and LHCII) that confer the energy via exciton transfer to the chlorophyll-containing photosystem reaction centers. The chlorophyll absorbs the energy while losing an electron which is subsequently translocated through the thylakoid membrane complexes. Finally, this electron is reducing ferredoxin, thereby producing the reducing equivalent NADPH. This electron transfer creates a proton gradient across the chloroplast membrane that is used for ATP synthesis by the ATP synthase complex (Rochaix, 2011b). The chlorophyll molecule regains the lost electron from oxidation of a water molecule in the lumenal oxygen-evolving-complex releasing a dioxygen (O_2) molecule. The reducing equivalents NADPH in turn are used for carbon fixation, a process that converts carbon dioxide

(CO_2) into sugars. However, the light energy that is absorbed through the reaction centers cannot be quantitatively used for photosynthesis and is thus partially reflected as heat or fluorescence. Spectroscopic measurement of this fluorescence can shed light on the physiological state of the photosynthetic apparatus, since, e.g. fluorescence is increased if electron transfer is partly restricted (Schreiber, 1986; Schreiber *et al.*, 1986).

1.3 Nuclear Control of Plastid Gene Expression

Despite its cyanobacterial origin, plastid gene expression is regulated in a different manner than in eubacteria or in the cytoplasmic system of eukaryotes (Allen, 2003 and 2005; Bollenbach *et al.*, 2005). Chloroplast biogenesis is mainly requiring adaptation of transcript metabolism (Barkan, 2011) which is characterized through increased transcription rates as well as mRNA decay. An important characteristic of chloroplast gene regulation is the predominance of post transcriptional control, which is exerted at gene-specific, gene-cluster, and genome-wide levels (Cho *et al.*, 2009; del Campo, 2009; Stern *et al.*, 2010). Although the chloroplast has reduced its coding capacity to less than 100 proteins, a highly sophisticated system of transcript maturation including endo- and exonucleolytic activities, splicing, editing, and modulation of RNA stability has been developed which is not exploited to the same extent in the free-living cyanobacterial ancestor. Numerous nuclear-encoded factors have been acquired for processing and other post-transcriptional modifications of plastid transcripts (Stern *et al.*, 2010; Barkan, 2011). Some of these factors act as global players, whereas others have specific functions in maturation, stabilization, and editing of plastid transcripts. Especially chloroplast RNA-binding proteins, including members of the pentatricopeptide repeat (PPR) protein family, are involved in post-transcriptional control (Nickelsen, 2003; Schmitz-Linneweber and Small, 2008). Genetic and molecular approaches demonstrated that higher-order protein complexes are often involved in processing of plastid transcripts (Fisk *et al.*, 1999; Ossenbühl and Nickelsen, 2000; Kroeger *et al.*, 2009). Altogether several hundred nucleus-encoded factors are thought to be required for proper expression of the organellar genome. Interestingly, most of these factors are gene specific, one factor being required for the expression of one, or a few, organellar mRNA(s). The frequent occurrence of plant-specific genes important for chloroplast mRNA homeostasis demonstrates that regulation at the post-transcriptional level represents a fast evolving process during endosymbiosis.
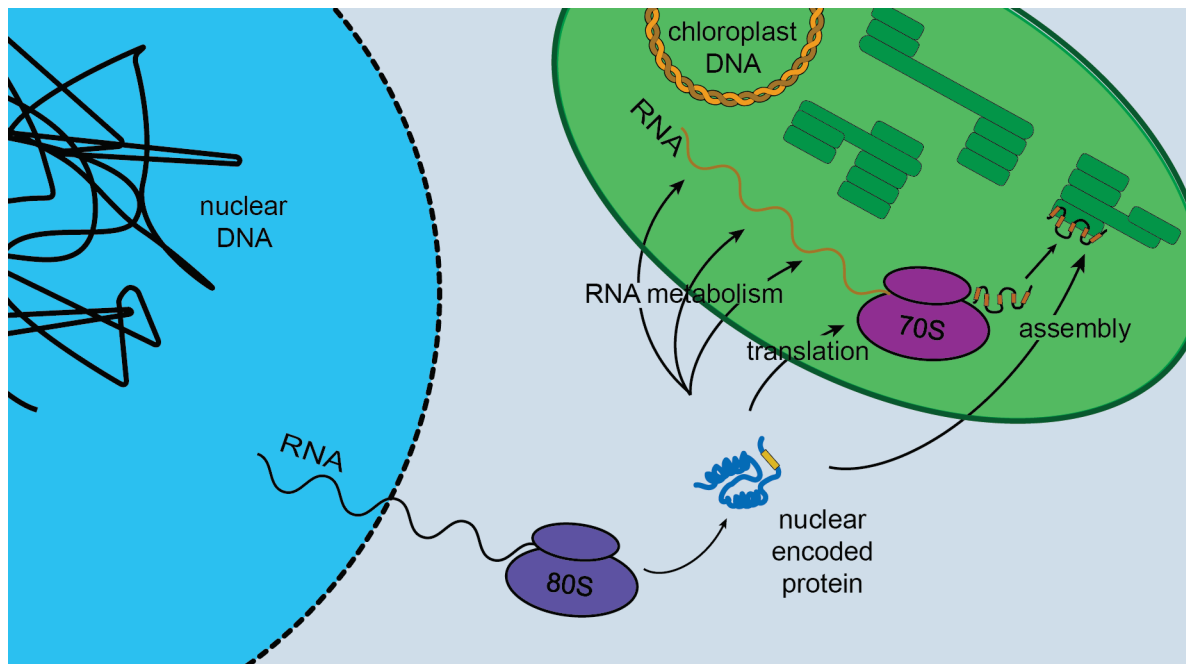
Figure 3. Nuclear-Encoded Factors Involved in the Control of Plastid Gene Expression.

Most of the genes encoded in higher plant chloroplasts are organized in transcription units, which are often processed prior to translation producing mono- and oligocistrons. Post-transcriptional RNA metabolism is mediated by nuclear-encoded proteins and includes intercistronic cleavage, intron splicing and editing. RNA stabilization involves either the formation of stem-loop structures or binding of specific proteins to prevent exonucleolytic degradation. Control by nuclear-encoded factors is also mediated on translational level and on the assembly of proteins in the thylakoid membrane.

1.4   Ribonucleases in the Chloroplast

The massive gene transfer which occurred after functional integration of the chloroplast organelle into the host cell, asides with its differentiation into various types of plastids, resulted in a dramatically elevated complexity of the higher plant. Tight control of complex chloroplast RNA processing events and global regulation of chloroplast translation turned out to be indispensable.

Though chloroplasts originate from cyanobacteria and have retained part of the general prokaryotic endonuclease-exonuclease RNA degradation system, gene expression differs widely from that of their ancestors. Unlike in bacteria, nearly if not all polycistronic transcripts are processed by endo- and exonucleases, splicing activities and editing events in the chloroplast (Bollenbach *et al.*, 2007; Barkan, 2011). Processing within intergenic regions is required for subsequent translation as transcription termination is very inefficient in chloroplasts (Bollenbach *et al.*, 2004). Additionally, transcript half-lives differ dramatically from an average of 3-8 minutes in bacteria to several hours in chloroplasts (Bernstein *et al.*, 2002; Klaff and Gruissem, 1991). Not

only the abundance of mRNAs but also the availability of other RNA species, like noncoding RNAs, rRNAs and tRNAs, is an important parameter in determining translation rates, and therefore the amounts of proteins produced. Most RNAs undergo an extensive maturation process in order to become functional. Processing and degradation of plastid RNA is mediated by ribonucleases. This offers a means of rapidly adjusting RNA abundance in response to changing environmental conditions, determining the half-life of individual RNAs and serving as a tool for quality control.

In Prokaryotes one major factor involved in post-transcriptional regulation of gene expression is the well-characterized endoribonuclease E (RNase E) (Arraiano *et al.*, 2010). In *E. coli* RNase E forms part of a multiprotein complex called the degradosome, which harbors RNase E, PNPase, Rhl B, and Enolase as major components (Carpousis, 2007). The N-terminal catalytic part of the large multidomain protein RNase E is essential for cell viability. Mutations or deletions in this region lead to a reduced rate of RNA decay (Mudd *et al.*, 1990) and accumulation of partly degraded fragments with increased lifetimes (Carpousis *et al.*, 1994). The C-terminal non-catalytic domain serves as scaffold for the degradosome and helps targeting RNase E to RNA, but is not essential in *E. coli*, since the catalytic activity of the N-terminus is only little affected when part or all of the C-terminus is deleted (Kido *et al.*, 1996). RNase E homologs can be found in cyanobacterial and land plant genomes but it remains uncertain whether they originate from the highly similar RNase E or the shorter form RNase G (Lee and Cohen, 2003; Stoppel and Meurer, 2011). RNase G is another *E. coli* endonuclease with overlapping but not identical cleavage specificity that resembles 50% sequence similarity to the highly conserved catalytic part of RNase E (Lee, 2002; Ow *et al.*, 2003). Plant RNase E (RNE) differs from known bacterial forms mainly by an insertion in the RNA-binding S1 motif of the catalytic domain, the lack of the C-terminal degradosome scaffold which is replaced by a shorter chloroplast-specific region (Figure 4) and the acquisition of a large N-terminal extension (Schein *et al.*, 2008).
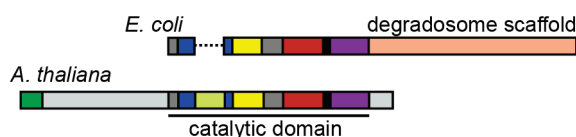
Figure 4. Schematic View of *E. coli* and *Arabidopsis thaliana* RNE Proteins.

Domains are colored as follows: transit peptide, dark green; N-terminal extension, light grey; RNase H, dark gray; S1 domain, blue; S1 addition in plants, light green; 5' sensor, yellow; DNase I-like, red; Zn-link, black; small domain, purple; C-terminal extension in plants, light grey; *E. coli* degradosome scaffold, rose.

Although chloroplasts are descendants of photosynthetic eubacteria, the presence of a characteristic degradosome and the formation of a multiprotein complex involved in RNA processing and decay has yet not been reported. The presence of RNase E in a previously described multiprotein complex involved in RNA processing (Hayes *et al.*, 1996) was proven to be an artifact due to cross-reaction with antibodies raised against *E. coli* RNase E (Baginsky *et al.*, 2001). The fact that the plastid PNPase, one of the degradosome components in some bacteria like *E. coli*, forms a homo-multimer not associated with other proteins (Baginsky *et al.*, 2001; Rott *et al.*, 2003) along with the lack of the degradosome scaffold and the formation of homo-oligomers of the plastid RNE *in vitro* (Schein *et al.*, 2008) led to the assumption that a degradosome homolog is not present in chloroplasts.

The Arabidopsis nuclear genome encodes one RNE protein (At2g04270), which has been characterized in several recent studies, supporting its endonucleolytic function within the chloroplast stroma (Schein *et al.*, 2008; Mudd *et al.*, 2008). RNE has been found in a proteomics study of triton-insoluble fractions of pea, where it co-sedimented with nucleoids and large multi-enzyme complexes (Phinney *et al.*, 2005). It was proposed that the *rne* mutation causes mainly defective processing of the *rpl22* mRNA coding for an essential ribosomal protein (Walter *et al.*, 2010). However, the nature and necessity of interaction partners as well as an involvement of factors conferring binding specificity to RNA targets still remained unknown. Importantly, it is unclear, whether chloroplast RNase E still fulfills endonucleolytic and RNA degradation functions previously carried out by its counterpart in the bacterial degradosome.

1.5   Ribonucleases and RNA Maturation as Exemplified by Ribosomal RNA

Chloroplast ribosomes comprise two subunits of 50S and 30S, which together form the 70S ribosome that decodes mRNAs and translates them into the appropriate polypeptide chains (Harris *et al.*, 1994). Ribosomal subunits are composed of more than 50 ribosomal proteins (Yamaguchi and Subramanian, 2000; Yamaguchi *et al.*, 2000) together with four ribosomal RNAs that are encoded in one gene cluster and have been proposed to play a role in the catalytic activity of the ribosome (Nissen *et al.*, 2000). In spite of the vast evolutionary distance, the chloroplast rRNA gene cluster still resembles that of bacteria in terms of organization of coding sequences and co-transcription of genes (Strittmatter and Kössel, 1984). The clusters in eubacteria encode mature rRNAs of 16S, 23S, and 5S, while those of eukaryotes specify 18S, 5.8S, 28/25S, and 5S rRNAs (Figure 5). Eukaryotic 5.8S and 28/25S correspond to the 23S rRNA of eubacteria

(Evguenieva-Hackenberg, 2005). In plastids homologs of eubacterial 23S rRNA are split into 23S and 4.5S, the latter sharing high homology with the 3'-end of the bacterial 23S. In the plastid genome, 16S and 23S sequences flank a region encoding tRNAs for isoleucine and alanine and an additional tRNA for arginine is encoded downstream of the 5S rRNA (Figure 5).
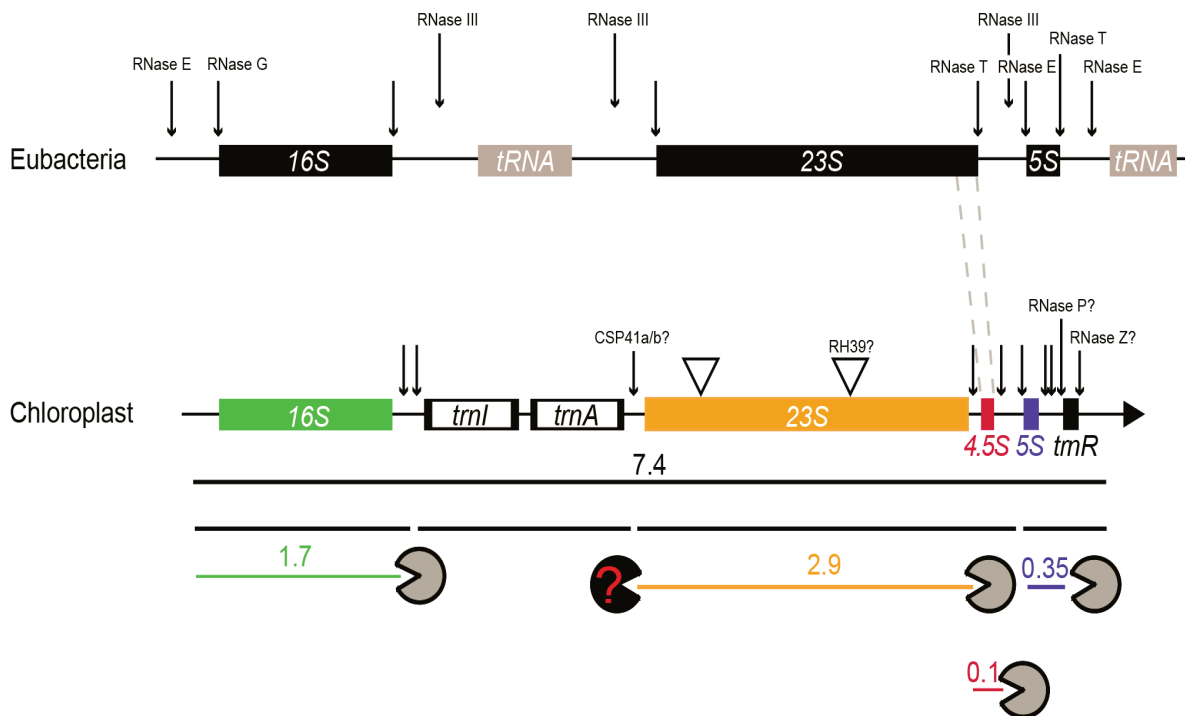
Figure 5. Maturation of rRNA Precursors in Eukaryotes, Eubacteria and Chloroplasts.

In eukaryotes the 28/25SS, 18S, and 5.8S rRNAs are cleaved from an 18S-5.8S-28/25S precursor transcript transcribed by RNA polymerase I, while the 5S rRNA genes form separate clusters that are transcribed by RNA polymerase III (Haeusler and Engelke, 2006). The bacterial *rrnC* operon shown here is one of seven rRNA operons in the *E. coli* genome. The primary transcript is first cleaved by RNase III and the resulting intermediates are then trimmed by the RNases E, G and T (Davies *et al.*, 2010). The RNases (arrows) responsible for maturation of the primary transcript in chloroplasts are still unknown. It has been suggested that tRNA[ARG] is cleaved by the RNases P and Z, and 5' maturation of 23S rRNA has been attributed to CSP41a/b. RH39 was proposed to function in cleavage of the second 'hidden break' (triangle). Endonucleolytic cleavage intermediates are subsequently trimmed at their 3'-ends by PNPase and/or RNase R (grey) and possibly also at their 5'-ends by an exonuclease that could be RNase J (black).

Ribosomal RNA abundance and processing is of great importance for ribosome assembly. Thus bacterial cells usually have multiple copies of the ribosomal RNA operon, located in different parts of the genome and arranged in a similar but not identical manner. Accordingly rRNA operons in eukaryotic nuclear genomes cluster in large tandem regions containing up to 400 copies in human or many thousands in some plant species (Long and Dawid, 1980). By contrast,

there are only two rRNA operons in the chloroplast genome, which are located in the inverted repeats. Maturation of rRNA precursor transcripts performed by endo- and exoribonucleases is a prerequisite for accurate chloroplast ribosome biogenesis. Furthermore some parts of chloroplast rRNA processing occur in an assembly-assisted manner.

In *E. coli*, mutants defective in pre-rRNA processing have been used to elucidate the process of ribosomal RNA maturation (Gegenheimer and Apirion, 1981). It was shown that RNase III in concert with RNase E and G are responsible for the endonucleolytic cleavages, while RNase T performs the exonucleolytic 3'-trimming step (Davies *et al.*, 2010). In vascular plant chloroplasts several mutants with putative defects in rRNA processing and ribosome assembly have been identified to date (Bellaoui *et al.*, 2003; Bisanz *et al.*, 2003; Bollenbach *et al.*, 2005; Komatsu *et al.*, 2010; Lu *et al.*, 2011; Nishimura *et al.*, 2010). However, the precise mechanism of rRNA maturation in chloroplasts remains an open question, since a biochemical characterization of mutants is often lacking and secondary effects cannot always be excluded.

In chloroplasts, the 7.4 kb rRNA precursor is thought to be cleaved by an as yet unidentified endonuclease, releasing pre-tRNAs for isoleucine and alanine and pre-rRNA for 16S, as well as the dicistronic intermediates 23S-4.5S and 5S-tRNA^{ARG} (Figure 5). The pre-tRNAs are subsequently processed at their 5'- and 3'-ends by RNase P and RNase Z, respectively (Canino *et al.*, 2009; Gobert *et al.*, 2010). The processing intermediate 23S-4.5S is first matured at the 23S 5'- and 4.5S 3'-end, and then endonucleolytically cleaved in several steps at the 5'-end of 4.5S. Intercistronic cleavage requires both assembly of the dicistron into pre-ribosomal subunits and prior 3'-end maturation of 4.5S rRNA (Bellaoui *et al.*, 2003). Mutants defective in rRNA 3'-processing or ribosome assembly accumulate this 23S-4.5S processing intermediate (Bellaoui *et al.*, 2003; Bisanz *et al.*, 2003; Bollenbach *et al.*, 2005). The subsequent 3'-end trimming of 23S rRNA is performed by PNPase and the RNase R homolog RNR1 (Yehudai-Resheff *et al.*, 2001; Bollenbach *et al.*, 2005). The mature 23S rRNA is then cleaved internally at so-called 'hidden breaks', as revealed by electrophoresis on agarose gels under denaturing conditions (Leaver, 1973). Although a DEAD-box helicase with a proposed function in formation of one of the hidden breaks was recently identified (Nishimura *et al.*, 2010), the need for such additional modifications of rRNAs in the large ribosomal subunit is not understood.

In contrast to bacteria, precursors of chloroplast 16S RNA are not processed close to their mature termini. Thus they possess long 3'-tails requiring 3'→5' exonucleolytic processing which is performed, as in the case of 23S, by RNR1 and/or PNPase as reported previously (Yehudai-Resheff *et al.*, 2001; Bollenbach *et al.*, 2005). The 5S RNA is co-transcribed with the downstream

tRNA[ARG] in Brassica and Arabidopsis (Leal-Klevezas, 2000; Sharwood *et al.*, 2011) followed by endonucleolytic cleavage and exonucleolytic 3'-end trimming.

1.6 Regulation of Site Specificity and Transcript Abundance

Various mechanisms can determine the stability of chloroplast mRNAs, including protection of RNA termini by proteins or RNA secondary structures. Since untranslated regions are not protected by ribosomes they are typical sites of endonucleolytic cleavage by RNase E/J or CSP41, making accessibility to such sequences a key determinant of mRNA stability. Processing of polycistronic transcription units generates RNA 5'- and 3'-ends thus creating a complex pattern of mono- and oligo-cistronic RNAs (Barkan, 2011). Gene-specific transacting factors encoded in the nucleus can bind the 5' UTR of mRNAs to protect them against 5'→3' exonucleases (Drager *et al.*, 1998) while the transcript 3'-end can in turn be stabilized by stable stem-loop structures or proteins, protecting from digestion by 3'→5' exonucleases (Figure 6).
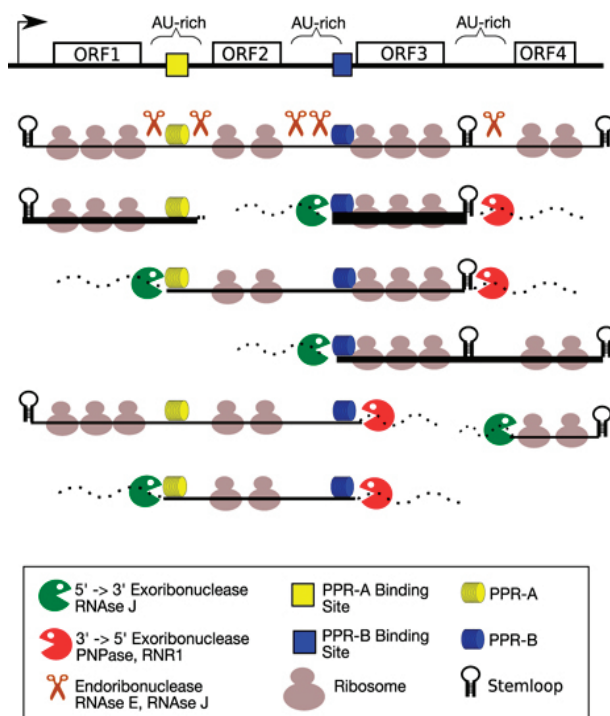
Figure 6. Model for mRNA Stability Mediated by Protein Binding to 5' and 3' Regions of Chloroplast Transcripts.
In this model, processing and RNA decay are both initiated by endonucleolytic cleavage of sequences that are not masked by RNA structure, ribosomes, or proteins. The cleaved products are substrates for 3'→5' and 5'→3' exonucleases, which proceed until blocked by an RNA stem-loop or a bound protein. The ribonucleases proposed to be involved in RNA cleavage are indicated. Protective functions attributed to PPR proteins here, could also be taken over by non-PPR proteins. Line thickness indicates the relative accumulation of different transcripts (picture from Pfalz *et al.*, 2009).

One major group of proteins mediating post-transcriptional control is the pentatricopeptide repeat (PPR) family, characterized by the presence of repeated units of 35 amino acid residues (aa). PPR proteins are widespread among vascular plants with more than 450 members in

Arabidopsis thaliana that are located either in chloroplasts or in mitochondria (Lurin *et al.*, 2004). PPR proteins like CRP1 and PGR3 have been implicated in both RNA stability and translation (Schmitz-Linneweber *et al.*, 2005; Cai *et al.*, 2011), similarly to the *Clamydomonas* protein MCA1, which interacts with the *petA* transcript (Loiselay *et al.*, 2008; Boulouis *et al.*, 2011). Recently a PPR-protein, PPR10, was reported to serve as a barrier to exonucleolytic RNA decay, substituting for RNA stem-loop structures (Pfalz *et al.*, 2009). In addition to pentatricopeptide proteins, members of the tetratricopeptide family (TPR) have also been characterized. The TPR-protein HCF107 for example is reported to be responsible for processing or stability of the *psbH* transcript (Sane *et al.*, 2005). Further evidence for the existence of site specific RNA-binding proteins give the recently identified small RNAs, representing 'footprints' of presumably PPR- or TPR-binding sites (Ruwe and Schmitz-Linneweber, *personal communication*). By binding of the protein the RNA remains protected from cleavage and endures exonucleolytic digestion. The nature of these protective proteins is not necessarily restricted to the PPR family but could also apply to other proteins with RNA-binding capability. Thus binding of proteins at both 5'- and 3'-ends can define chloroplast RNA transcript termini and abundance without the need for sequence specificity of ribonucleases (Figure 6).

For example, endonucleases like CSP41 and RNase E were shown to cleave RNA without any specificity *in vitro* (Schein *et al.*, 2008; Yang *et al.*, 1996). But while RNases E and J are postulated to cleave rather non-specifically *in vivo* also, giving exonucleases access to internal RNA regions, CSP41a displays a preference for RNAs containing hairpin structures, making it a candidate for determining transcript half-life in the chloroplast (Bollenbach *et al.*, 2003). Among the exonucleases, PNPase preferentially degrades polyadenylated sequences (Lisitsky and Schuster, 1999) while the activity of RNR1 could, like that of the *E. coli* RNase II (Coburn and Mackie, 1996), be modulated by RNA secondary structures *in vivo*. An interaction with other proteins like helicases is also conceivable, as it would facilitate the cleavage of highly structured substrates, as is the case for the *E. coli* degradosome, in which PNPase is associated with the RNA helicase RhlB. Last but not least translational events have been shown to influence RNA stability (Meurer *et al.*, 2002).

1.7   Aims of the Thesis

The aim of this work was to extend the knowledge of RNA metabolism in the chloroplast. Although many aspects of post-transcriptional mechanisms have been investigated so far, the underlying molecular mechanisms and the nature of factors involved are still largely unknown. To

assess the function of nuclear-encoded factors acting globally or in contrary exhibiting high sequence specificity, we chose both a forward and reverse genetics approach using *Arabidopsis thaliana* as a well-established model plant. The project focused on (1) identification and characterization of mutant phenotypes, (2) determination of the chloroplast gene expression defects, (3) identification and characterization of the nuclear-encoded products, and (4) functional analyzes of the components.

For identification of interacting proteins we chose a co-immunoprecipitation (Co-IP) approach of complexes from cell extracts. A cell extract is prepared under non-denaturing conditions where proteins are present in their native conformation often associated with other proteins. This protein-protein complex is then precipitated using specific antibodies and unspecific proteins are removed by a series of washes. Precipitated complexes are then evaluated by SDS-PAGE followed by Western blotting with specific antibodies for the bait or prey partners or subjected to mass spectrometry analyses. It was necessary to (5) generate antibodies against the previously identified nuclear-encoded factors, (6) complement mutant lines with tagged versions of these proteins, (7) perform the Co-IP analyzes, and (8) characterize the identified interaction partners and corresponding mutant alleles.

In order to provide a coherent picture, I included some analyses performed by colleges or collaboration partners. People involved in the analyses are either mentioned in the figure legends or in case of already published material the reference is given.

2 MATERIALS

2.1 Database Analysis

Analyzes of gene models

Ensembl Genome Browser	http://atensembl.arabidopsis.info/index.html
TAIR	www.arabidopsis.org
NCBI	www.ncbi.nlm.nih.gov

Identification of protein homologues

Chlamydomonas reinhardtii	www.chlamy.org/cgi-bin/webblast.pl
Cyanidioschyzon merulae	http://merolae.biol.s.u-tokyo.ac.jp/blast/blast.html
Cyanobacteria	http://blast.kazusa.or.jp/blast_search/cyanobase/genes
Galdieria sulphuraria	http://genomics.msu.edu/cgi-bin/galdieria/blast.cgi
NCBI Blast	http://blast.ncbi.nlm.nih.gov/Blast.cgi
Oryza sativa	http://rice.plantbiology.msu.edu/blast.shtml
Ostreococcus tauri	http://bioinformatics.psb.ugent.be/blast
Phaeodactylum tricornutum	http://avesthagen.sznbowler.com
Physcomitrella patens	http://www.plantgdb.org
Populus trichocarpa	http://www.phytozome.net/poplar
Red algae	http://gobase.bcm.umontreal.ca/index.php
Selaginella moellendorffii	http://www.plantgdb.org
Thalassiosira pseudonana	http://genome.jgi-psf.org/

Identification of duplicated genes

PGDD	http://chibba.agtec.uga.edu/duplication/index/locus

Sequence alignments

CLUSTAL-W2	http://www.ebi.ac.uk/Tools/msa/clustalw2/
Geneious	Biomatters
NCBI Blast 2 sequences	http://blast.ncbi.nlm.nih.gov/Blast.cgi
Vector NTI 10.0	Invitrogen

Digital Northerns

Genevestigator	www.genevestigator.com

Co-regulated gene relationships

ATTED-II   www.atted.jp

Proteomics database

Plant Proteome Database   http://ppdb.tc.cornell.edu

SUBA II   http://suba.plantenergy.uwa.edu.au/

Prediction of organellar targeting

BaCelLo   http://gpcr.biocomp.unibo.it/bacello

ChloroP   http://www.cbs.dtu.dk/services/ChloroP

MitoProt   http://ihg.gsf.de/ihg/mitoprot.html

Predotar   http://urgi.versailles.inra.fr/predotar/predotar.html

PSORT   http://psort.ims.u-tokyo.ac.jp/form.html

SLP   http://sunflower.kuicr.kyoto-u.ac.jp/~smatsuda/slplocal

TargetP   http://www.cbs.dtu.dk/services/TargetP

Wolf Psort   http://wolfpsort.org/

Structure prediction and visualization

Genesilico   https://genesilico.pl/meta2/

JMol   http://www.jmol.org/

2.2 Bacterial Strains

Escherichia coli:

BL21(DE3)pLysS   Novagen/Merck

DH5α   Bethesda Research Laboratory

Stbl2   Invitrogen

Agrobacterium tumefaciens:

GV3101 (pMP90RK)   Koncz *et al.*, 1994

2.3 Plant Material

The *Arabidopsis thaliana* T-DNA insertion lines *prfB3-1* (SALK_133921) and *rne-1* (SALK_093546) both of ecotype Columbia-0 were obtained from the SALK collection (http://signal.salk.edu/). Seeds of the *Arabidopsis thaliana* ecotype Columbia-0 line *rne-2* (formerly named *hcf2*) originated from a collection of EMS induced mutants (Dinkins *et al.*, 1994) and were kindly provided by R. Dinkins (Kentucky, USA). The mutant line *prfB3-2*, ecotype Wassilewskija, was selected from a T-DNA mutant collection (Bechtold *et al.*, 1993) and was provided by P. Westhoff. Seeds of *Arabidopsis thaliana* ecotypes Columbia-0, Landsberg erecta and Wassilewskija were obtained from PD Dr. Meurer. Seeds for mutant lines *cry1*, *cry2*, *phyA*, *phyB* and corresponding double mutants were obtained from SALK.

2.4 Vectors

Detailed maps of all vectors used in this work can be found in the appendix.

Gateway vectors pENTR/D-TOPO, pDONR207, and pDEST17 were purchased from Invitrogen. The Gateway TAP-tag vector was kindly provided by Dr. Karin Meierhoff. The vector pSEX001-VS (Reiss *et al.*, 1996) was used for complementation studies of *prfB3-1*.

2.5 Oligonucleotides

Oligonucleotide primers used for amplification of certain DNA regions were purchased through MWG Biotech AG or Metabion international AG. A list of all primers used in this work can be found in the appendix.

2.6 Antibodies

Antibodies used in this work raised against subunits of the thylakoid membrane were either described in Meurer *et al.* (1996a) or purchased from Agrisera. Peroxidase-conjugated secondary antibodies as well as an anti-polyHistidine antibody were purchased from Sigma-Aldrich. The monoclonal, high affinity anti-HA-Peroxidase antibody was obtained from Roche and the anti-phosphothreonine antibody derived from Cell Signaling.

RNE: In order to generate antibodies against RNE, the recombinant protein (Schein *et al.*, 2008; kindly provided by Prof. Gadi Schuster, Haifa, Israel) was injected into rabbits at different time intervals (Pineda-Antikörper-Service).

At-PrfB3: For production of antibodies against At-PrfB3, a fragment of the cDNA (aa 35-407) lacking the putative transit peptide was amplified using primers PrfB3-Topo17-f and PrfB3-Topo17-r and Phusion Pfu polymerase (NEB), cloned into Gateway pDEST17 vector via Gateway pENTR/D-TOPO and overexpressed together with an N-terminal 6xHis-tag in BL21(DE3)pLysS cells. The PrfB3-HIS antigen was isolated from urea-solubilized inclusion bodies to almost purity and injected into rabbits at different time intervals (Pineda-Antikörper-Service).

PAC: The cDNA of *PAC* (aa 23-314) lacking the putative transit peptide was amplified using Phusion Pfu polymerase (NEB) and primers Pac-Topo17-f and Pac-Topo17-r. After cloning the fragment into Gateway pDEST17 vector via Gateway pENTR/D-TOPO the protein was overexpressed in BL21(DE3)pLysS cells and purified from urea-solubilized inclusion bodies to almost purity. The resulting antigen was injected into rabbits at different time intervals (Pineda-Antikörper-Service).

3 METHODS

General molecular methods, e.g. cultivation and transformation of bacteria, phenol/chloroform extraction, precipitation, gel electrophoresis, staining and quantification of nucleic acids, PCR and others were performed according to standard protocols (Sambrook *et al.*, 1989) or using kits consistent with the manufacturer's instructions.

3.1 Seed Sterilization, Plant Growth and Mutant Selection

Seed sterilization and growth conditions for wild-type and mutant plants on 1x MS-medium (Murashige and Skoog, 1962) supplemented with 1.5 % Sucrose (Suc) were as described in Meurer *et al.* (1996a). After 2 days at 4°C to synchronize germination, seedlings were grown under continuous light of 20-40 μmol photons m^{-2} s^{-1} and constant temperature of 21°C. Selection of mutant plants was facilitated by a chlorophyll fluorescence video imaging system (FluorCam690M, Photon Systems Instruments). Mutants were distinguishable from wild-type plants because of their failure to quench chlorophyll fluorescence, therefore displaying a *high chlorophyll fluorescence* (*hcf*) phenotype. Propagation of the seedling lethal mutants occurred via heterozygous plants grown on soil. Wild-type plants and complemented mutant lines were grown on soil in a growth chamber in a 12-h-light (20°C)/12-h-dark (18°C) cycle under heterochromatic light of 80 μmol photons m^{-2} s^{-1}. In all experiments 3-4 week old plants were used.

3.2 DNA Analyses

3.2.1 Rapid DNA Isolation for PCR

Plant material of young leaves was homogenized in 400 μl extraction buffer (200 mM Tris/HCl, pH 7.5, 250 mM NaCl, 25 mM EDTA, 0.5% w/v SDS) using microbeads and a bead-beater (MM300, Retsch) for 2 min at a frequency of 30 s or a mechanical stirrer (RW16 basic, Kika Labortechnik). The extract was centrifuged for 3 min at 16,000 g, 300 μl supernatant was transferred to a new reaction tube and 300 μl isopropanol was added. After vortexing and incubation at room temperature for 2 min the mixture was centrifuged for 5 min at 16,000 g. The supernatant was discarded, and the pellet was air-dried and resuspended in 100 μl TE buffer. For PCR amplification 1 μl DNA was used.

3.2.2 Radioactive Labeling of DNA

DNA labeling was performed using the Random Primed DNA Labeling Kit (Roche) according to the method of Feinberg and Vogelstein (1983).

3.3 RNA Analyses

3.3.1 Isolation of Total RNA

Total RNA was isolated from 1-2 g of leaf material homogenized in liquid nitrogen and incubated for 5 min with 700 µl TRIzol reagent (Invitrogen). After adding the same volume chloroform and vortexing 2 min, phases were separated through centrifugation at 10,000 g for 15 min. One volume of phenol/chloroform/ isoamylalcohol was added to the upper phase and centrifuged for 10 min at 12,000 g. After transferring the upper phase to a new tube, one volume of isopropanol and 100 µl of 3 M Na-acetate (pH 6.0) was added, gently mixed and RNA was precipitated over night at -20°C. Centrifugation for 45 min at 10,000 g and subsequent air-drying of the RNA and resolution in 50-200 µl of RNase-free water resulted in RNA concentrations of 0.5 – 2 µg/µl which were determined by spectroscopic measurement of the extinction at 260 nm.

3.3.2 Reverse Transcription (RT)-PCR

Reverse transcription and PCR of specific RNAs in one single step was carried out using the Titan One Tube RT-PCR Kit (Roche). Total cDNAs were amplified with 1 µg RNA using SuperScript III Reverse Transcriptase (Invitrogen) and hexanucleotides (Roche). Ribonuclease-free DNase I (Roche) was used for removal of DNA from RNA preparations prior to RT-PCR reactions.

3.3.3 Quantitative Real-Time RT-PCR

Quantitative two-step RT-PCR was carried out using the LightCycler Thermal Cycler System (Roche) and a commercially available master mix containing Taq DNA polymerase, SYBR-Green I dye and dNTPs (FastStart DNA master SYBR-Green I; Roche). Serially diluted samples of Arabidopsis total cDNA, corresponding from 15 ng to 1.5 pg of DNA were used for calibration with the *prfB3-1* mutant using primers *psaA*-f and *psaA*-r. Quantification of spliced *petB* or *petD*

transcript was carried out using primers *petB*-f/*petB*-r and *petD*-f/*petD*-r, respectively. Additionally, PCR products were analyzed by 1% agarose gel electrophoresis and stained with ethidium bromide to obtain an independent validation check of the presence of a single product.

3.3.4   Northern Analyses

For Northern analysis 10 μg of total RNA was denatured through incubation with 30% glyoxal (McMaster and Carmichael, 1977), electrophoretically separated in 1.2% agarose gels in MOPS buffer (0.2 M MOPS, 50 mM Na-acetate, 10 mM EDTA, pH 7.0) and capillary transferred onto a Biodyne B nylon membrane (0.2 μm; Pall) in 20x SSC buffer (Grüne and Westhoff, 1988). RNA was fixed to the membrane by exposure to UV light of 12,000-120,000 μjoules (Khandijan, 1986).

3.3.5   Hybridization of Nucleic Acids

Hybridization of radioactive labeled DNA probes was performed in ULTRAhyb hybridization buffer (Applied Biosystems/Ambion) at 42°C according to the manufacturer's instructions. After hybridization filters were washed 2x for 5 min in washing buffer I (2x SSC/0.05% SDS) and 2x for 15 min in washing buffer II (0.1x SSC/0.1% SDS). Hybridization images were read with a digital scanner (Typhoon, GE Healthcare).

3.3.6   Polysome Analysis

Polysomes were isolated from leaf tissue essentially as described in Barkan (1998). Polysome aliquots (0.5 ml) were layered onto 3.2 ml of 15-55% sucrose gradients and centrifuged for 65 min at 250,000 g at 4°C. Fractions of 0.4 ml were collected, the RNA was purified, denatured with 30% Glyoxal and subjected to RNA gel blot analysis.

3.3.7   Translation Inhibition Experiments

For application of plastid translation inhibitors, three-week-old plants of *prfB3* and wild type were used. To avoid embolism, hypocotyls were clipped in a ½ MS solution containing 500 mg/L

chloramphenicol or 400 mg/L lincomycin, respectively. Leaves were not immersed to ensure increased uptake of the antibiotics by transpiration. 24 hours after incubation in ambient light, leaves of the seedlings were harvested. Control plants were incubated for the same time in a solution containing ½ MS nutrients. Total RNA was isolated from the harvested material and used for Northern analysis. The *petB* and *petD* probes used for hybridizations were amplified using primers *petB*-f/ *petB*-r and *petD*-f/*petD*-r, respectively.

3.3.8   RIP-Chip Array Design, Hybridization and Slot-Blot Analyses

Labeling of RHON1^{TAP}-copurified RNA and its hybridization on the Arabidopsis chloroplast microarray was carried out as described previously (Schmitz-Linneweber *et al.*, 2005). The length of spotted probes was about 800 bp. Control experiments were performed using wild-type extracts. Hybridization of probes and array analyses was performed by Prof. Christian Schmitz-Linneweber (Berlin, Germany). For slot-blot hybridizations RNA was isolated as for RIP-chip analysis and 1/12 of the flow through and 1/6 of the pellet were spotted onto nylon membranes and hybridized with the probes indicated.

3.4   Protein Biochemical Analyses

3.4.1   Isolation of Soluble Chloroplast Proteins

Arabidopsis leafs were homogenized in isolation media (0.3 M Sorbitol, 20m M Hepes/KOH, 10 mM NaHCO$_3$, 5 mM EGTA, 5mM EDTA, 5 mM MgCl$_2$, pH 8.0) using a warring blender following centrifugation at 1,500 g for 8 min with medium break. Chloroplasts were lysed in RIPA buffer containing 0.1, 0.5 or 1% NP-40 and after centrifugation at 18,000 g membrane and soluble proteins were separated.

3.4.2   Isolation of Thylakoid Membrane Complexes

Thylakoid membranes were separated according to Ossenbühl *et al.* (2004). Approximately 3 g Arabidopsis leafs were homogenized in a Warring blender in 50 mM Hepes/KOH pH 7.5, 330 mM Sorbitol, 1 mM MgCl$_2$, 2 mM EDTA, 5 mM Ascorbat, 10 mM NaF. The homogenate was filtered through two layers Miracloth (100 μm, Calbiochem) and centrifuged for 3 min at 1,000 g.

The thylakoid pellet was washed in washing buffer (50 mM Hepes/KOH pH 7.5, 5 mM Sorbitol, 10 mM NaF) and resuspended in 150 μl TMK buffer (50 mM Hepes/KOH pH 7.5, 100 mM Sorbitol, 5 mM MgCl$_2$, 10 mM NaF). The suspension obtained was incubated for 10 min on ice and then centrifuged for 3 min at 1,000 g. The sediment was again resolved in TMK buffer and membrane fractions equivalent to 20-30 μg chlorophyll were used for further analyses.

3.4.3   Measurement of Protein and Chlorophyll Concentration

Concentrations of soluble proteins were measured according to Bradford (1976). Protein amounts of mutants were equalized to amounts in wild type (100 μg) according to Coomassie-stained gels. Chlorophyll concentrations were measured according to Arnon (1949).

3.4.4   Sodium Dodecyl Sulfate Polyacrylamide Gel Electrophoresis (SDS-PAGE)

Proteins were separated by SDS-PAGE as described in Meurer *et al.* (1996a).

3.4.5   Two-Dimensional Blue Native / SDS-PAGE

Blue Native (BN)-PAGE analysis was performed as described earlier for tobacco with some modifications (Schwenkert *et al.*, 2006). Thylakoid membranes equivalent to 30 μg of chlorophyll were solubilized with 1% *n*-dodecyl-β-D-maltoside and separated on a 5-15% acrylamide gradient gel. After electrophoresis, lanes of the BN polyacrylamide gel were excised, denatured by incubation in an SDS/β-Mercapto-ethanol containing buffer and run in the second dimension in SDS-PAGE with 15% acrylamide and 4 M urea. Subsequently, the gels were silver-stained.

3.4.6   Two-Dimensional Clear Native / SDS-PAGE

Clear Native (CN)-PAGE gels used for separation of soluble complexes were substantially the same like for BN besides a reduced Coomassie content (0.002%) and a lower acrylamide concentration (5-12%). Lanes of the CN gels were denatured as for BN and run on the second dimension in SDS-PAGE with 10% acrylamide.

3.4.7 Size-Exclusion Chromatography

Three-weeks-old Arabidopsis wild-type and mutant leaves were homogenized in isolation media as described above. Chloroplasts were lysed in a buffer containing 25 mM Tricine pH 7.9, 50 mM KCl and 1% Protease Inhibitors. The soluble stromal fraction was obtained after a two-step centrifugation for 20 min at 18,000 g and 245,000 g. Supernatants were concentrated in Amicon Ultra filtration devices (Millipore) at 4°C, with or without 250 units of RNaseOne (Promega). Samples (5 mg protein) were loaded onto a Superdex 200 10/300 GL column (GE Healthcare) and eluted with the same buffer using an FPLC device (Äkta, GE Healthcare). Elution fractions were precipitated with trichloroacetic acid and loaded onto SDS-PAGE gels with subsequent immunoblotting. The column was calibrated with a HMW calibration kit (GE Healthcare).

3.4.8 Western Analyses

For immunodetection, proteins separated on SDS-PAGE gels were transferred to polyvinylidene difluoride (0.45 μm; GE Healthcare) or nitrocellulose membranes (0.45 μm; Whatman) using a discontinuous buffer system (Khyse-Andersen, 1984) and a semi-dry transfer device. After blocking membranes in TBS-T buffer (10 mM Tris/HCl pH 8.0, 150 mM NaCl, 0.1% Tween-20) containing 5% dry milk powder, hybridization with primary antibodies was performed for 1 h at room temperature or overnight at 4°C in the same buffer conditions. Washing steps after antibody-incubation were performed in TBS-T. Signals could be visualized after incubation with secondary antibodies for 1 h at room temperature using the enhanced chemiluminescence technique.

3.4.9 *In Vivo* Labeling of Chloroplast Proteins with ^{35}S-Methionine

For radioactive labeling of chloroplast proteins leafs of three-week-old Arabidopsis plants were pre-incubated for 30 min in IVL-buffer (1 mM KH_2PO_4 pH 6.3, 0.1% Tween-20, 20 μg/ml cycloheximide) to block the synthesis of nuclear-encoded proteins and subsequently vacuum-infiltrated in a syringe in 5 ml of the same buffer supplemented with 1 mCi [35S]-L-methionine/cysteine. After incubation and illumination with 100 μmol photons $m^{-2}s^{-1}$ for 2 h leafs were homogenized as described in 3.4.2 using a mechanical stirrer (RW16 basic, Kika Labortechnik). Soluble and membrane proteins were separated by centrifugation for 10 min at 10,000 g and loaded onto SDS-PAGE gels, which were either dried or subjected to a semi-dry

blotting transfer as described above. Signals were quantified using the Typhoon scanner (GE Healthcare).

3.4.10 Co-Immunoprecipitation of Protein Complexes

a) using antibodies raised against a native protein

10 µl of α-RNE antibody was bound to 50 µl Dynabeads coupled to Protein A (Invitrogen) following the manufacturer's instructions. After several washing steps the Protein A-α-RNE complex was incubated for 30 min with 1 ml of a soluble chloroplast fraction. RNE complexes bound to the Protein A-antibody mix and could be used for subsequent analyses after elution.

b) using antibodies raised against epitopes of tagged proteins

Soluble chloroplast extracts of at least 30 g of four-week-old mutant plants complemented with tagged versions of the respective gene and grown on soil were prepared as described above. After loading onto a Strep-Tactin Column (IBA) the tagged proteins were purified following the manufacturer's instructions. The combined eluates were concentrated using Amicon Ultra filtration devices (Millipore) and either used for further analyses or in a second purification step incubated for 1 h with 50 µl of an HA-matrix (Anti-HA-affinity matrix, Roche). After final elution samples were either separated on CN-PAGE and SDS-PAGE-gels for western analyses or used for identification of interaction partners via mass spectrometry. If necessary, Co-IP-purified and concentrated complexes were treated with 1% RNase One (Promega) before loading onto the CN gel.

3.4.11 Mass Spectrometry

Samples for analysis with mass spectrometry were loaded onto SDS-PAGE gels, run for 30 min and stained with Coomassie. If visible, bands were cut out or otherwise proteins were cut out in total and subjected to mass spec analysis (Mass Spectrometry Unit, Department I, Biologie, LMU Munich).

3.5   Fluorometric and Spectroscopic Methods

3.5.1   Visualization of GFP and Chlorophyll Autofluorescence

The cDNA of *PrfB3* encoding the N-terminal part was PCR-amplified using primers At-PrfB3-Sal-f and At-PrfB3-Sal-r. The resulting product was digested with *SalI* and cloned in-frame into the *SalI* site of the GFP expression vector pOL-LT (Mollier *et al.*, 2002). Transient expression was performed in polyethylene glycol-treated tobacco protoplasts and fluorescence was visualized 18 hours after transformation using a Fluorescence microscope in ApoTome mode (Axio Imager, Zeiss). Cloning of the GFP construct and transformation of protoplasts was performed by Elli Gerick, microscopy images were taken by PD Dr. Jörg Meurer. Analysis of chlorophyll autofluorescence took place with isolated protoplasts of *Arabidopsis thaliana* (Dovzhenko *et al.*, 2003) and fluorescence was visualized as described above.

3.5.2   Chlorophyll *a* Fluorescence Analyses

A pulse amplitude-modulated (PAM) fluorometer (Dual-PAM101, Walz) equipped with a data acquisition system (PDA-100, Walz) was used to measure and analyze *in vivo* chlorophyll *a* fluorescence from plants of the same age grown under identical conditions. Plants were dark adapted for 20 min and minimal fluorescence (F_0) was measured. Saturating pulses (0.8 s) of white light (5,000 µmol photons m^{-2} s^{-1}) were used to determine the maximum fluorescence (F_m) and the ratio F_v / F_m (maximum quantum yield of PSII) was calculated. After 10 min of illumination with actinic light of varying intensities, one more saturating pulse (0.8 s) of 5,000 µmol photons m^{-2} s^{-1} light intensity was applied to estimate F_m' and the effective quantum yield of PSII. Additionally the photosynthetic parameters qP (photochemical quenching) and NPQ (non-photochemical quenching) were determined.

Photochemical quenching: $qP = (F_m' - F_s) / (F_m' - F_0)$

Non-photochemical quenching: $NPQ = (F_m - F_m') / F_m'$

Effective quantum yield PSII: $\Phi_{PSII} = (F_m' - F_s) / F_m'$

Maximum quantum yield PSII: $F_v/F_m = (F_m - F_o) / F_m$

3.5.3   Light-Induced Changes of the P700 Redox State

Light-induced changes of the P700 redox state were recorded by absorbance changes at 830 nm, with the above described PAM system equipped with a dual wavelength emitter-detector unit (101-ED, Walz). Multiple turn-over flashes of 50 μs were induced by a Xenon lamp and saturating light pulses of 1 s were applied by halogen lamps.

3.6   Genetic Methods

3.6.1   Map-Based Cloning of *rne-2* and *rhon1*

In order to identify the precise chromosomal location of the *rne-2* gene a mapping population was generated by crossing heterozygous *rne-2* plants of ecotype Columbia-0 with wild-type plants of ecotype Landsberg erecta. 768 plants of the F2 generation were examined using a set of SSLP and CAPS markers. The genotype of recombinants was identified by screening the progeny for mutant segregates. Segregating mutations were confirmed by fluorescence imaging of the F3 offspring. The *rne-2* mutation could be fine-mapped to a 69 kb region on BAC T23O15. The *rne-2* mutation was found in gene At2g04270 by sequencing. Flowers of the wild type (accession Landsberg erecta) were pollinated with heterozygous *rhon1* plants giving rise to F2 and F3 generations, which were screened accordingly. Mapping of *rhon1* was carried out by Elli Gerick and PD Dr. Jörg Meurer.

3.6.2   Complementation of *rne* and *rhon1* Mutants

The cDNA for *RNE* splice variant 1 was kindly provided by Prof. Gadi Schuster (Haifa, Israel). For complementation of the *rne* phenotype the cDNA beginning six nucleotides upstream of the start codon and missing the stop codon was amplified using Pfu polymerase (NEB) and the product was cloned into the TAP vector via pDONR207 using the Gateway technology and stbl2 competent cells (Invitrogen). This allowed a C-terminal fusion of the Strep-HA-tag. Heterozygous *rne-1* plants were transformed using *Agrobacterium tumefaciens* (floral dip method; Clough and Bent, 1998) and complemented transgenic plants were selected through BASTA resistance and named *rne*[TAP]. A full-length cDNA of *RHON1* was generated by RT-PCR. Cloning into the TAP-tag vector and transformation of heterozygous *rhon1* plants occurred in the same way as for *rne-1*. The selected homozygous mutant lines were named *rhon1*[TAP]. Homozygosity of

complemented lines was confirmed by PCR analyzes using primers flanking the T-DNA insertion. Both mutants were functionally complemented using the tagged protein versions.

3.6.3   Complementation of the *prfB3-1* Mutation

The cDNA of *PrfB3* RAFL09-18-I15 (Accession number AY128374) was obtained from the RIKEN BioResourse Center (Seki *et al.*, 2002) and amplified with Pfu polymerase (NEB) using the 5′ phosphorylated PrfB3-P-f and PrfB3-Xba-r oligonucleotide primers, the latter including an *Xba*I restriction site. The resulting *Xba*I-digested PCR product was ligated into the *Sma*I/*Xba*I sites of vector pSEX001-VS (Meurer *et al.*, 1998). The construct obtained, *pbinatprfB3*, was introduced into *Agrobacterium tumefaciens* GV3101 (pMP90RK) and subsequently transformed into progenies of mutant segregants using the floral dip method (Clough and Bent, 1998). After propagation lines were tested for antibiotic resistance conferred by the T-DNA and homozygous mutants were selected by PCR using gene specific intron primers PrfB3-f and PrfB3-r and the left border primer (LBb1) of the T-DNA insertion. Cloning of the construct and transformation of plants was performed by Lina Lezhneva.

3.6.4   Accession Numbers

Accession numbers are NP_850987 (At2g04270.1, RNE protein), 814965 (At2g04270.1, *RNE* gene), NP_563761 (At1g06190, RHON1 protein), 837128 (At1g06190, *RHON1* gene), NP_191278.2 (At3g57190, At-PrfB3 protein) and 824886 (At3g57190, *At-PrfB3* gene).

4   RESULTS

4.1   Global Players in RNA Metabolism

4.1.1   Genetic Mapping of *HCF2* Identified the Endoribonuclease RNE

The *rne-2* mutant (*hcf2*) was originally identified in a screen of EMS-mutagenized Arabidopsis plants, exhibiting a *high chlorophyll fluorescence* (*hcf*) phenotype and affecting accumulation of certain sets of chloroplast transcripts (Dinkins *et al.*, 1994). We assigned the mutation in our mapping population using 1536 meiotic chromosomes to bacterial artificial chromosome (BAC) T23O15 between two adjacent markers with 3 and 10 recombination events (Figure 7A). Sequencing of genes located in between revealed a mutation in the *RNE* gene At2g04270 with a single G-to-A transition of the last nucleotide of the seventh intron (Figure 7B).

Figure 7. Mutations, Mapping and Structure of the *Arabidopsis thaliana RNE* Gene.

(A) Positions of molecular markers A-G on chromosome 2 used for mapping of *rne-2* and the corresponding numbers of recombinant events (below) are shown. **(B)** Exons (gray boxes) and introns (gray lines) show the structure of the 6 kb genomic *RNE* gene (At2g04270). The T-DNA insertion and the point mutation representing mutant lines *rne-1* and *rne-2* are indicated. The *rne-2* mutation is based on a G-to-A-transition of the last nucleotide of the 7th intron, resulting in splicing 18 nucleotides farther downstream. Arrows indicate the positions of primers used for PCR analysis. **(C)** Exon specific primers P4 and P5 were used for RT-PCR analysis of the *rne-2* mutant line. The sizes (bp) and sequences of RT-PCR products demonstrate the splice

defect. **(D)** Immunoblot analyses using an antibody raised against RNE detected the protein in the soluble chloroplast fraction of wild type and *rne-2* but not in *rne-1*. The PAC protein serves as loading control.
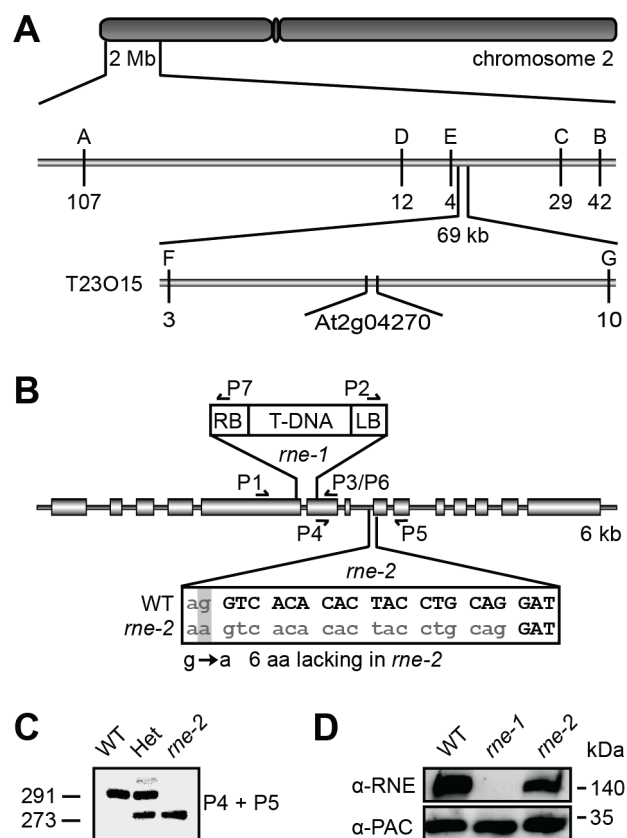
Sequencing of RT-PCR products uncovered an alternative splice site 18 nucleotides farther downstream within exon eight (Figure 7B+C) resulting in a deletion of six aa in the RNase H fold. The T-DNA insertion of the SALK line *rne-1* was accompanied by a small deletion between

nucleotides +2381 and +2538 relatively to the start codon as confirmed by sequencing of PCR products generated with T-DNA border and genomic primers. Antibodies raised against the C-terminal subdomain of RNE localized the protein in the soluble stroma fraction as reported previously (Schein *et al.*, 2008). RNE is absent in the *rne-1* knockout line whereas in *rne-2* the protein lacking the six aa is expressed at normal levels (Figure 7D). The protein runs at about 140 kDa although the predicted size of the mature protein lacking the transit peptide for chloroplast import is around 104 kDa. This anomaly in migration of the protein has also been reported for RNase E in *E. coli* and was mentioned in previous reports about plastid RNE as well (Casaregola *et al.*, 1992; Schein *et al.*, 2008; Mudd *et al.*, 2008).

In cooperation with the lab of Prof. Gadi Schuster it was shown that a recombinant protein corresponding to RNE-2 lacking the six aa 688-693 has no catalytic activity *in vitro* (Stoppel *et al.*, *submitted*) when compared with the previously characterized, truncated Arabidopsis wild-type protein comprising aa 284-996 (Schein *et al.*, 2008). This explains why the overall *rne-2* phenotype is very similar to that of the *rne-1* knockout line and demonstrates that the internal six aa in the RNase H fold are essential for catalytic activity.

4.1.2 Complementation and Epitope-Tagging of *rne-1*

When grown on Suc-supplemented medium under sterile conditions *rne* mutant plants showed a pale green phenotype but their size and morphology was comparable to wild-type and heterozygous plants (Figure 8).
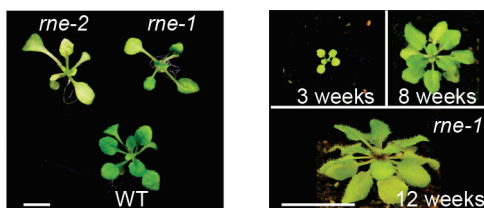
Figure 8. Phenotype of WT and *rne* Mutant Plants.
Wild type (WT) and mutant lines *rne-1* and *rne-2* were grown on Suc-supplemented MS-media for 3 weeks (left). *rne-1* mutants were grown on soil for three, eight and 12 weeks, respectively (clockwise, right). Bars indicate the size of 1 cm.

Homozygous *rne* seedlings developed pale cotyledons when grown photoautotrophically on soil, but were reported to be lethal at the stage of primary leaf formation (Mudd *et al.*, 2008). However, when kept under optimal watering and light conditions some of the homozygous mutants were able to survive on soil albeit with severe growth retardations as reported recently (Walter *et al.*, 2010) and confirmed here (Figure 8).

Since the *hcf* phenotype indicates deficiencies in photosynthetic electron transport and to evaluate the effect of the mutations on protein assemblies, thylakoid membrane complexes were separated by blue-native polyacrylamide gel electrophoresis (BN-PAGE) on a first and by SDS-PAGE on a second dimension. The protein complex pattern revealed a comparable pleiotropic phenotype for both *rne* mutant alleles (Figure 9). All major thylakoid membrane complexes are present in the *rne* mutants, albeit at lower levels, demonstrating that generally translation and assembly of complexes is not the primary target of RNE.
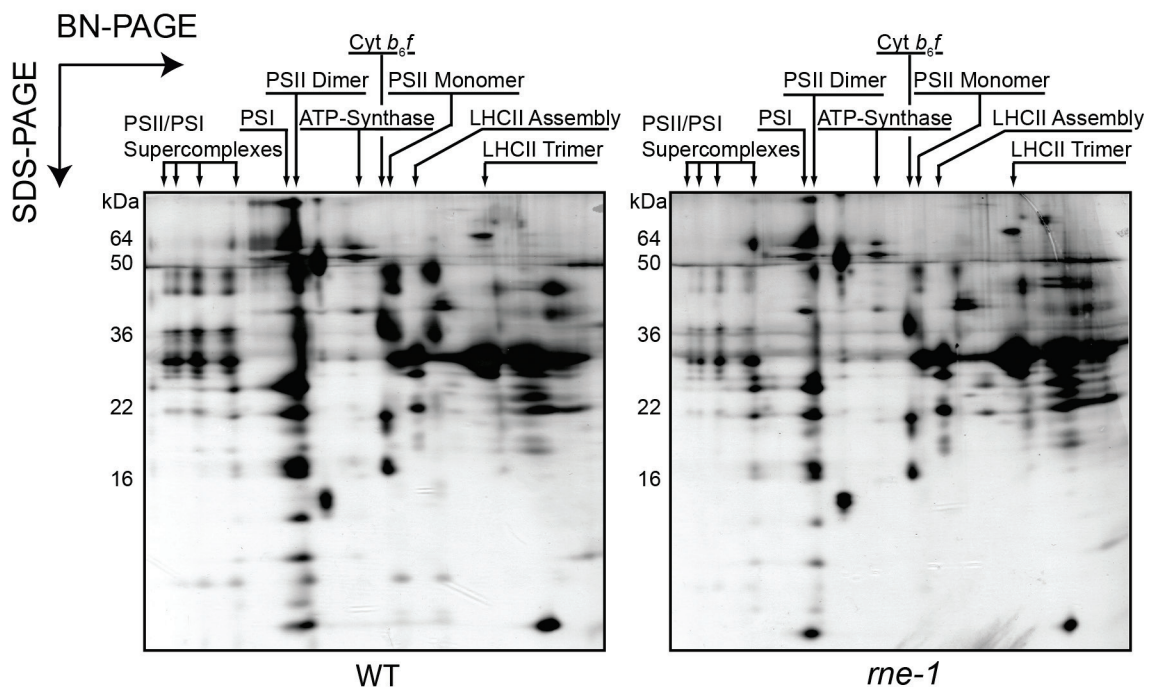
Figure 9. Representative Blue Native/SDS-PAGE Analysis of Solubilized Thylakoid Membrane Complexes of WT and *rne-1*.

Thylakoids were solubilized with 1% *n*-dodecyl-β-D-maltoside, and electrophoresis was performed in the first (BN-PAGE) and second (SDS-PAGE) dimension. Individual protein spots were silver stained. Although levels of proteins are reduced in *rne-1* with respect to the WT the protein complex pattern are comparable. The position of thylakoid membrane complexes is indicated.

To further investigate the function and potential interactions, we complemented homozygous *rne-1* mutants with the *RNE* full-length cDNA fused in frame to a TAP-tag, creating *rne*[TAP] lines. The TAP-tag consists of a tandem of three HA epitopes and one StrepIII epitope, separated by a short linker sequence (Figure 10A). The vector contains a weak promoter derived from the *HCF173* gene in order to avoid overexpression of the tagged protein (Schult *et al.*, 2007). This should allow identification of interaction partners using highly specific monoclonal antibodies raised against the epitopes of the tags in co-immunoprecipitation (Co-IP) experiments.

Homozygosity of 16 independently generated rne^{TAP} plants was confirmed by PCR using genomic and T-DNA-specific primers (Figure 10B). No visible differences could be observed between epitope-tagged mutant lines and wild-type plants, suggesting that the TAP-tag does not impair the function of RNE (Figure 10C). Immunoblot analyses of complemented *rne* lines revealed a signal at the expected size (RNE 140 kDa + TAP-tag = 147 kDa) in the chloroplast stroma using mono-specific HA-antibodies (Figure 10D). The StrepIII-tag allowed purification of RNE under native conditions using a Strep-tactin column (Figure 10D).
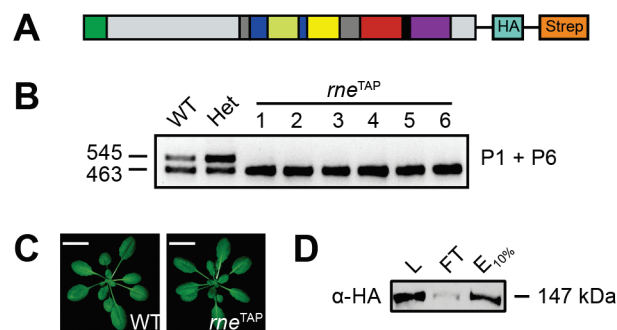
Figure 10. Complementation of *rne-1* with a Double Tag for Tandem Affinity Purification (TAP).
(A) Structure of the TAP-tag construct used for transformation of *rne-1* mutants. An HA and a Strep tag were fused in tandem to the C-terminus of the full-length cDNA of *RNE*. **(B)** Genotyping of WT, heterozygous (Het) and six independent *rne-1* lines complemented with the TAP-tag construct (rne^{TAP}) was performed using PCR. Primers P1 and P6 shown in Figure 7 amplified a 545 bp genomic DNA fragment (upper band) and a 463 bp fragment of the cDNA (lower band), thus confirming complementation of *rne-1* mutants. **(C)** Complementation of the *rne-1* line fully restored WT phenotype. WT and rne^{TAP} plants were grown on soil for four weeks (left). Bars indicate the size of 1 cm. **(D)** Stromal lysate (L), IP flow through (FT) and 10% of the IP eluate (E) collected during purification of RNE^{TAP} with the Strep-column were loaded. A monoclonal HA antibody detected the tagged protein in the lysate and IP eluate. The protein is migrating at a size of 147 kDa. The remaining 90% of the IP eluate were subjected to mass spectrometry.

4.1.3 Isolation of the First RNE Interacting Protein in Plant Chloroplasts

We took advantage of the Strep-tag to isolate potential interaction partners associated with the plastid RNE. Detergent-solubilized stromal fractions were prepared from isolated chloroplasts and subjected to co-immunoprecipitation using the Strep-tactin column. Co-IP eluates were shortly separated on a gel and subsequently in-gel digested with trypsin. The resulting peptides were analyzed through microcapillary liquid chromatography MS/MS followed by protein database searches of the generated spectra. Three independent experiments identified several peptides of RNE together with a protein that could be assigned to the At1g06190 gene (Table 1).

Table 1: RNE and RHON1 Peptides Identified in Co-IP Experiments with *rne*^TAP Lines.

Experiment	Sequence	Homology	Frequency
1	R.SAIVSAQQEQPPSR.L	RNE	1
	K.TLQPQGFGLTVR.T	RNE	2
	K.TNVQC#DSVYLGVITK.F	RNE	1
	R.AM*GQTLSVVQDYFNDK.V	RNE	2
	R.PGPQFSLSVPSSVNQDR.K	RNE	2
	R.SAIVSAQQEQPPSR.L	RNE	1
	R.TVAAGHSLEELQK.D	RNE	2
	R.VDSHMSSFLTTGK.R	RNE	1
	K.FSSQGEVQGDTVDKQDR.T	RHON1	1
	R.NGPLFNLSSSPK.F	RHON1	1
2	K.DLDGLLLTWK.N	RNE	1
	R.TVAAGHSLEELQK.D	RNE	1
	R.NGPLFNLSSSPK.F	RHON1	2
3	K.AILEVNLAAAR.Q	RNE	2
	K.LVELLLEPVK.T	RNE	2
	K.TLQPQGFGLTVR.T	RNE	1
	K.TNVQC#DSVYLGVITK.F	RNE	2
	R.VEALETTFSK.I	RNE	2
	-.NGPLFNLSSSPK.-	RHON1	3
	K.DNNASSFTRPTSSFR.R	RHON1	1

Peptide sequences were determined by mass spectrometry based sequencing in three independent experiments. C#, Carbamido-methylation; M*, Oxidation.

Both proteins were completely absent when untagged wild-type plants or lines expressing other TAP-tagged proteins, like HCF101 (Schwenkert *et al.*, 2009), PrfB3 (Stoppel *et al.*, 2011), and PAC (Meurer *et al.*, 1998) were subjected to the same procedure (unpublished data), indicating the reliability of the TAP-tag purification and suggesting that the At1g06190 gene product represents an interaction partner of RNE.

4.1.4   The At1g06190 Gene is Found Exclusively in Vascular Plants and its Product is Targeted to the Chloroplast

With the exception of *Chlamydomonas reinhardtii*, RNase E homologs can be found in all photosynthetic lineages including green algae, whereas At1g06190 holds only homologies among

vascular plants. We generated a full-length cDNA of the At1g06190 locus by RT-PCR. The obtained cDNA of 1,285 bp encodes a protein of 401 aa. Domain analysis of this protein revealed that the C-terminus contains a motif similar to the N-terminal part of the RNA-binding domain of bacterial transcription termination factor Rho (Allison *et al.*, 1998; Aravind and Koonin, 2001). This part of the RNA-binding domain has a helix-extended-helix (HEH) structure and is called Rho-N. Hence we named the At1g06190 protein RHON1. Besides *RHON1* the Arabidopsis genome encodes two other proteins with a putative Rho-N domain, predicted to be targeted to mitochondria (At4g18740) and cytoplasm (At2g41550) (Figure 11).

```
Sec. structure        HHHHHHHH..HHHHHHHHHHH........HHHHHHHHH

RHON1          359    EAVKDLSELKLVELRGIAKSRGLKGLSKMKKAELVELL
AT4G18740      205    EKASLIETMKLAELKEVAKNRGIKGYSKLRKSELLELI
At2g41550      420    LSISELKKKTGKELRSIAKDLKVQHYYKLKKEDLLQRI
Physcomitrella 479    AVSKNLSSYKLPELRSMAKAKGLKGYSKLKKGELVELI
Ostreococcus   549    DGRFRLRTMTRTELLELARQRGMTRYSKLNKPELVERL
Synechocystis    4    EDRPSLKDMTLRQLRRVASECNISRYSRMRKSQLLAEV
Rhodobacter      5    LNLSDLKAKSPKDLLAMAEDWEIENASTMRKGEMMFSI
E. coli          1    MNLTELKNTPVSELITLGENMGLENLARMRKQDIIFAI

consensus/90%         .....hp.b...pLb.bh.pbsl...pp.pK.pLl..l
```

Figure 11. Multiple Sequence Alignment of Rho-N Motifs.

The alignment shows the HEH structured Rho-N motifs of RHON1 and other proteins of unknown function in *Arabidopsis thaliana* (At4g18740, At2g41550), *Physcomitrella patens* (XP_001761620) and *Ostreococcus lucimarinus* (XP_001416615), as well as N-terminal sequences of Rho factors from *Synechocystis*, *Rhodobacter* and *E. coli*, starting with the aa indicated. The secondary structure shown above the alignment and the consensus sequence shown below were described in Aravind and Koonin (2001). Negatively charged aa are colored in red, positively charged are colored blue. H, helix; h, hydrophobic; p, polar; b, big; s, small; l, aliphatic.

A third genomic locus (At2g31150) displaying high similarity (43%) to the entire *RHON1* is present in Arabidopsis. However, annotation data, RT-PCR analyses as well as available EST data could identify only transcripts, which do neither encode an entire open reading frame nor the corresponding C-terminal Rho-N domain because of the presence of several premature stop codons and annotated intron sequences. This locus most likely originated from a gene duplication of *RHON1* because of a collinear genomic context. We conclude that At2g31150 has been converted into a pseudogene after duplication. This is consistent with single copy genes in monocot and most dicot species.

The previously described rice protein OsBP-73 (Os03g0183100) was assumed to bind DNA (Chen *et al.*, 2003) and exhibits 35% sequence similarity to RHON1. An *in vitro* interaction with the promoter of the nuclear *waxy* gene in rice suggested localization of OsBP-73 in the nucleus and function as a transcription factor. However, the localization of OsBP-73 was not addressed experimentally. Several subcellular localization algorithms predicted that RHON1 and

OsBP-73 are present in the chloroplast (ChloroP, TargetP, PCLR). A C-terminal in-frame fusion to GFP was previously investigated in our group and confirmed targeting of RHON1 to chloroplasts (not shown). This is consistent with several chloroplast proteomics data and the immunological identification of RHON1 in chloroplast extracts (see below).

4.1.5 Molecular Mapping, Complementation and Phenotype of *rhon1* Mutants

An Arabidopsis seedling-lethal T-DNA mutant affected in chloroplast RNA metabolism and exhibiting an *hcf* phenotype was previously identified in our group. Segregation analysis using 2448 F2 progenies and 638 individual F3 plants derived from backcrossed mutant plants revealed that the mutation is either caused by or very closely located to one insertional event because the kanamycin resistance conferred by the T-DNA strictly co-segregated with the mutant phenotype.

Figure 12. Mapping, Phenotype, and Complementation of *rhon1*.

(A) Molecular markers H-M used for fine-mapping of *rhon1* on chromosome 1 and the corresponding numbers of recombinant events are shown. Southern blot analysis of BACs T21E18 and F9P14 as well as sequencing of T-DNA border regions revealed that the T-DNA was inserted into the At1g06190 gene (*RHON1*). **(B)** Exons (gray boxes) and introns (black lines) show the structure of the genomic *RHON1* gene. The T-DNA insertion at position +481 is marked. Arrows indicate the positions of primers used for PCR analysis. The phenotype of a *rhon1* mutant plant as compared to WT grown for three weeks under heterotrophic conditions is shown. **(C)** The N-terminus of RHON1 includes the sequence predicted to constitute a chloroplast transit peptide (TP). In addition, the protein contains two conserved regions (red) and the C-terminal motif Rho-N (yellow). For complementation of the mutant a construct of the full-length protein fused to an HA-Strep TAP-tag was used. **(D)** WT and complemented *rhon1*[TAP] plants were grown on soil for four weeks in 12/12 hours light/dark conditions. **(E)** PCR analysis demonstrates orientation of the T-DNA insertion in exon 2 of *rhon1*, as well as homozygosity of independent complemented lines.
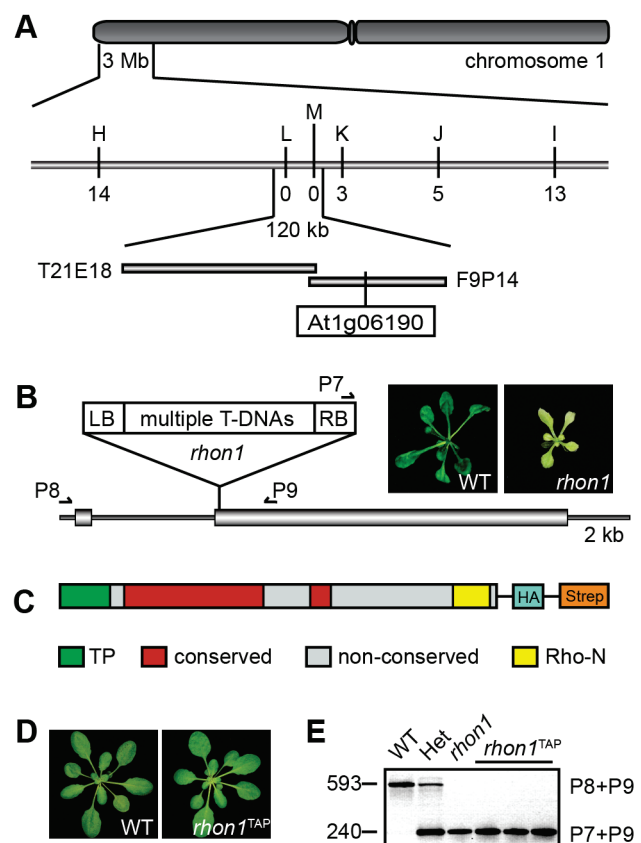
It was impossible to identify the T-DNA flanking sequences by inverse PCR because of multiple truncated T-DNA insertions in this locus as revealed by genomic Southern analysis. Therefore, we fine mapped the mutation on the upper part of chromosome 1 (Figure 12A) and localized the T-DNA insertions at position +481 relative to the start codon of *RHON1*. *RHON1* has a size of about 2 kb organized in two exons (Figure 12A+B). The protein contains a predicted transit peptide (TP) for transfer to the chloroplast (ChloroP) and two conserved regions with unknown functions followed by a stretch consisting of highly negatively charged aa. Since all attempts to express the full-length RHON1 in *E. coli* cells and to immunize rabbits against synthetic peptides in order to get functional antibodies failed, we complemented the *rhon1* mutant with the cDNA fused to the same TAP-tag as described for RNE (Figure 12C+D). PCR analysis of 49 selected plants confirmed homozygosity of 3 lines using genomic primers in combination with the right border primer of the T-DNA (Figure 12E). Complemented *rhon1*[TAP] lines could not be distinguished phenotypically from the wild type (Figure 12D) indicating that the phenotype is solely caused by the multiple T-DNA insertions in the *RHON1* gene.

The phenotype of *rhon1* mainly resembles that of *rne*, but in contrast to *rne*, the defect leads to seedling lethality, and homozygous *rhon1* mutants could be grown only on Suc-supplemented medium (Figures 12B). Chlorophyll *a* fluorescence imaging of isolated leaf protoplasts revealed a dramatic decrease in chloroplast size accompanied with an increase in chloroplast number in both mutants as compared to the wild type (Figure 13).
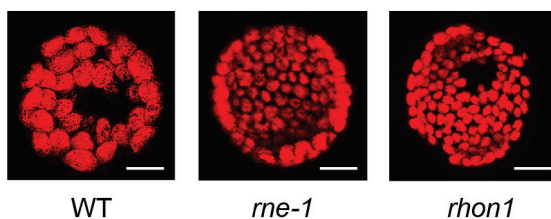
Figure 13. Chloroplast Number and Size as Revealed by Chlorophyll Autofluorescence.
Chlorophyll fluorescence was imaged from protoplasts isolated from WT, *rne-1* and *rhon1*. Bars show the size of 10 μm.

WT   *rne-1*   *rhon1*

4.1.6   RHON1 Precipitates RNE

To further confirm the RNE-RHON1 interaction, we investigated Co-IPs of *rhon1*[TAP] lines applying the same method as described above. Using the HA antibody we could observe a distinct signal in lysate, flow through, and eluate of *rhon1*[TAP] but not in untagged wild-type lines. The same immunoblot probed with the RNE antibody detected RNE in lysate and flow through of *rhon1*[TAP] and wild type, but only in the eluate of *rhon1*[TAP] (Figure 14A). Control experiments using antibodies raised against HCF101 or PAC, which are involved in plastid Fe/S cluster biogenesis (Schwenkert *et al.*, 2009) and RNA metabolism (Meurer *et al.*, 1998; Stoppel *et al.*,

2011), respectively, did not give any notable signal in *rhon1*[TAP] or wild-type eluates, suggesting that *rhon1*[TAP] precipitated specifically RNE. This data confirms a true interaction between both proteins (Figure 14A).
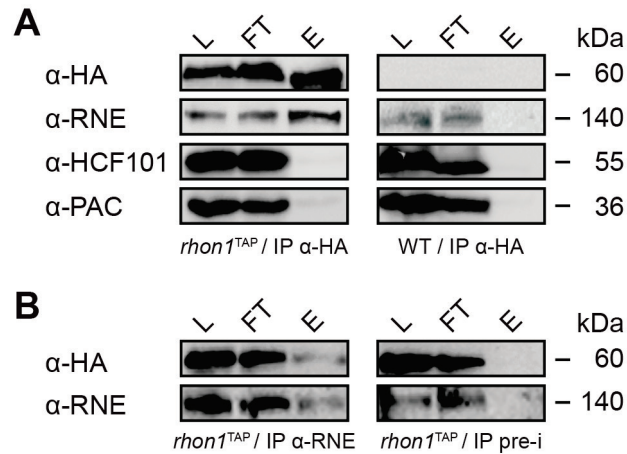
Figure 14. RNE and RHON1 Reciprocal Precipitations.
(A) Soluble protein extracts from *rhon1*[TAP] or WT were immunoprecipitated using a Strep-Tactin column. Samples from stromal extract (L), IP flow-through (FT), and the IP eluate (E) were separated in 10% polyacrylamide gels and subjected to immunoblot analysis using the antibodies indicated (left). Protein sizes are given in kDa (right). **(B)** A Co-IP using the RNE antibody and protein extracts from *rhon1*[TAP] was able to precipitate RNE as well as RHON1 while the pre-immunserum was not, as shown by immunoblot analysis. pre-i, pre-immunserum.

Moreover, a Co-IP using *rhon1*[TAP] plants and RNE antibodies coupled to Protein A coated magnetic beads, precipitated both RNE and RHON1, while pre-immune sera of the same rabbit failed to do so, again substantiating the interaction (Figure 14B).

Levels of RNE were severely reduced in *rhon1* mutants to about 25% as compared to wild type, while the PAC protein used as loading control accumulated normally (Figure 15A). Lower levels of RNE could also be observed in both *rne*[TAP] and *rhon1*[TAP] TAP-tagged lines presumably because of the weak promoter driving expression of the tagged proteins (Figure 15B). The HA antibody gave a distinct signal of both tagged proteins in stromal fractions (Figure 15B). The tagged RHON1 protein shows the same anomaly of migration in SDS-gels like RNE, running at 60 kDa, which is about 13 kDa higher than expected, probably due to the high amount of negatively charged aa (Figure 15B).

Figure 15. RNE Levels of WT, Mutants, and Tagged Lines.

(A) Comparison of RNE levels in WT, *rne*, and *rhon1* mutants. Levels of the protein PAC were used as a loading control. **(B)** Levels of RNE were compared between wild type, *rne*^TAP, and *rhon1*^TAP lines. Note the difference in size between wild-type RNE and the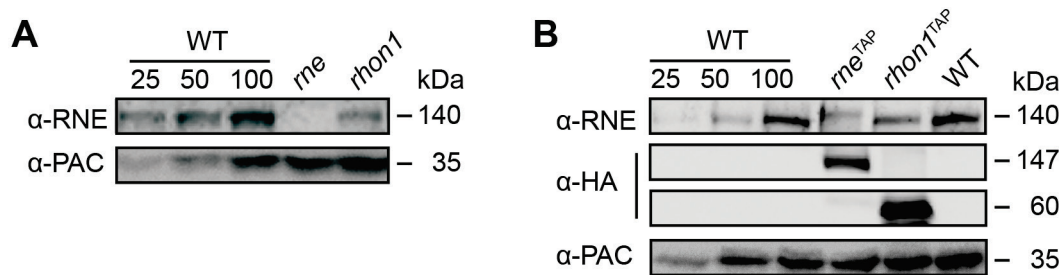 tagged version. The same blot was probed with an HA-antibody and gave signals at the expected sizes of 147 kDa and 60 kDa in *rne*^TAP and *rhon1*^TAP, respectively. Levels of PAC served as loading control.

4.1.7 Spectroscopic and Fluorometric Analyses Revealed a Pleiotropic Phenotype of *rne* and *rhon1*

The *hcf*-phenotypes of pale *rne* and *rhon1* mutant plants indicated defects in the photosynthetic apparatus and were compared with each other. In order to rule out the possibility of photosynthetic defects in complemented mutants we included *rne*^TAP and *rhon1*^TAP lines in our analyses. If feasible, measurements were conducted on plants grown on soil. *In vitro* cultured *rhon1* plants were compared with wild type and *rne-2* grown under the same conditions. However, no significant discrepancy between *rne* mutant plants grown on sucrose or soil could be observed. The activities of PSI and PSII were determined using spectroscopic and fluorometric methods. The maximum quantum yield of PSII (F_v/F_m), a standard parameter of PSII integrity, was reduced to more than 50% in both *rne* and *rhon1*. The effective maximum quantum yield of PSII (Φ_{PSII}) in the steady state was 0.72±0.03 in the wild type and significantly reduced to comparable levels in *rne* (0.20±0.06) and *rhon1* (0.16±0.11). An equal decrease in photochemical quenching (qP) could be observed in both mutants as compared to the wild type (Figure 16A). This behavior was due to elevated ground fluorescence and a decreased level of variable fluorescence. Measurements of the P700 redox state under increasing actinic light intensities revealed elevated levels of oxidized P700 in both mutants as compared to wild type. This demonstrates that activity of PSI is significantly reduced and that electron transport at the acceptor site of PSI is limited in the mutants (Figure 16B). The epitope-tagged complemented lines behaved comparably to wild type (Figure 16A+B).

A

		Φ_{PSII}	F_v/F_m	qP
MS media	WT	0.720	0.838	0.922
	rne-2	0.204	0.398	0.380
	rhon1	0.158	0.312	0.528
soil	WT	0.622	0.836	0.776
	rne-1	0.204	0.394	0.278
	rne^{TAP}	0.592	0.839	0.777
	rhon1^{TAP}	0.628	0.843	0.805

B
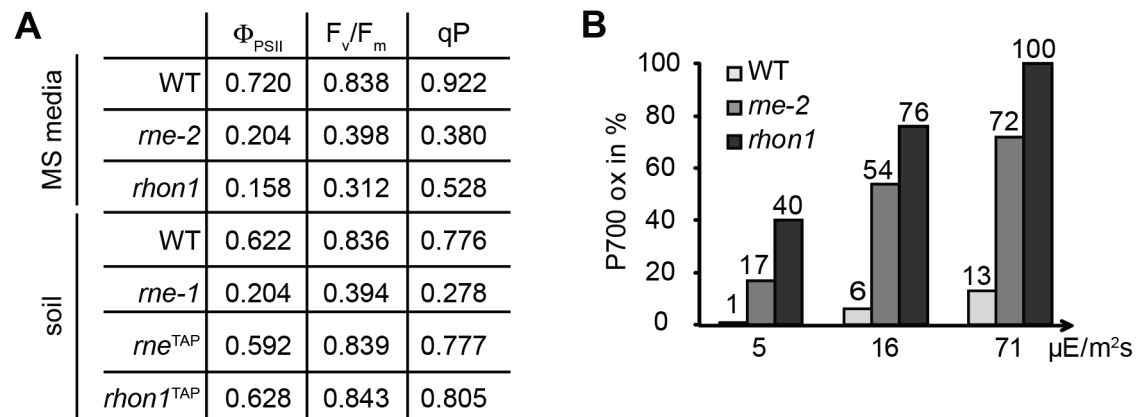
Figure 16. Photosynthetic Parameters of WT, *rne*, *rhon1* and Tagged Lines.

(A) Fluorescence parameters show a severe reduction in effective quantum yield of PSII (Φ_{PSII}), maximum quantum yield of PSII (F_v/F_m), and photochemical quenching (qP) indicating decreased PSII activity in *rne-2* and *rhon1* grown on MS-medium. No significant difference between *rne-1* grown on soil or on Suc-supplemented medium was detectable. Complemented TAP-tagged lines all showed wild type characteristics. **(B)** PSI redox state was measured. Amounts of oxidized P700 under increasing actinic light intensities are elevated in *rne-2* and even more in *rhon1* as compared to the wild type.

Since these data pointed out severe pleiotropic effects on photosynthetic capacity we determined the content of photosynthetic proteins by immunoblot analyses. Levels of most PSI and PSII proteins and the ATP synthase were reduced to equal amounts of less than 25 % in both mutants whereas amounts of the cytochrome b_6f complex were more affected in *rhon1* than in *rne-1* (Figure 17).

Figure 17. Immunoblot Analyses of Thylakoid Membrane Proteins.

Dilution series of membrane protein extracts from three-week-old wild-type plants were compared with *rne-1* and *rhon1* using antibodies raised against proteins of the thylakoid membrane. Loading of 100% corresponds to 10 µg chlorophyll.
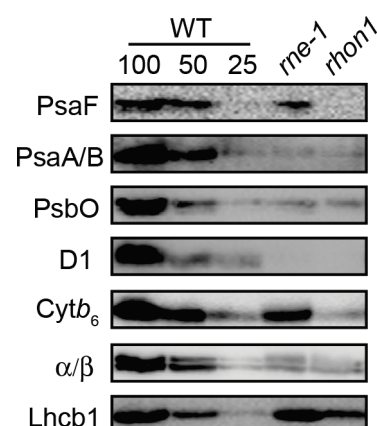
Taken together, the phenotype of *rhon1* is comparable to but to a certain extent more severe than that of *rne-1* displaying an elevated importance and/or additional functions of RHON1 in comparison with RNE.

4.1.8 Double Knockouts of *rne-1* and *rhon1* Display an Additive Phenotype

The nature of both *rne-1* and *rhon1* mutations was strictly recessive. F_v/F_m levels were more reduced (0.07±0.07) and the pale phenotype appeared to be more intense in the homozygous *rne rne/rhon1 rhon1* double knockout mutants than in the individual knockouts indicating an additive effect of the mutations on photosynthetic parameters and chloroplast development (Figure 18).
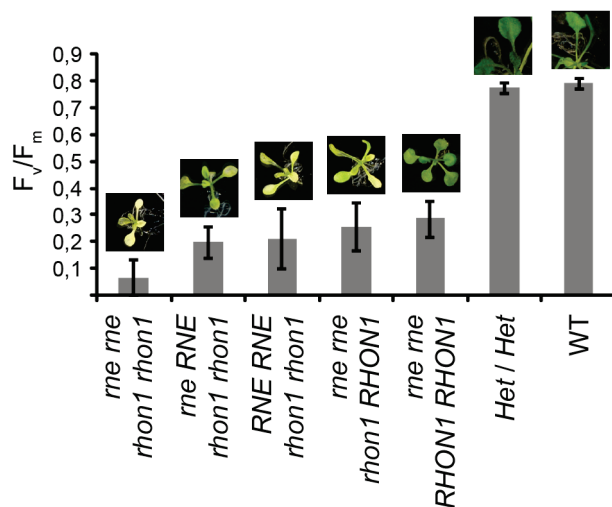
Figure 18. Phenotype of *rne rne/rhon1 rhon1* Double Knockouts.

Double knockouts were created by crossing heterozygous *rne-1* and *rhon1* mutants and selfing of the selected double heterozygous F1. The average F_v/F_m rate and standard deviation was determined from ten independent plants. Representative mutant plants are shown above each column, while wild-type and double heterozygous plants are only shown in parts in order to maintain the same scale. Note that the *rne* mutants in the background of heterozygous *rhon1* are paler than those in the WT background.

4.1.9 RNE and RHON1 are Located in the Same Complex

Since we confirmed that RHON1 represents one of the interaction partners of plastid RNE we intended to clarify if they are stably associated in the same complex *in vivo*. Bacterial RNase E is extremely sensitive to proteolysis and tends to form larger assemblies when overexpressed in *E. coli* cells (Coburn and Mackie, 1999). A similar high degree of sensitivity was observed for plastid RNE even when using protease inhibitors. The biochemical characterization of the plastid enzyme is even more difficult because freezing results in a severe loss of protein stability, necessitating biochemical analysis only with fresh preparations. After applying several separation methods we found Clear Native polyacrylamide gel electrophoresis (CN-PAGE) of Co-IP-enriched RNE[TAP] or RHON1[TAP] to work best for identification of the RNE-containing complex. Our results show, that both RNE[TAP] and RHON1[TAP] are located in the same complex running at about 800 kDa in the separating gel (Figure 19).

Figure 19. RNE Associates with RHON1 in the Degradosome-Like Complex.

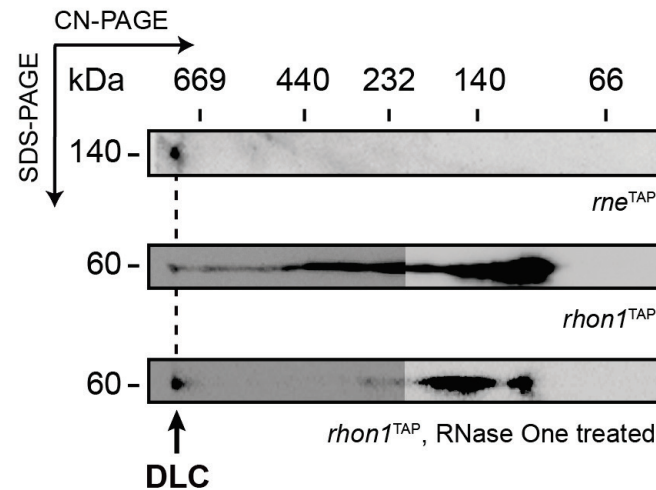Soluble chloroplast fractions of *rne*[TAP], *rhon1*[TAP], and *rhon1*[TAP] treated with RNase One (Promega) were purified on Strep-columns and complexes were separated in the first (CN-PAGE) and second (SDS-PAGE) dimension. Blotted gels were immunodecorated with an HA antibody and sizes of complexes estimated using a HMW-marker set (GE). The left parts of *rhon1*[TAP] immunoblots were overexposed. The high-molecular-weight degradosome-like complex (DLC) of ~800 kDa containing both RNE and RHON1 did not disappear upon RNase One treatment (not shown for *rne*[TAP]).

As the *in vitro* processing activities of RNase E homologs in eubacteria and plastids are comparable and as the *E. coli* enzyme is the characteristic scaffold protein of the degradosome associated with different proteins, we suggest naming the 800 kDa assembly degradosome-like complex (DLC). DLC did not change its size when treated with RNase One, indicating that either it contains no RNA or that RNA is bound to the complex in a compact form, which is not accessible by RNase One. In addition, RHON1 forms a dominant sub-complex of about 100 kDa and further complexes ranging from 100 to 800 kDa. Sub-complexes >150 kDa almost completely disappeared upon RNase One treatment and gave rise to a prominent and distinct RHON1[TAP]-containing complex of 150 kDa, indicating interactions presumably with RNAs of different sizes resulting in this broad molecular weight range (Figure 19).

4.1.10   RHON1 Associates with 16S and 23S rRNA

As an initial survey experiment to identify potential plastid RNA targets of RHON1, we performed RIP-chip assays. Co-immunoprecipitated RNAs from TAP-tagged lines and wild type as negative control were isolated from flow-through and eluates using both HA and Strep-tags and subsequently labeled with red- or green-fluorescing dyes, respectively. These RNAs were

combined and hybridized to a tiling microarray of the Arabidopsis chloroplast genome (Schmitz-Linneweber *et al.*, 2005). Replicate experiments revealed that the RNAs most strongly enriched in Co-IPs using *rhon1*[TAP] were the ribosomal 16S and 23S RNAs (Figure 20A). Slot-blot hybridization of immunoprecipitated RNAs from flow through and eluate verified the enrichment of 16S and 23S rRNA using full-length gene probes (Figure 20B), while 4.5S, 5S, *ycf1* and *rbcL* RNAs were not bound efficiently.
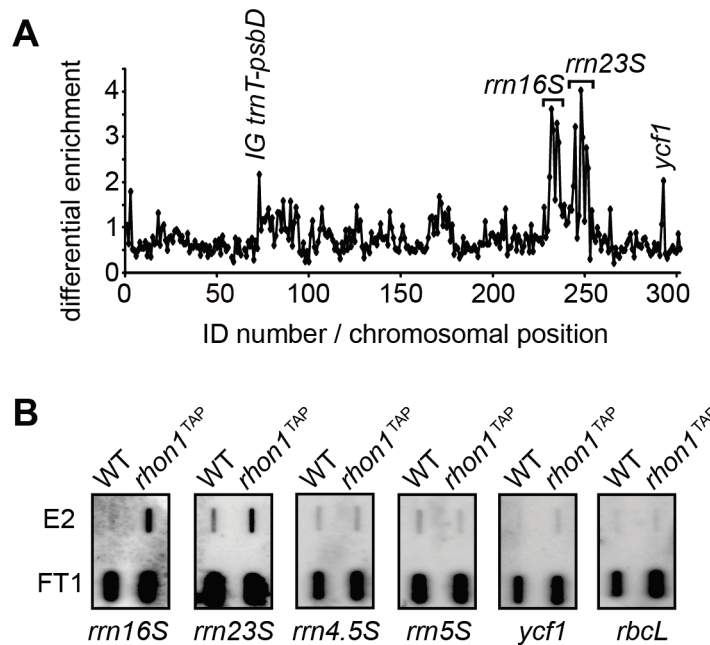
Figure 20. Association of RHON1 with Chloroplast Transcripts.

(A) Stroma of *rhon1*[TAP] or WT (control) was subjected to tandem IP with Strep-Tactin column and HA-matrix. Co-purified RNAs after the second purification step were labeled with Cy5 and RNAs of the flow-through from the first purification step were labeled with Cy3. The enrichment ratios (FCy5:FCy3) were normalized between two assays using tagged protein extracts and two assays using wild-type extracts. The median normalized values for replicate spots from the RHON1[TAP] purifications were divided by those from WT data and plotted according to fragment number on the Arabidopsis chloroplast genome tiling microarray. Fragments are numbered according to their chromosomal position. Labeling, hybridization and analysis of the array data was performed by Prof. Christian Schmitz-Linneweber **(B)** RIP-chip data were validated by slot–blot hybridization. 1/12 of the RNA purified from the IP flow-through of the first purification steps (FT1) and 1/6 of the RNA from the IP eluate of the second purification steps (E2) was applied to slot-blots and hybridized with the indicated probes.

This suggests that RHON1 associates with the highly abundant 16S and 23S rRNAs. However, it remains uncertain if RHON1 is also associated with lower abundant mRNAs. Notably, RIP-chip analysis using RNE[TAP] did not detect any association with RNAs speaking in favor of the idea that DLC contains no RNA. Since the resolution of our RIP-chip and slot-blot analysis is limited

to several hundred nucleotides, electrophoretic mobility shift assays were performed in the group of Jörg Meurer suitable for narrowing down the target sequence. It appeared that the over-expressed C-terminal 40 aa comprising the Rho-N motif fused to a GST tag binds to all investigated RNAs although with quite different stringencies. These data indicate that RHON1 represents a novel RNA-binding protein recognizing specific regions of quite diverse rRNAs and mRNAs via the Rho-N domain.

4.1.11 General Processing of Chloroplast Transcripts is not Affected in *rhon1* and *rne* Mutants

Recently in the group of Jörg Meurer, a chloroplast genome-wide transcriptomic approach was used to study the differential expression of plastid genes under changing environmental conditions and in various nuclear mutants affected in chloroplast functions (Cho *et al.*, 2009). The *rne-2* and *rhon1* (formerly named *crp102* and *crp135*, respectively) mutant transcriptomes appeared to cluster closely together. Levels of >50% of the 94 tested genes were differentially expressed in comparison to wild type (Cho *et al.*, 2009). Genes transcribed by the nuclear- and plastid-encoded polymerase were generally up- and down-regulated, respectively. Thus *RNE* and *RHON1* fall into the same class of genes exerting global functions in plastid gene expression.

A comparison of macroarray data with RNA gel blot analysis has not only confirmed alterations in the mutants' transcript levels, but also revealed dramatic changes in the pattern of chloroplast transcripts in both mutants as compared to wild type, indicative for processing defects and altered RNA stability. For example, accumulation of high-molecular-weight transcripts, like that of *rbcL*, results from inefficient processing of precursor transcripts (Figure 21). The same phenomenon could also be observed in *rne* mutants. Appearing precursor transcripts of 8.5 and 5.4 kb of the *rbcL* transcription unit comprise sequences of the downstream located genes *accD*, *psaI*, *ycf*4, *cem*A, and *pet*A in both mutants (Figure 21B+C). Notably, none of the processed transcripts present in the wild type (not shown) is completely missing in both mutants indicating that processing basically takes place although with reduced efficiency (Figure 21B+C). This finding is indicative for the presence of additional redundant endonucleases, like RNase J (Sharwood *et al.*, 2011), which are also supported by RHON1 and possibly can partially replace the catalytic function of RNE.
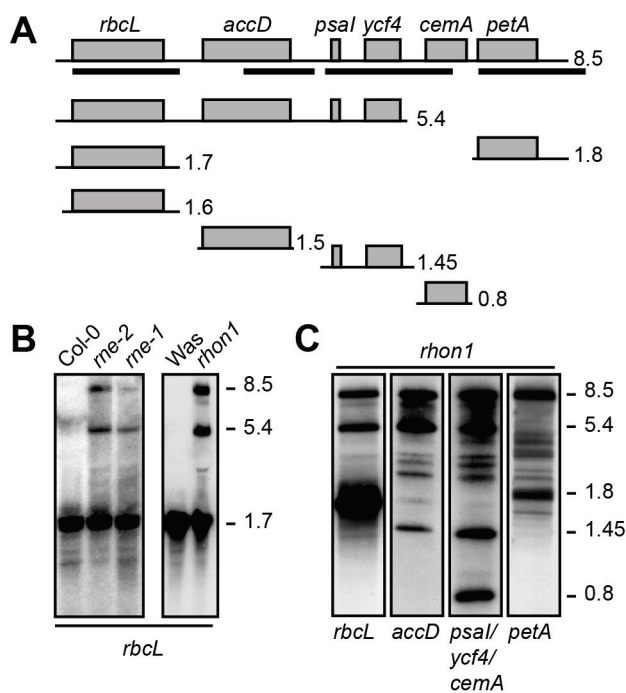
Figure 21. The *rbcL* Gene Cluster and Processing Products in WT, *rne*, and *rhon1*.
(A) The *rbcL* gene cluster, comprising genes *rbcL*, *accD*, *psaI*, *ycf4*, *cemA*, and *petA* and processing products are shown down to scale. Transcript lengths are indicated in kb, probes used for hybridization by black lines. **(B)** Transcript levels of *rbcL* are shown in WT Columbia (Col-0), *rne-1*, *rne-2*, WT Wassilewskija (Was), and *rhon1*. 10 µg leaf RNA of three-week-old plants, grown on Suc-supplemented MS-media, were loaded. **(C)** Total RNA of *rhon1* mutants was separated on the same gel and subjected to RNA gel blot analysis using strand-specific probes (performed by PD Dr. Jörg Meurer).

4.1.12 Levels of Plastid Ribosomes are Severely Reduced in *rhon1* Mutants

Binding of RHON1 to ribosomal 16S and 23S RNAs suggested a crucial involvement in processing and/or stability of ribosomal RNAs. We stained a blot of denatured RNAs of isolated polysome fractions of WT and *rhon1* with methylene blue to visualize the integrity of plastid ribosomal RNAs (Figure 22).
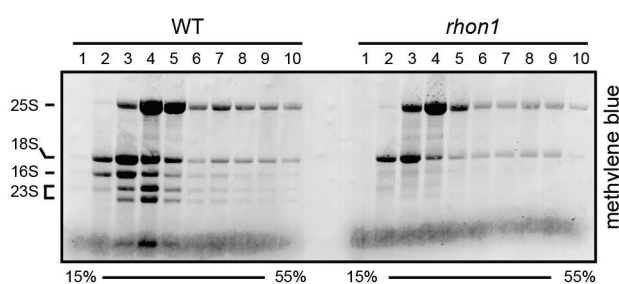
Figure 22. Visualization of Polysome Integrity of WT and *rhon1*.
Polysomes of wild type and *rhon1* were separated by 15-55% sucrose gradient centrifugation and collected in 10 fractions. Ribosomal RNAs as indicated on the left were visualized by methylene blue staining.

Blots were then subjected to hybridization with a full-length probe of 23S rRNA and a probe of *rbcL*. Both RNAs did not accumulate to the same extent in polysomal fractions of *rhon1* as compared to wild type, indicating that polysomal loading and translation is affected in *rhon1* (Figure 23). This implies that translation takes place on monosomes and/or that small amounts

of transcripts present in polysomal fractions are sufficient to translate proteins albeit at reduced levels.

Figure 23. RNA Gel Blot of Separated Polysomes of WT and *rhon1*.

Polysomes of wild type and *rhon1* were hybridized with full-length probes of 23S and *rbcL*. Sizes indicated on the left are given in kb.
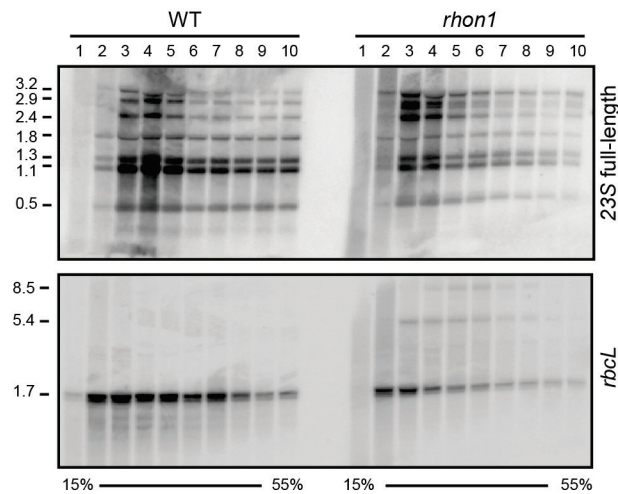
4.1.13   Processing of Ribosomal RNAs is Affected in *rne* and *rhon1*

We also investigated the processing pattern of the rRNA transcription unit by performing RNA gel blot analysis in *rne* and *rhon1* mutants. RNA staining of filters revealed a severe reduction of both 16S and 23S rRNAs in *rhon1* but not in *rne-1* (Figure 24). The 16S rRNA is correctly processed in both mutants and levels were almost unchanged in *rne* but markedly decreased in *rhon1* as compared to the wild type (Figure 24). Accumulation of the 3.2 kb 23S-4.5S dicistronic precursor transcript was observed in *rne* and even more in *rhon1* mutants indicating loss of efficient endonucleolytic processing. This is accompanied by reduced levels of processed transcripts in *rhon1* and to some extent in *rne*, like the 0.5 kb, 1.1 kb, and 1.8 kb RNAs originating from the 23S rRNA. Hybridization with the 4.5S probe revealed an additional band of 2.7 kb in both mutants, which is not present in the wild type or other rRNA processing mutants (Bellaoui *et al.*, 2003; Bisanz *et al.*, 2003; Bollenbach *et al.*, 2005; Nishimura *et al.*, 2010). Since this band could not be detected with the probe of the 23S 5' region it still comprises sequences of the 4.5S rRNA but lacks 0.5 kb of the 5' region (Figure 24). The 5S probe could not detect any high-molecular-weight band although levels of the monocistronic 5S rRNA were reduced in *rhon1*, supporting that the 2.7 kb band does not comprise the 5S rRNA. Therefore, RNE and RHON1 are not only required for efficient cleavage of mRNA but also of the 23S-4.5S rRNA intergenic region.
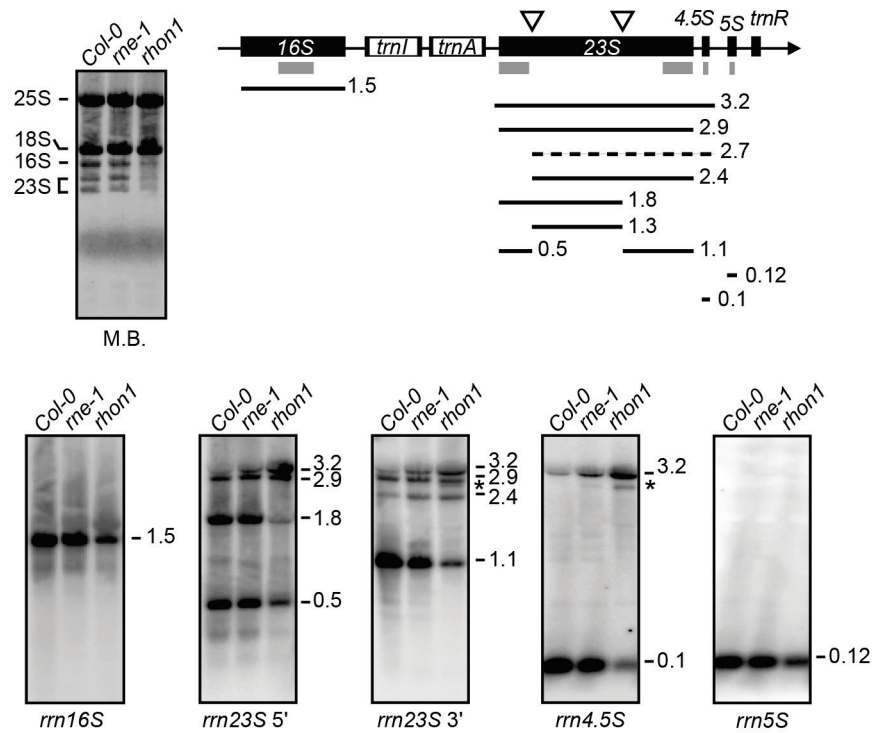
Figure 24. Transcript Analysis of the rDNA Gene Cluster in WT, *rne* and *rhon1*.

The rDNA gene cluster and all processing products (black lines) of rRNAs is shown down to scale. RNA gel blot analyses were performed using probes *rrn16S*, *rrn23S*, *rrn4.5S*, and *rrn5S* as indicated in grey boxes. A 2.7 kb transcript (dotted line and asterisks) is detected only in *rhon1* and *rne-1* mutant lines. Equal loading was confirmed using methylene blue (M.B.) staining. The transcript lengths are indicated in kb.

4.2 A Site Specific Factor for Regulation of RNA Stability

4.2.1 Identification and Origin of the Nuclear-Encoded Factor PrfB3 in Arabidopsis

Up to now little attention has been paid to the functions of translation termination in chloroplasts (Meurer *et al.*, 1996b and 2002). In contrast to the omnipotent eukaryotic and archaebacterial ribosomal release factors (RF), two peptide chain release factors are present in eubacteria, chloroplasts and plant mitochondria, *prfA* (RF1) for UAA and UAG and *prfB* (RF2) for UAA and UGA (Meurer *et al.*, 2002; Motohashi *et al.*, 2007). Functional and structural comparisons on the basis of a common GGQ motif present in all release factors described so far revealed its essential function in the hydrolytic activity (Kisselev and Buckingham, 2000) and may reflect a common evolutionary origin of the eukaryotic/archaebacterial and eubacterial proteins both of which are supposed to mimic tRNAs when bound to ribosomes (Nakamura and Ito, 2003; Loh and Song, 2010). The other highly conserved motif SPF for recognition of UGA stop codons is present in all eubacterial and related plastid and mitochondrial PrfB proteins (Meurer *et al.*, 2002). Previously, the essential roles of the GGQ- and SPF-containing *Arabidopsis thaliana* plastid RF2 homolog, At-PrfB1 (formerly designated At-PrfB), in translational termination and stabilization of chloroplast UGA stop codon-containing transcripts were identified in our group (Meurer *et al.*, 1996a and b; Meurer *et al.*, 2002).

A fifth release factor-like protein, PrfB3, is a PrfB1-homolog of eubacterial origin. Its full-length cDNA encodes a protein consisting of 406 aa with a deduced size of ~45 kDa. PrfB3 can be found only in vascular plants and displays 36.5, 37.5, and 31% sequence similarity over the whole length with the corresponding RF2 and only 23.3, 22.6, and 21.7% with the corresponding RF1 homologous proteins of mitochondria, chloroplasts, and *Synechocystis*, respectively. PrfB3 has so far not been found in proteomic approaches, indicating that this protein represents a minority factor, as is found for many regulatory proteins. Remarkably, *PrfB3* neither contains the otherwise conserved tripeptide anticodon SPF, which determines release factor specificity *in vivo* in PrfB proteins (Ito *et al.*, 2000; Nakamura *et al.*, 2000), nor the universally conserved GGQ motif, which is essential for the hydrolytic activity and represents a structural counterpart on the CCA-3' acceptor stem of the tRNA-aminoacyl group (Frolova *et al.*, 2000). Moreover, the corresponding nucleotides of both motifs were not simply replaced but rather cut out from the genes by deletion events (Figure 25). Therefore, PrfB3 must have lost its function to terminate translation and potentially could have been recruited by the chloroplast for a new function that is not directly related to ribosomal release.

```
At-PrfB1  267  ..AYGYISGEKGTHRIVRQ SPF NSKGLRQTSFSGVEVMPLLPEEAVGIEIPEEDLDISFTRAGGK GGQ NVNKVETAVRITHIPTGVAVRCTEERS..
Os-PrfB1  307  ..AYGYLSGEKGTHRIVRQ SPF NAKGLRQTSFAGVEVMPLLPEESMDVEIPEEDLEISFTRAGGK GGQ NVNKVETAVRMVHIPTGIAVRCTEERS..
At-PrfB2  296  ..AYGYAKAEVGVHRLVRI SPF DSGKRRHTSFAAVAVIPILGDGSTRVEINDSDLRIERFRSGGA GGQ HANTTDSAVRIVHIPTGITATCQNERS..
Os-PrfB2  285  ..AFGYAKAEVGVHRLVRI SPF DSGKRRHTSFAAVAVVPILGDGSTRYQIKDSDLRIERFRSGGP GGQ HANCTESAVRIVHIPTGITATCQNERS..
Synech.   151  ..AYGYLKSEKGTHRLVRI SPF NANGKRQTSFAGVEVMPLLGEEAISLDIPDKDLDISTSRAGGK GGQ NVNKVETAVRIVHLPTGLAVRCTQERS..
E. coli   188  ..AYGWLRTETGVHRLVRK SPF DSGGRRHTSFSSAFVYPEV-DDDIDIEINPADLRIDVYRASGA GGQ HVNRTESAVRITHIPTGIVTQCQNDRS..
At-PrfB3  233  ..AYGYLLGERGVHRLII- --- -SSTSNEECSATVDIIPLFLRASPDFEVKEGDL-IVSYPAKED --- HK-IAENMVCIHHIPSGVTLQSSGERN..
Os-PrfB3  239  ..MFGTLTGEKGTHRMIYP SV- DNAGTYEATSARVDIIPLFLDRPVNLHLDENDLEISPSPSDHK --- RRDHRNSAIRVQHIRTGVTAESSGERS..
```

Figure 25. Partial Sequence Alignment of Eubacterial PrfB and Homologous Plant Proteins.

The conserved part of all functional RF2 in eubacteria (*Synechocystis* and *E. coli*), plastids (At-PrfB1 and Os-PrfB1) and mitochondria (At-PrfB2 and Os-PrfB2) was compared with the corresponding region in At-PrfB3 and Os-PrfB3 in *Arabidopsis* and rice, respectively. The essential tripeptide motifs SPF and GGQ are highlighted in red. Conserved aa, which are also present in At-PrfB3 and Os-PrfB3, are shaded in gray. Amino acid residues specific for the functional release factors are shaded in yellow. Conserved aa, which only occur in the plastid At-PrfB3 and Os-PrfB3 proteins are shaded in green. The deduced positions of introns are underlined and labeled in blue.

4.2.2 At-PrfB3 Is Targeted to the Chloroplast

Several publicly available programs did not predict an amino terminal transit peptide for import of At-PrfB3 into the chloroplast but instead identified a putative mitochondrial transit peptide. Moreover, it has been suggested previously that At-PrfB3 might be involved in termination of translation of transcripts lacking stop codons and might be a mitochondrial protein (Raczynska *et al.*, 2006).

Figure 26. Localization of At-PrfB3 in the Chloroplast Stroma.

(A) The 206 N-terminal aa were fused in frame to the GFP reporter under the control of the 35S promoter and the construct was transiently expressed in tobacco protoplasts. The GFP fluorescence perfectly matched with chlorophyll fluorescence confirming chloroplast targeting of At-PrfB3. Fluorescence pictures were taken by J. Meurer.

(B) Membrane and soluble proteins of WT, *prfB3* mutants (*prfB3-1* and *prfB3-2*) and complemented lines (*prfB3-1-c*) were subjected

to immunoblot analysis using antibodies raised against At-PrfB3, the membrane protein CP43 and the soluble protein PAC. At-PrfB3 has a size of 45 kDa and was only present in the soluble fraction of wild type and complemented lines. Protein amounts were adjusted according to stained Coomassie gels.
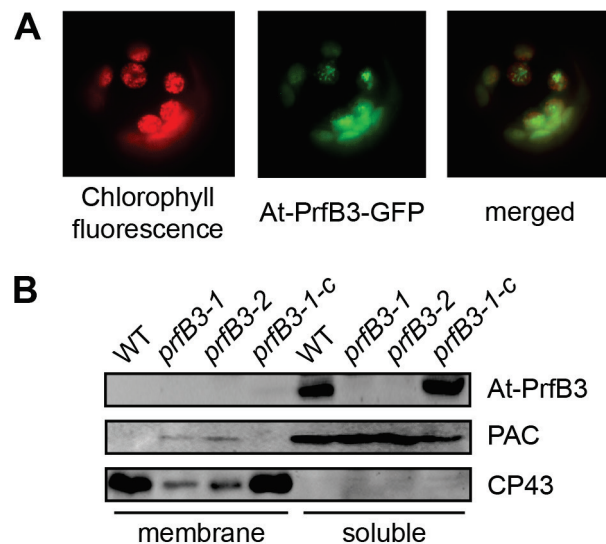
4.2.3   PrfB3 is an Essential Chloroplast Protein

To assess the function of PrfB3, we applied a reverse genetics approach and studied a Salk_133921 T-DNA insertion line (*prfB3-1*) of the At3g57190 gene of Arabidopsis encoding PrfB3 (Figure 27A). Sequencing of the PCR product obtained with genespecific and left border T-DNA primers confirmed that the insertion occurred in the fourth exon at position +961 relative to the start codon. Homozygosity of the T-DNA insertion line was confirmed by PCR using adequate control primers (Figure 27B).
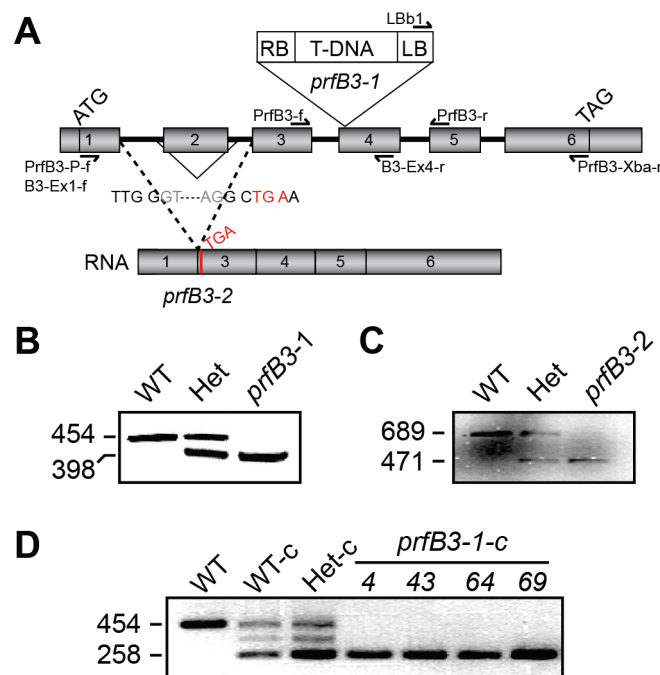
Figure 27. Gene Structure and Mutations of *PrfB3*.

(A) The structure of the *PrfB3* gene, composed of 6 exons (gray boxes), the T-DNA insertion in line *prfB3-1*, the deletion in *prfB3-2* with the resulting splice product, the corresponding sequences (lower part), and the primers used for PCR analysis (arrows) are indicated. The positions of start (ATG) and stop (TAG) codons of translation are assigned. The resulting premature stop codon in *prfB3-2* is labeled in red. **(B)** To test homozygosity of the T-DNA insertion, PCR analysis was performed using primers specific for the T-DNA left border (LBb1) and the *PrfB3* gene (PrfB3-f and PrfB3-r). The gene specific primers only amplified a 454 bp product in wild type and heterozygous plants. The border primer and PrfB3-r amplified a 398 bp fragment in heterozygous and mutant plants. The T-DNA insertion in homozygous lines prevented PCR amplification of the corresponding locus. Sequencing of the PCR product obtained with LBb1 and PrfB3-r primers confirmed that the T-DNA was inserted in the fourth exon at position +961 relative to the start codon. Size of PCR products is given in bp. **(C)** RT-PCR products using gene specific primers B3-Ex1-f and B3-Ex4-r amplified a 689 bp fragment in the wild type and a 471 bp fragment in the *prfB3-2* mutants corresponding to the loss of exon 2 and border regions as revealed by sequencing. Both fragments were amplified in heterozygous plants. **(D)** Successful complementation of four lines number *4*, *43*, *64*, and *69* was tested with the same primers as used in (B). The genomic fragment could only be amplified in wild-type and heterozygous plants. In the complemented mutants only the inserted cDNA gave rise to a PCR product of 258 bp.

A forward genetics screen identified a mutation, *prfB3-2*, showing the same phenotype. Sequencing of the PrfB3 locus in *prfB3-2* identified a deletion of 273 bp at position +282 relative to the start codon. The deletion includes the entire exon 2 and adjacent intron regions (Figure 27A). Sequencing of RT-PCR products revealed that the deletion produces a premature stop codon and, correspondingly, leads to expression of a truncated protein encoded mainly by exon 1 (Figure 27C). Both mutations segregated in a Mendelian manner. The stromal PrfB3 protein was lacking in both mutants but was expressed at wild-type-comparable levels in the complemented lines (Figure 26B). Homozygous mutants exhibited an *hcf* phenotype characteristic for plants with deficiencies in the photosynthetic apparatus (Meurer *et al.*, 1996a) and, accordingly, died in the seedling stage and could grow further only under sterile heterotrophic conditions. Plants grown under very low light of 10 μmol photons m^{-2}s^{-1} were somehow pale but their size and leaf morphology was comparable to the wild type (Figure 28A). Expression of the full-length cDNA under the control of the constitutive 35S promoter in homozygous *prfB3-1* lines fully restored the wild-type phenotype and photoautotrophic growth (Figures 27D and 28A). Functional complementation indicates that the phenotype was exclusively due to the mutations in the *PrfB3* gene. Endogenous PrfB1, expressed in the *prfB3* mutant background, apparently fails to rescue the mutant defect, supporting the idea that PrfB3 recruited a novel function.

4.2.4 The Intersystem Electron Transport is Abolished in *prfB3-1* and *prfB3-2*

To gain insights into the primary photosynthetic defect in the mutants, chlorophyll *a* fluorescence primarily emitted by PSII at room temperature was measured. The maximum quantum yield of PSII, F_v/F_m, was reduced to 0.54 ± 0.04 in the mutants compared with 0.82 ± 0.01 in the wild type. Under the chosen light conditions, ~85% of the variable fluorescence is lost by photochemical and non-photochemical quenching in the wild type (Figure 28B). In *prfB3-1* and *-2*, the actinic light-induced fluorescence remained at its maximum level (qP and NPQ = 0), indicating disruption of the photosynthetic electron transport behind PSII (Meurer *et al.*, 1996a). To further estimate the primary defect in both mutants, the redox state of PSI was assessed. Light intensities of 50 μmol photons m^{-2} s^{-1} induced ~10% oxidation of PSI in the wild type. Although the P700 signal was a bit weaker in the mutants, the actinic light oxidized P700 to 100% (Figure 28C). This indicates that PSI operates but its activity is limited by deficiencies in the intersystemic electron transport chain due to disruption of PrfB3. The photosynthetic

characteristics of the complemented lines were comparable to those of the wild type (Figure 28B+C).
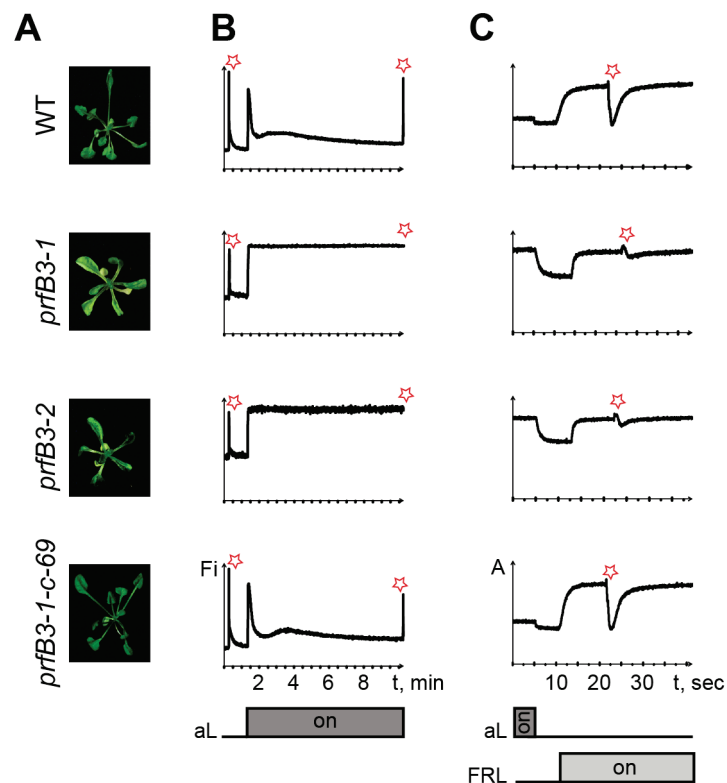
Figure 28. Phenotype and Functional Analysis of *prfB3* Mutants and Complemented Lines.

(A) Phenotype of 25-d-old wild type (WT) and mutant plants grown on Suc-supplemented medium under low light of 10 μmol photons m^{-2} s^{-1}. Under these conditions mutant plants are paler than wild-type plants but similar in size. Knockout line *prfB3-1-c-69* complemented with the *PrfB3* cDNA were undistinguishable from wild type and able to grow photoautotrophically. **(B)** Chlorophyll *a* fluorescence induction was measured after application of a saturating light pulses (red stars) to dark-adapted plants. The ratio F_v/F_m of 0.82 ± 0.01 in the wild type was reduced to 0.54 ± 0.04 in *prfB3* mutants. Actinic light (aL) of 50 μmol photons m^{-2} s^{-1} was applied, and the photosynthetic parameters qP and NPQ were measured in the steady state after 9 min illumination. Fi, fluorescence intensity (arbitrary units). **(C)** Absorbance of P700 at 830 nm is a measure of the P700 redox state. Light-to-dark switches and application of far-red light (FRL) induced redox changes of P700, indicating that PSI is active in *prfB3* mutants, although the overall signal is somehow decreased. Saturating light pulses (red stars) in the background of far-red light were sufficient for the complete PSII-dependent reduction of PSI in the wild type. However, these conditions did not significantly reduced P700 in the mutants, indicating that the electron transport is interrupted before PSI. A, relative absorbance.

4.2.5 PrfB3 is Required for Accumulation of the Cytochrome b_6f Complex

Immunological analyses showed that the amounts of the major subunits of the cytochrome b_6f complex, such as cytochrome f, cytochrome b_6, and the Rieske Fe-S protein, constituted around 4% of wild-type levels in *prfB3-1* (Figure 29). By contrast, PsaF, a representative subunit of PSI as well as PsbI and PsbH from PSII accumulated at wild-type-comparable levels. Levels of the α- and β-subunits of the ATP synthase were increased in *prfB3* mutants (Figure 29), which is likely to represent a secondary effect of the mutation since cytochrome b_6f complex knockout lines in Arabidopsis, *Oenothera*, and tobacco (*Nicotiana tabacum*) showed the same phenomenon (Schwenkert *et al.*, 2007) presumably to compensate for the loss of the cytochrome b_6f complex.

Figure 29. Accumulation of Thylakoid Membrane Proteins in *prfB3* Mutants.

Immunoblot analyses of *prfB3-1* and the wild type (WT) are shown. Levels of cytochrome b_6f complex subunits PetA (Cyt$f$), PetB (Cytb_6), and the Rieske protein, the PSII subunits PsbI and PsbH, the PSI subunit PsaF, and α- and β-subunits of the ATP synthase were analyzed. Loading of 100% corresponds to 10 μg of chlorophyll. Parts of these analyses were performed by Serena Schwenkert. Cyt, cytochrome.
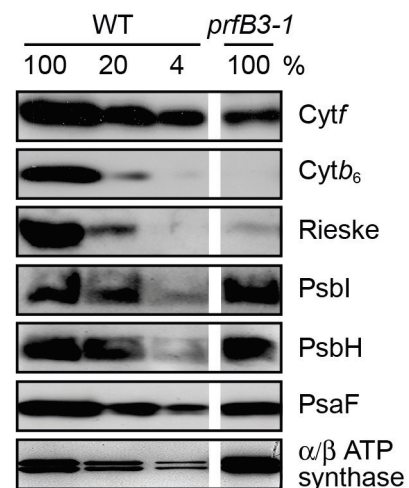
To investigate whether the assembly of higher-order photosynthetic membrane complexes was affected in the mutants, two-dimensional resolution of thylakoid protein complexes was performed by Blue Native/SDS-PAGE. The spot pattern clearly demonstrates that thylakoid membrane complexes of the ATP synthase, PSI, and PSII were able to assemble efficiently in *prfB3-1* (Figure 30). By contrast, both the dimeric and monomeric cytochrome b_6f complexes were below the limits of detection by staining in the mutants (Figure 30). Therefore, we conclude that the deficiency in *prfB3* caused a severe and specific defect in the accumulation of the cytochrome b_6f complex. Immunoblot analysis of the second dimension demonstrated that the high ratio of dimeric/monomeric complexes was comparable in mutants and the wild type (Stoppel *et al.*, 2011). This indicates that assembly and stability of the cytochrome b_6f complex are not affected in the mutants. Taken together, the results of the fluorometric, spectroscopic, and protein analyses allowed the conclusion that accumulation of the cytochrome b_6f complex, but not its assembly or stability, is the primary defect in the *prfB3* mutations.
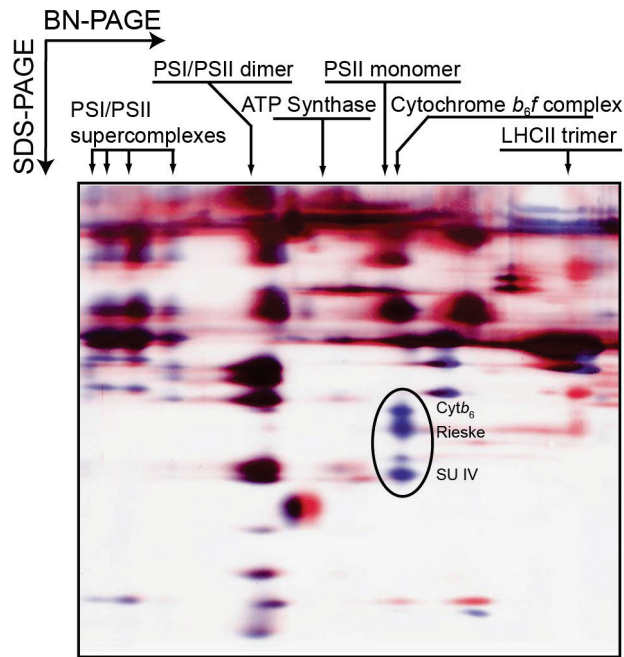
Figure 30. Assembly of Thylakoid Membrane Complexes in *prfB3* Mutants.
Chloroplast protein complexes were solubilized by treatment with 1% (w/v) *n*-dodecyl-β-D-maltoside and separated by Blue Native/PAGE (BN-PAGE) in the first and SDS-PAGE in the second dimension followed by silver staining. Macromolecular protein complexes of thylakoid membranes are indicated. The protein spots of the wild type (blue) and *prfB3-1* mutant (red) were selectively stained *in silico* (Photoshop), and subsequently merged. The proteins cytochrome b_6, Rieske and subunit IV of the dimeric cytochrome $b_6 f$ complex, which appeared only in the wild type, are circled. This experiment was performed by Serena Schwenkert.

4.2.6   3' Processed *petB* Transcripts Fail to Accumulate in *prfB3* Mutants

To assess whether lack of the cytochrome $b_6 f$ complex was caused by deficiencies in transcript patterns, numerous plastid transcripts were probed by RNA gel blot hybridizations (Figure 31). With the exception of mRNAs for the *psbB* gene cluster, all of the transcripts analyzed accumulated in size and abundance comparable to the wild type in both allelic *prfB3* mutants, indicating that global plastid gene expression is not affected by the mutations (Stoppel *et al.*, 2011). The plastid pentacistronic *psbB-psbT-psbH-petB-petD* gene cluster has a promoter for the plastid-encoded polymerase and is conserved among vascular plants. It encodes the subunits CP47 (*psbB*), T (*psbT*), and H (*psbH*) of PSII as well as cytochrome b_6 (*petB*) and subunit IV (*petD*) of the cytochrome $b_6 f$ complex (Figure 31A). Each of the *petB* and *petD* genes contains an intron. The processing pattern of this gene cluster is rather complex and differs between plant species. Accumulation of most transcripts derived from the *psbB* gene cluster was unchanged in both allelic mutants (Figure 31C). However, both mutants showed the same striking deviation from the wild-type transcript pattern. The 3' processed and spliced *petB*-containing transcripts, the monocistronic *petB*, and the dicistronic *psbH-petB* transcripts were barely detectable in the mutants. Also, transcript precursors lacking the *petB* intron (i.e., *psbB-psbT-psbH-petB-petD*, *psbH-petB-petD*, and *petB-petD*) were slightly reduced in both mutants as shown by RNA gel blot analysis (Figure 31C, transcripts 3, 6, and 7). Quantitative RT-PCR analysis revealed that *prfB3-1*

accumulates 67% ± 2% spliced *petB* RNA and 105% ± 6% *petD* RNA compared with the wild type. This reduction is due to the apparent lack of 3' processed *petB* transcripts and reduced levels of spliced precursors. Amounts of all precursor transcripts that include the *petB* intron were unchanged in the mutants, indicating that splicing takes place efficiently (Figure 31C, transcripts 1, 2, 4, and 5).
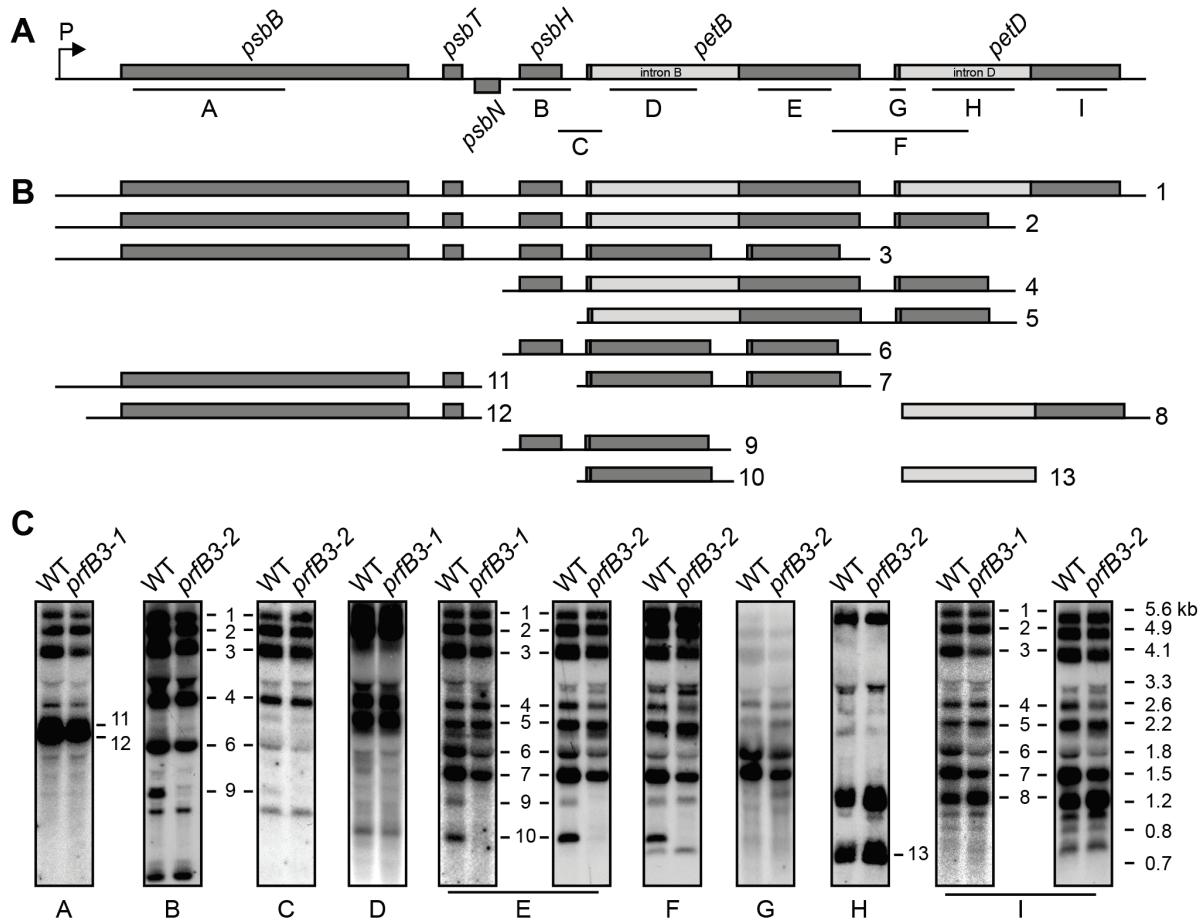
Figure 31. RNA Gel Blot Analysis of the *psbB* Gene Cluster.

(A) The structure of the *psbB* gene cluster and probes A-H used in RNA gel blot analysis in (C) are shown. P, promoter of the plastid-encoded polymerase. The gene cluster has been drawn to scale. **(B)** The precursor transcript and its most prominent processed and spliced products are numbered from 1-13. Transcripts have been drawn to scale. **(C)** RNA gel blot analysis of the *psbB* gene cluster in the wild type (WT) and *prfB3* mutants. Probes used A-I and labeled transcripts 1-13 are shown in (A) and (B), respectively. The size of the transcripts is indicated. Mutant plants were compared with wild-type plants of the same accession. RNA gel blot analyses were performed in cooperation with Lina Lezhneva and Susanne Felder.

All this attests that the *prfB3* mutation affects only 3' processed *petB* transcripts of the *psbB* gene cluster. Therefore, PrfB3 is involved either in processing of the *petB-petD* intergenic region or in the stabilization of 3' processed *petB* transcripts. In contrast with maize (*Zea mays*) and presumably

all other monocots (Barkan, 2011), monocistronic and spliced *petD* transcripts of ~600 nucleotides do not accumulate to significant levels in Arabidopsis and other dicots. In Arabidopsis wild-type plants, *petD* transcripts, which result from endonucleolytic cleavage in the *petB-petD* intergenic region, are rapidly degraded irrespective whether they are spliced or not (Figures 31B+C) (Felder *et al.*, 2001; Meierhoff *et al.*, 2003). In the *prfB3* mutants, intron- and 3' exon-containing *petD* transcripts of 1.2 kb (Figure 31C, transcript 8), which lack the first exon, accumulate to even slightly higher amounts presumably due to increased cleavage of the 5' splice site, indicating that splicing of *petD* occurs efficiently in the mutants (Figure 31C, transcript 8). Spliced *petB* transcripts in the wild type are either processed in the *petB-petD* intergenic region or the *petD* intron is also missing (Figures 31B+C). This indicates that *petB* splicing depends either on processing of the intergenic region or on *petD* splicing. The fact that the abundance of these spliced but unprocessed precursors is slightly reduced in both mutants suggests that processing of the *petB-petD* intergenic region occurs efficiently. The finding that the spliced *petB* intron of 0.8 kb accumulated to wild-type comparable levels again suggests that *petB* splicing is not affected in the mutants (Figure 31C). This all speaks in favor of the idea that PrfB3 evolved to stabilize 3' processed *petB* transcripts.

4.2.7 Proposed Function of PrfB3 in Stabilization of 3' Processed *petB* Transcripts

Several nuclear and chloroplast mutants have been identified that are affected primarily in splicing or processing of plastid precursor transcripts. In all cases, unspliced or unprocessed precursors accumulated at higher levels (e.g., Jenkins *et al.*, 1997; Meierhoff *et al.*, 2003; Asakura and Barkan, 2007; Petersen *et al.*, 2011). This is not the case for *petB* precursors in *prfB3* mutants. They are instead slightly decreased, again supporting the assumption that spliced and 3' processed *petB* transcripts are efficiently generated but are rapidly subjected to degradation in the mutants.

Chloroplast mRNA stability is known to be dependent on the state of transcript termini. Therefore, in cooperation with the group of Prof. Peter Westhoff (Düsseldorf, Germany), the mature 5'- and 3'-ends of transcripts from the *psbB* gene cluster were precisely determined by S1 nuclease mapping in both the wild type and *prfB3-2* (Stoppel *et al.*, 2011). 3' processing of *petB* transcripts could only barely be detected in the mutant, again indicating that PrfB3 is required for accumulation and/or stabilization of 3' processed *petB* transcripts.

Taken together we conclude that PrfB3 is required for stabilizing 3' processed *petB* transcripts. Obviously, accumulation of almost unchanged amounts of spliced *petB*-containing precursors in the mutants is not sufficient to ensure translation of *petB*. This indicates that either only 3' processed *petB* transcripts are translational competent or that PrfB3 plays an additional role in translation of *petB* or other transcripts encoding subunits of the cytochrome b_6f complex.

4.2.8 The Function of PrfB3 in *petB* RNA Stabilization is Independent of Translation

Since PrfB3 originated from a duplication of the functional release factor PrfB1, we addressed the question whether the role of PrfB3 is still related to translational events. In contrast with transcripts that are targeted by PrfB1 (Meurer *et al.*, 2002), polysomal loading of *petB* and *petD* transcripts is unaltered in *prfB3-1* mutants (Figure 32).

Figure 32. Polysome Analysis of WT and *prfB3-1*.

Polysomes were isolated, separated on sucrose gradients and subsequently subjected to RNA gel blot analysis using *petB* and *petD* specific probes.
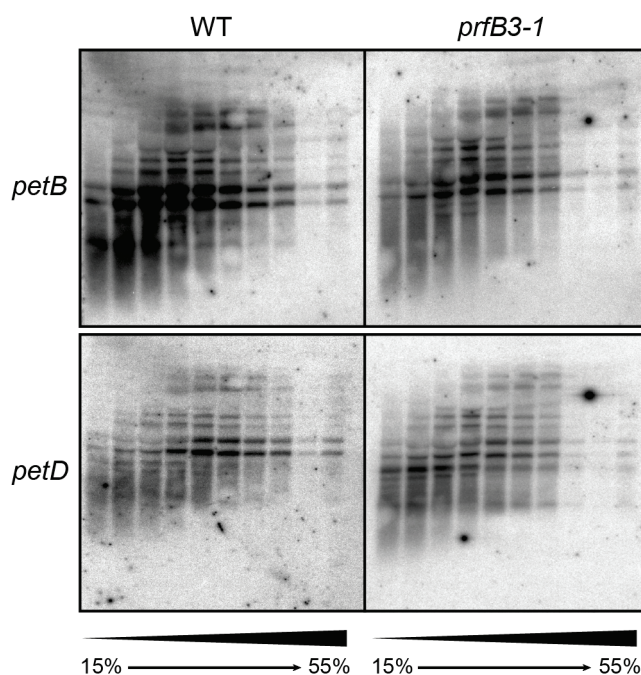
Inhibition of plastid translation in *prfB1* induced normal accumulation of transcripts, which are otherwise lacking (Meurer *et al.*, 2002). By contrast, neither inhibition with lincomycin nor with chloramphenicol induced an increase in *petB* transcript abundance in *prfB3-1* (Figure 33). This indicated that the function of PrfB3 in *petB* RNA stability has been completely uncoupled from translational events.

Figure 33. RNA Gel Blot Analysis of WT and *prfB3-1* Treated with Plastid Translation Inhibitors.

20-d-old plants were incubated for 24 h with the plastid translation inhibitors lincomycin (L) (400 mg/L) and chloramphenicol (C) (500 mg/L) in ½ MS medium. Control plants (-) were incubated for the same time in a solution containing ½ MS nutrients.
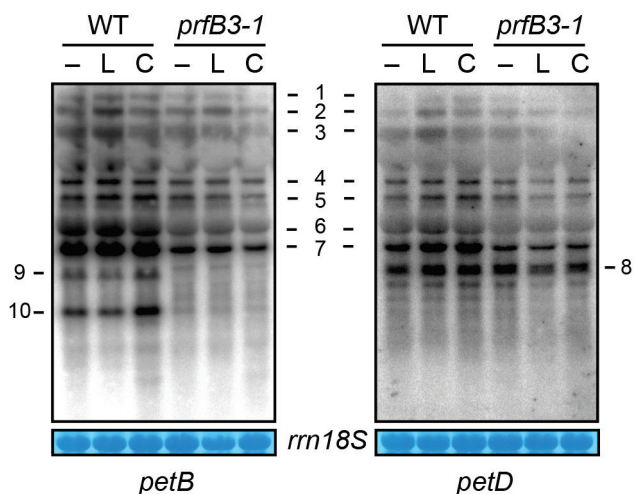
4.2.9 PrfB3 is Part of a *petB* RNA-Containing Complex

To investigate whether PrfB3 acts as part of a protein complex, we analyzed native soluble proteins by size-exclusion chromatography. Collected fractions were subjected to immunological analysis. PrfB3 was found to be part of a 400-kDa complex when RNA digestion was inhibited from the beginning of sample extraction (Figure 34).
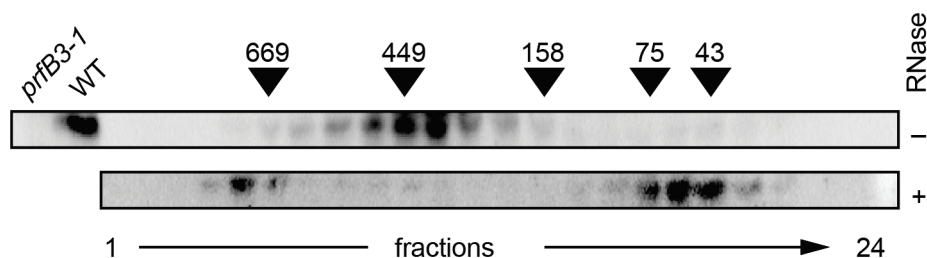
Figure 34. PrfB3 is Part of an RNA-Containing Complex.

Native soluble proteins were separated by size-exclusion chromatography in the presence of RNase inhibitors, and fractions (1-24) were subjected to immunoblot analysis together with wild-type (WT) and *prfB3-1* proteins using PrfB3 antibodies (top part). Extracts were RNase treated before subjecting to chromatography (bottom part). The molecular mass of marker proteins is indicated in kDa.

However, when samples were treated with RNase before they were subjected to chromatography, the 400 kDa complex disappeared and most PrfB3 could be found as free protein. In addition, upon RNase treatment, small amounts of a PrfB3-containing complex of ~700 kDa were assembled, possibly due to the formation of unspecific aggregation products or a multimeric complex when RNA is lacking (Figure 34). Electrophoretic mobility shift assays were performed

with the purified PrfB3 protein and indeed it appeared that PrfB3 efficiently binds to the *petB* 3'
UTR (Stoppel *et al.*, 2011).

4.2.10   Reduced PrfB3 Amounts Effect Stabilization of *petB* mRNA

The potentially regulatory function of PrfB3 in stabilizing *petB* transcripts was first investigated by
selecting partially complemented mutant lines (Figure 35). When grown under normal light
regime (>20 µmol photons m^{-2} s^{-1}) mutant plants were smaller in size and much paler as
compared to wild type indicating that the mutants are extremely light sensitive because under
very low light of 10 µmol photons m^{-2} s^{-1} their size was comparable to wild type (Figure 28).
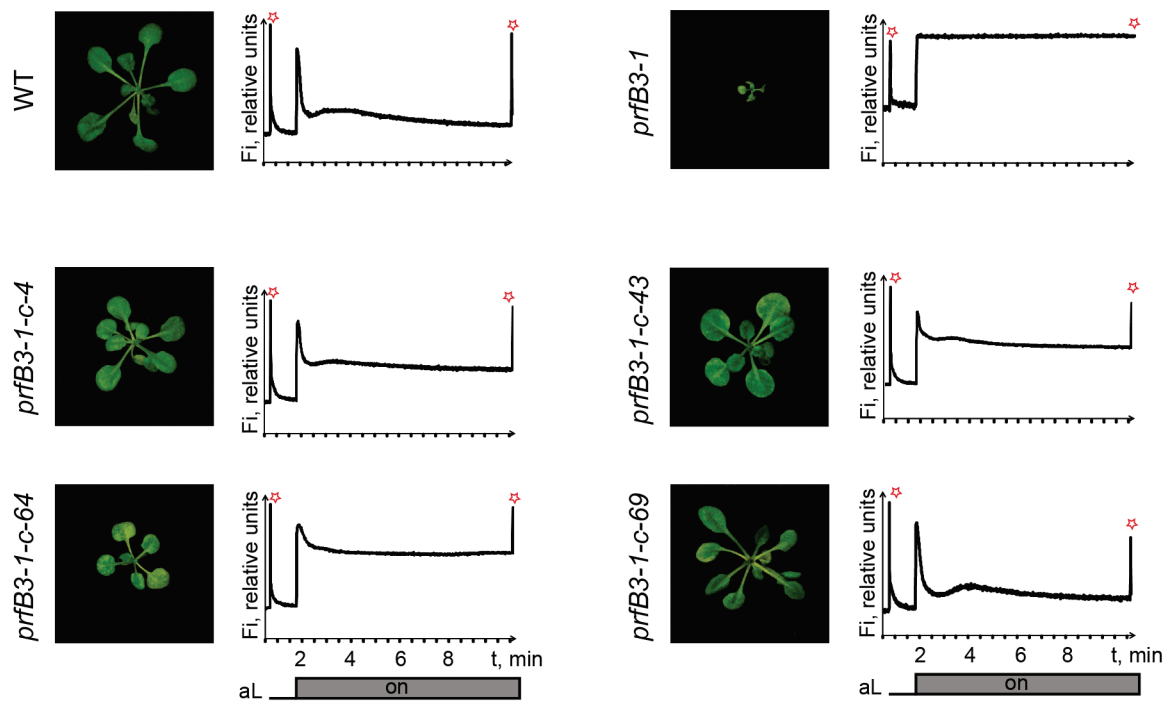
Figure 35. Phenotype and Functional Analysis of *prfB3* Mutants and Complemented Lines.
21-d-old WT and mutant plants were grown on Suc-supplemented medium under light intensities of 40 µmol
photons m^{-2} s^{-1}. At this light intensity mutant plants were much paler and smaller as compared to those grown
under 10 µmol photons m^{-2} s^{-1} indicating increased light sensitivity of the mutants (for comparison see Figure
28). In contrast to mutant plants, partially complemented lines *4*, *43*, and *64* were smaller and/or paler than the
WT but compared to the mutants they looked much healthier and were able to grow photoautotrophically. Line
number *69* precisely showed WT behaviour indicating complete complementation. Chlorophyll *a* fluorescence
induction was measured after application of a saturating light pulse (red star) to dark-adapted plants. Note that
the partially complemented lines *4*, *43*, and *64* showed an intermediate level of variable fluorescence, lower than
in the mutants and higher than in WT and line *69*. aL, Actinic light of 50 µmol photons m^{-2} s^{-1}. Fi, fluorescence
intensity.

Three lines, numbers *4*, *43*, and *64*, showed increased steady state chlorophyll fluorescence levels and a lowered qP (Figure 35) but were able to grow photoautotrophically. Line number *69* showed fluorescence characteristics that are typical for the wild type. It appeared that expression of PrfB3 is reduced in lines number *4*, *43*, and *64*. Only those lines (numbers *43* and *64*) in which PrfB3 accumulated below a threshold of ~25% of wild-type levels also accumulated <25% of cytochrome *b*6 (Figure 36A). Down-regulation of PrfB3 levels to >50% of wild-type levels in line *4* was insufficient to reduce amounts of cytochrome b_6 comparably. Levels of the PSI protein PsaF were unaffected by the lower accumulation of PrfB3, indicating that PrfB3 levels are crucial for determining levels of cytochrome b_6 and accordingly of the entire cytochrome b_6f complex. The effect of reduced PrfB3 levels in the partially complemented lines on *petB* mRNA stability was tested by RNA gel blot analysis. Only lines number *43* and *64* had significantly lower levels of the monocistronic *petB* mRNA, indicating that accumulation of PrfB3 above 50% had no effect on *petB* mRNA levels (Figure 36B).
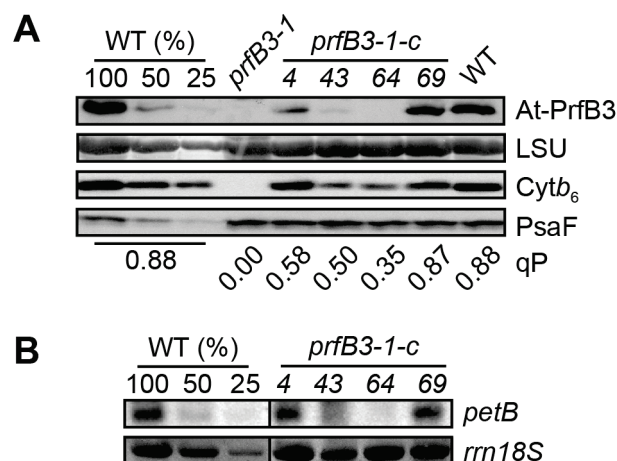
Figure 36. Regulatory Role of PrfB3 in *petB* RNA Stability and Cytochrome b_6 Accumulation.

(A) Levels of the soluble protein PrfB3 and the membrane proteins cytochrome b_6 and PsaF were investigated in the WT, mutant, and partially (numbers *4*, *43*, and *64*) as well as completely complemented (number *69*) lines by immunoblot analysis. For the WT, dilution series of membrane proteins corresponding to 10 (100%), 5, and 2.5 μg chlorophyll and to 100 (100%), 50, and 25 μg of soluble proteins were loaded. As loading control for the soluble proteins, an imidazole stain of the RuBisCO large subunit (LSU) is shown. The qP value for each line is indicated below. **(B)** Accumulation of monocistronic *petB* transcripts in WT and complemented lines. A dilution series of 8 (100%), 4, and 2 μg of total WT RNA was loaded. As loading control the 18S rRNA is shown.

4.2.11 Light- and Stress-Dependent Regulation of PrfB3 Levels

The general increase in chloroplast transcript abundance upon illumination of dark-adapted plants is known to depend highly on increased RNA stability (Monde *et al.*, 2000). Therefore, a possible role of light in PrfB3 abundance was investigated. Interestingly, levels of PrfB3 were severely reduced in light-grown plants adapted to darkness, low heterochromatic (2 μmol photons m^{-2} s^{-1}), blue (5 μmol photons m^{-2} s^{-1}), or far-red light (0.1 μmol photons m^{-2} s^{-1}) for 3 d (Figure 37A). Reduced expression of PrfB3 correlated with reduced amounts of cytochrome b_6 but levels of the large subunit of the RuBisCO as well as of the α- and β-subunits of the plastid ATP synthase remained unchanged, reflecting the specificity with which PrfB3 regulates cytochrome b_6 levels. Expression of PrfB3 and, thus, cytochrome b_6 was comparable to the wild type under red light illumination (70 μmol photons m^{-2} s^{-1}) and under heterochromatic light of 100 and 20 μmol photons m^{-2} s^{-1} (Figure 37A).
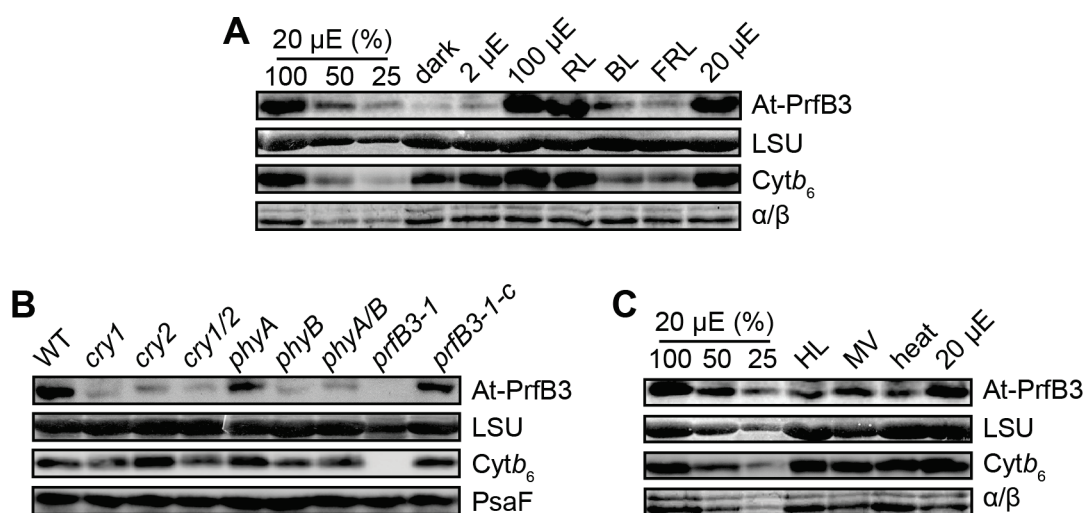
Figure 37. Effect of Light Quantities, Qualities and Stressors on PrfB3 and Cytochrome b_6 Expression.
(A) PrfB3 levels under different light conditions were investigated by immunoblot analysis. As loading control, an imidazole stain of the RuBisCO (LSU) (soluble protein) and the α/β subunits of the ATP synthase (membrane proteins) are shown. Plants were grown for 14 d under heterochromatic light (100 μmol photons m^{-2} s^{-1}) on soil and were then adapted for 3 d to different light regimes. The intensities of heterochromatic light are indicated. μE, μmol photons m^{-2} s^{-1}; RL, red light (70 μmol photons m^{-2} s^{-1}); BL, blue light (5 μmol photons m^{-2} s^{-1}); FRL, far-red light (0.1 μmol photons m^{-2} s^{-1}). **(B)** Expression of PrfB3, cytochrome b_6, and PsaF was analyzed in photoreceptor mutants. Levels of LSU are shown as loading control. Plants were grown on soil under heterochromatic light (100 μmol photons m^{-2} s^{-1}) for 3 weeks. c, complemented. **(C)** Stress-dependent expression of PrfB3 and cytochrome b_6 was analyzed. Controls are the same as in (A). HL, high light (800 μmol photons m^{-2} s^{-1}, 3 h); MV, methylviologen (50 μM in 0.1% Tween, 2x 4 h incubation); heat (38°C, 3 h).

The light intensities used differed and were quite weak for blue and far-red light. Therefore, we could not differentiate between light quantity and quality. To address this issue, we performed immunoblot analyses using mutants of several photoreceptors. PrfB3 is severely down-regulated in cryptochrome mutants *cry1*, *cry2*, and *cry1 cry2*. Additionally, expression of PrfB3 is severely reduced in *phyB* and *phyA phyB* double mutants (Figure 37B). This is consistent with normal expression of PrfB3 under red light, which is sensed only by phytochrome B (Quail *et al.*, 1995), and in *phyA* mutants. Reduced PrfB3 expression below a certain threshold is apparently accompanied by lower cytochrome b_6 levels. These data indicate that expression of PrfB3 highly depends on light receptors and accordingly on light quality in addition to light intensity. Since the cytochrome $b_6 f$ complex is known to be responsible for redox signaling (e.g., to balance light absorbance of the two photosystems by triggering phosphorylation of the LHCII kinase; Lemeille and Rochaix, 2010), a possible role of PrfB3 in stress responses was also investigated (Figure 37C). It appeared that application of high light (3 h), oxidative stress as induced by methylviologen treatment (H_2O_2 production) (8 h), and heat stress (3 h) caused a decrease in PrfB3 amounts to ≤50% of wild-type levels. However, no simultaneous loss of cytochrome b_6 could be observed, again indicating that a certain threshold of PrfB3 levels is needed to mediate regulation of cytochrome b_6 levels. In conclusion, expression of PrfB3 is quite sensitive to environmental changes, indicating an important regulatory role in adjusting *petB* RNA and consequently cytochrome b_6 protein levels.

5 DISCUSSION

Ribonucleases have long been considered as purely degradative enzymes, cleaving without any sequence specificity. But nowadays a greater awareness of the significance of both endo- and exoribonucleases is emerging, in particular because it has become apparent that many RNases can display specificity for sequences or structures, allowing them to regulate transcript abundance according to the needs of the cell. It is becoming obvious that RNases play a central role in RNA metabolism, including RNA decay, maturation of RNA precursors and end-trimming of certain RNAs. A contribution of RNases to the implementation of molecular processes in response to environmental signals is emphasizing the importance of RNA metabolism in adjusting chloroplast functions. A single cell or organelle contains various RNases with sometimes overlapping functions and specificities, and high-molecular-weight complexes function together with stabilizing elements in order to control overall RNA accumulation (Stoppel and Meurer, 2011). Besides the protection of RNA termini by RNA secondary structures, RNA stability is influenced by polyadenylation or ribosome binding and *in vivo* RNA cleavage specificity is thought to be imposed by auxiliary RNA-binding proteins, which protect RNAs from non-specific nucleolytic attack by masking otherwise vulnerable sites.

5.1 Global Players: Evidence for a Degradosome-Like Complex in Arabidopsis Chloroplasts

5.1.1 Divergence of Evolution, Structure and Function of RNE

RNase E is a well-studied and highly conserved eubacterial enzyme, which in *E. coli* is part of the so-called degradosome that functions in mRNA decay and post-transcriptional gene expression. The shorter form RNase G is lacking the degradosome scaffold and acts independent from RNase E in *E. coli*. Cyanobacterial and red algae plastid genomes encode only one form, which cannot be assigned to RNase E or G with certainty (Stoppel and Meurer, 2011). This cyanobacterial RNase E/G gene is likely to be the ancestor of the plant *RNE* gene. The *Arabidopsis thaliana* homolog RNE is localized in the chloroplast and shares *in vitro* biochemical similarities with the eubacterial protein (Schein et al., 2008). In this work we present a new allele of the chloroplast RNase E, *rne-2* (Figure 7), which was identified as an *hcf* mutant, formerly called *hcf2* (Dinkins *et al.*, 1994). Mapping and sequencing of the mutant locus revealed that the EMS induced mutation caused a deletion of six aa within the RNase H domain, leading to a

significant loss of RNase activity, although the RNE-2 protein is expressed at normal levels (Figures 7D). This is similar to *E. coli* where the replacement of single aa in the RNase H domain can severely affect the catalytic activity of the enzyme (Callaghan *et al.*, 2005). Despite all similarities, RNE diverged in many respects in plants. For example the highly conserved RNA-binding S1 domain (Callaghan *et al.*, 2005) is interrupted in plant RNEs by an insertion of more than 100 aa (Figure 4). Plant RNE is also lacking the large C-terminal degradosome scaffold typical for bacterial RNase E enzymes, which is replaced by a plant-specific 130 aa extension (Figure 4). Furthermore, a novel, large N-terminal extension was acquired. Both terminal regions are of so far unknown function but could serve as scaffold for associated proteins.

5.1.2 RNE Forms a High-Molecular-Weight Degradosome-Like Complex Together with RHON1

Eubacterial RNase E protein complexes are rate-limiting for RNA decay and processing and vary among different organisms. This could be attributed to the fact that the C-terminal degradosome assembly site is highly plastic in length and sequence. For example in the gram-negative γ-proteobacterium *E. coli* RNase E forms the degradosome mainly together with PNPase, Rhl B, and Enolase but without the presence of RNase G, which acts independently (Carpousis, 2007). In contrast to *E. coli*, which is lacking RNase J, the gram-positive γ-proteobacterium *Bacillus subtilis* has two RNase J forms (J1 and J2) but no RNase E (Condon, 2010). In the purple α-proteobacterium *Rhodobacter capsulatus* RNase E forms a degradosome-like complex acting in concert with two DEAD-box helicases and the termination factor Rho, which is an RNA helicase as well (Jäger *et al.*, 2001). Notably, this degradosome-like complex is lacking PNPase. Cyanobacteria possess, similar to land plants, both RNase J and RNase E/G (Kaberdin *et al.*, 1998; Rott *et al.*, 2003; Even *et al.*, 2005). The presence of processed transcripts in *rne* albeit at reduced amounts indicates that loss of RNE in Arabidopsis is partially compensated by RNase J or other RNases rendering the mutant viable. This is in contrast to the essential function of RNase E in *E. coli*, which is lacking RNase J. Apparently the presence of RNE is neither essential nor a prerequisite for general processing and degradation of plastid RNA and thus RNE gained specific targets via RHON1.

The first successful complementation of the *rne* mutant using the TAP-tag allowed purification and concentration of the low-abundant protein and thus discovery of the degradosome-like complex *in vivo* (Figure 19). RNE was not found in any other complexes or as a

monomer indicating that the protein is present only in the DLC, which does not seem to contain RNA (Figure 19).

Sequencing of co-precipitated proteins using antibodies raised against RNE and the TAP-tag identified RHON1 as an interaction partner (Table 1). Vice versa, Co-IPs of RHON1^{TAP} also precipitated RNE. Several more factors, like ribosomal proteins, helicases, and other ribonucleases were identified in RNE co-precipitates but they still have to be confirmed to be true interaction partners.

5.1.3 RHON1 is an Essential Key Player in Plastid Gene Expression

The vascular plant-specific RHON1 protein plays an indispensable role in plastid gene expression as revealed by seedling lethality and the *rhon1* phenotype. The data indicate physical interaction, tight co-regulation of RHON1 and RNE protein expression, and close functional relationship between the two proteins (Figures 13, 15-19). This is also reflected by tight clustering of both mutant transcriptomes (Cho *et al.*, 2009).

Besides being a component of the DLC, RHON1 forms smaller complexes, which are associated with certain plastid RNAs (Figure 19). Since we did not find RNAs associated with DLC, we suggest that transcripts are only transiently bound in the course of endonucleolytic cleavage. It is tempting to speculate that RHON1 targets these transcripts to the DLC in order to contribute to the efficient catalytic activity of RNE similar to one of the degradosome functions in *E. coli* (Figure 38). This function of RHON1 is supported by the finding that RNA processing still occurs in *rhon1* although less efficiently. The additive effect in the corresponding double mutant hints to additional roles of RHON1, e.g. supporting the function of other RNases such as RNase J.

RIP-chip and slot-blot analysis have shown that RHON1 associates with RNA (Figure 20). As revealed by electrophoretic mobility shift assays the short C-terminal Rho-N domain of RHON1 is responsible for RNA-binding (Stoppel *et al.*, *submitted*). Similar to related nucleic acid-binding domains, like the SAP motif (Aravind and Koonin, 2001), the Rho-N domain has been recruited by quite diverse proteins of plants including mosses and some green algae and has often been transferred to their C-terminus (Figure 11). The Rho-N domain of RHON1 binds to specific regions of plastid RNAs with different strength attesting sequence and/or secondary structure specificity, which may be supported further by the remaining part of RHON1 *in vivo*.
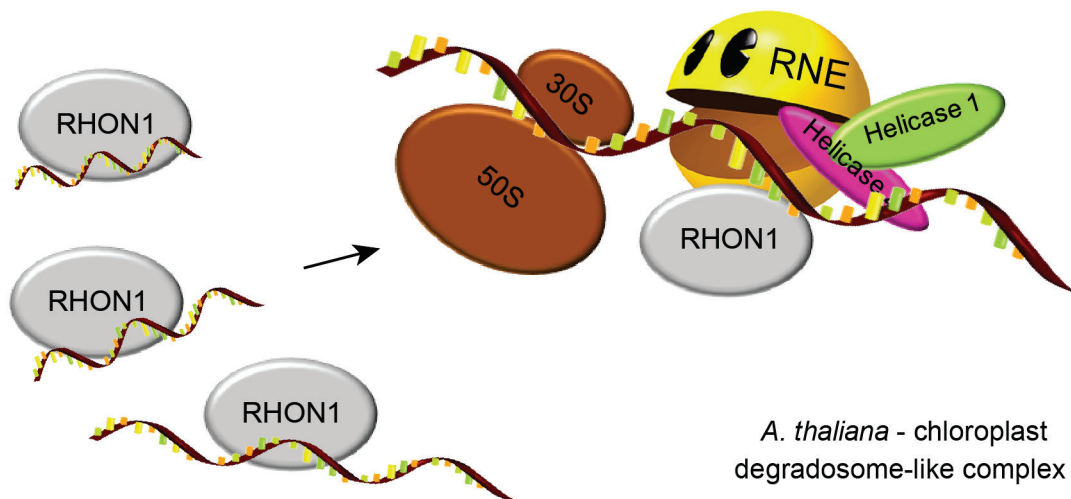
Figure 38. Model of the Degradosome-Like Complex in Arabidopsis Chloroplasts.
Using Co-IP analyses RNE (yellow) has been found to be associated with RHON1 (grey) and several other proteins, like helicases and ribosomal proteins, which still have to be confirmed as true interaction partners. Together they form a high-molecular-weight degradosome-like complex, primarily involved in RNA processing. In addition, RHON1 is part of various smaller complexes associated with RNAs of different sizes. It is tempting to speculate that RHON1 targets these RNAs to the DLC in order to ensure efficient processing of transcripts by RNE.

One of the most striking characteristics in *rne* and *rhon1* mutants is the accumulation of unprocessed high-molecular-weight transcripts within the chloroplast. For example, processing of the *rbcL-accD* intercistronic region is inefficient in both mutants as compared to the wild type leading to appearance of large transcripts, which harbor sequences of the downstream located *accD*, *psaI*, *ycf4*, *cemA*, and *petA* genes (Figure 21).

Association of RHON1 to 16S and 23S RNA revealed an important role in facilitating rRNA maturation at least in part through RNE (Figures 22-24). In turn, defective rRNA processing and thus ribosome assembly would explain the severe loss of polysomes in *rhon1* and to a certain extent in *rne* mutants (Figures 22, 23). This is evidenced by a severe loss of 16S rRNA in *rhon1* and accumulation of the 3.2 kb dicistronic 23S-4.5S precursor and a transcript of 2.7 kb, which appears in both mutants. The 2.7 kb transcript originates from an incorrectly processed 23S-4.5S precursor that is lacking the 23S 5'-end of 0.5 kb (Figure 24). Processing of one of the two hidden breaks generates this 0.5 kb fragment upon incorporation into ribosomes and usually depends on prior 23S-4.5S intercistronic cleavage (Leaver, 1973). Therefore, it is likely that initial assembly of ribosomes takes place but loss of 4.5S cleavage in the mutants hinders subsequent assembly steps leading to translational deficiencies.

Several pleiotropic mutants exhibiting defects in maturation of ribosomal RNAs have been described so far. However, it is still unclear whether all these deficiencies are primary or secondary effects (Barkan, 1993) since the molecular mechanisms of rRNA maturation are rather unclear and numerous proteins were assumed to be involved (Stoppel and Meurer, 2011). AtPPR2 was proposed to bind 23S RNA in order to coordinate translation during embryogenesis (Lu *et al.*, 2011) while BPG2 was described playing a role in processing and maturation of ribosomal RNA (Komatsu *et al.*, 2010). Mutations in the maize *Whirly* gene (Prikryl *et al.*, 2008) and the dicot *DCL, DAL, RNR1,* and *RH39* genes (Bellaoui *et al.*, 2003; Bisanz *et al.*, 2003; Bollenbach *et al.*, 2005; Nishimura *et al.*, 2010) lead to reduced processing of the 23S-4.5S precursor. Defects in processing of 23S RNA of the endonuclease mutants CSP41a and b (Beligni and Mayfield, 2008) were recently proposed to represent secondary effects (Qi *et al.*, 2011). In none of these mutants the 2.7 kb transcript was detectable. This indicates a primary effect of RNE and RHON1 on ribosomal RNA processing.

Another intriguing observation is the high number of chloroplasts in *rne* and *rhon1* mutants, accompanied by a smaller size as compared to wild type. This is pointing to a faster plastid multiplication rate caused by diminished repression of division (Figure 13). This finding could not be observed in mutants with similar defects in chloroplast development or RNA metabolism, e.g. *dpa1* (Dal Bosco *et al.*, 2004), *prfB3* (Stoppel *et al.*, 2011) or other mutants generally affected in plastid gene expression (Cho *et al.*, 2009; unpublished data). *E. coli* degradosomes form cytoskeleton-like structures together with MinD, a repressor of cell division (Taghbalout and Rothfield, 2007). In analogy to *rhon1*, *minD* mutants in *E. coli* divide more frequently resulting in minicells (de Boer *et al.*, 1989). Interestingly, MinD was shown to directly associate with bacterial RNase E in a yeast-two-hybrid screen suggesting that the bacterial cytoskeleton is involved in compartmentalization of protein activities like RNA processing and degradation (Taghbalout and Rothfield, 2007). A functional interaction between RNE and MinD is presumably conserved in the chloroplast causing plastid division defects when RNE or RHON1 are lacking. Alternatively, defective processing of plastid transcripts could account for elevated chloroplast division rates. Candidates could be *ycf1* and *ycf2* genes with still unknown function. To our knowledge, RHON1 and RNE are the first proteins linking plastid RNA metabolism to chloroplast division.

The discovery of the essential role of RHON1 for RNE function and evolution of a plant specific DLC leads to the conclusion that the plastid RNA processing/degradation machinery is more sophisticated than previously thought. We anticipate that future research on the degradosome-like complex, its compartmentalization and association partners will shed new light on chloroplast gene expression, division and development.

5.2 Specificity Factors: Recruitment of a Ribosomal Release Factor for Light- and Stress-Dependent Regulation of *petB* Transcript Stability in Higher Plant Chloroplasts

5.2.1 Phylogenetic Origin, Divergence and Structure of PrfB3

The Arabidopsis genome encodes four functional organellar release factors of eubacterial origin which retained the highly conserved stop codon recognition and peptidyl-tRNA hydrolysis tripeptide motifs, indicating the similarity between termination of translation in eubacteria and organelles. It was previously shown that At-PrfB1 in addition to its involvement in ribosomal release, also affects stability of transcripts containing UGA stop codons (Meurer *et al.*, 2002). This phenomenon has not been described in eubacteria to date. Therefore, it appears that the regulatory functions of At-PrfB1 have been newly acquired by land plants and that they could represent the evolutionary constraints keeping the number of TGA stop codons high in plastids of land plants (Meurer *et al.*, 2002). Several algae, like *C. reinhardtii*, have lost the TGA stop codon in their plastid genomes and accordingly a gene encoding for the corresponding RF2 (Meurer *et al.*, 2002). The PrfB3 RF2-like protein arose from PrfB1 but has lost both characteristic tripeptide motifs indicating that it also lost its function as a release factor. In spite of the comparable similarity between PrfB3 and the plastid (37.5%) and mitochondrial (36.5%) RF2, we unequivocally demonstrate that PrfB3 only recently arose from the plastid-localized form, indicating a very fast divergence of this gene. We provide evidence that PrfB1 and PrfB3 are phylogenetically closely related but functionally distinct plastid proteins in vascular plants.

The high degree of divergence as well as the fluctuation of the gene and intron composition of the *psbB* gene cluster in plants also attests to the fast evolving gene cluster organization accompanied by the recent acquisition of many plant-specific factors involved in processing of the primary transcript (Barkan, 2011). This is consistent with the higher divergence (even between closely related species) of the target sequence elements in plastid UTRs and intergenic regions compared with that in coding regions, which are by far not targeted as extensively for the control of gene expression (Greiner *et al.*, 2008).

The absence of the *PrfB3* gene in the sequenced genomes of cyanobacteria, red, green, and diatom algae, the moss *P. patens*, and the fern *S. moellendorffii* again suggests that PrfB3 evolved in vascular plants just before divergence of monocots and dicots, as a result of a duplication of the ancestral *PrfB1* gene and subsequent loss of the peptide chain release function followed by the loss of the two conserved tripeptide motifs (Figure 25).

5.2.2 PrfB3 Protects 3' Processed *petB* Transcripts against 3'→5' Exonucleolytic Degradation

Mapping of transcript termini demonstrated that only spliced and 3' processed *petB* transcripts are missing almost completely in both allelic *prfB3* mutants. Several effects potentially could cause reduction of the amounts of these RNAs: reduced splicing, loss of processing, or increased 3' exonucleolytic attack. Three lines of evidence indicate that there are no primary splicing defects in *prfB3*: (1) RNA gel blot, S1 nuclease mapping, and quantitative RT-PCR analyses showed that *prfB3* was generally able to splice *petB* transcripts efficiently (Figure 31C); (2) in contrast with nuclear and chloroplast mutants affected in splicing precursor transcripts (Jenkins *et al.*, 1997; Ostheimer *et al.*, 2003; Barkan, 2011), unspliced forms of *petB* did not accumulate at higher levels in *prfB3* (Figure 31C); (3) the pattern and abundance of all *petB* intron-containing transcripts was identical in the mutant and wild type (Figure 31C, intron probe D). Levels of all *petB* intron-containing precursors are unaffected, and spliced *petB* precursors are rather slightly reduced in the mutant, indicating efficient processing of the *petB-petD* intergenic region. Therefore, we hypothesize that PrfB3 stabilizes 3' processed *petB* transcripts (Figure 39).
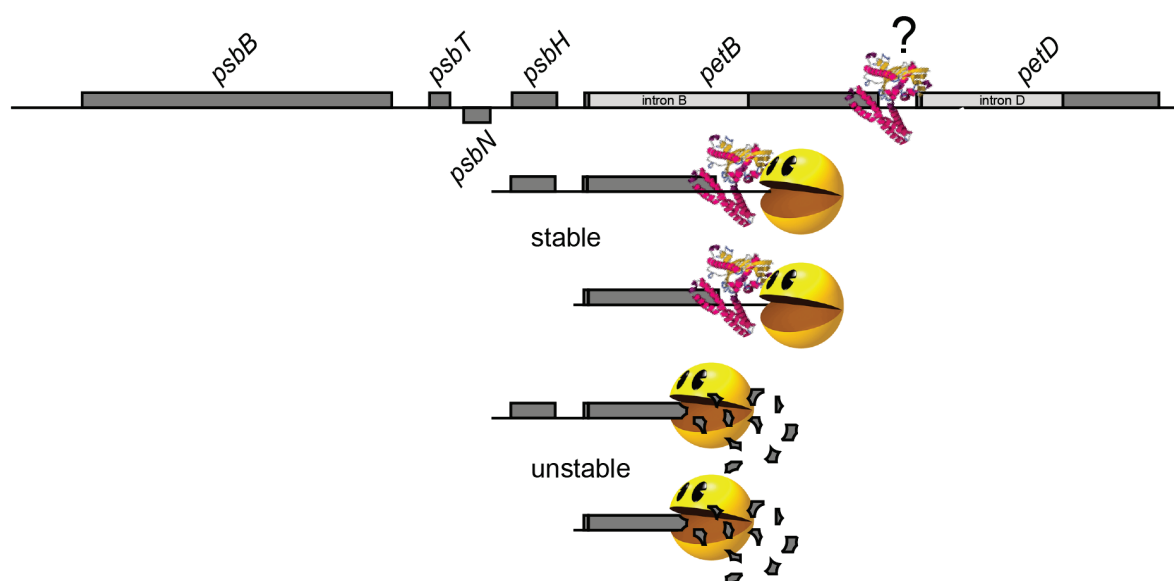
Figure 39. PrfB3 Protects 3' Processed *petB* Transcripts from 3'→5' Exonucleolytic Attack.
PrfB3 has been shown to protect 3' processed *petB* transcripts from digestion by exonucleases (yellow) by binding to the 3'-end of the *petB* RNA. The predicted three-dimensional structure of PrfB3 appears to be almost identical to that of the crystallized PrfB protein in *E. coli* (pdb 1GQE, Vestergaard *et al.*, 2001) with the exception of two loops harboring the SPF and GGQ tripeptide motifs in *E. coli*. It is still unclear whether PrfB3 already binds to unprocessed precursor transcripts or if structures built upon 3' processing are a prerequisite for PrfB3 binding capability. If PrfB3 is missing, 3' processed *petB* transcripts are highly unstable and rapidly digested.

The finding that PrfB3 is part of an RNA-containing complex also supports the role of the protein in *petB* RNA protection (Figure 34). The complex fell apart upon RNase treatment, but a shift toward heavier fractions was also observed. This indicates that the bound RNA is responsible for the formation of the complex running at ~400 kDa. Either the complex is shifted to a higher molecular weight because its structure is more relaxed when RNA is absent or, although less likely, a new association partner that replaces the RNA has been assembled. Alternatively, the RNA-free complex tends to form a multimeric assembly of 700 kDa. This may indicate that different transient assembly products are also present *in vivo*. A similar phenomenon has been described recently for MCA1 in *C. reinhardtii* (Boulouis *et al.*, 2011). As the RNA-containing complex is found in only a few fractions, we assume that it binds exclusively transcripts of a distinct and similar size like the 3' processed *psbH-petB* and monocistronic *petB* RNAs.

The slight reduction in the amounts of spliced *petB* precursors in the mutants indicates an increased cleavage of the *petB-petD* intergenic region and hints of a feedback regulation, when either cytochrome b_6 proteins or *petB* transcripts are of low abundance. Presumably, large amounts of accumulating precursor transcripts are translationally incompetent with respect to *petB* and are rapidly cleaved upon signaling to speed up cytochrome b_6 synthesis. This is supported by the fact that the cytochrome b_6f complex is virtually absent, although amounts of spliced *petB* precursors are only marginally reduced in the mutants.

Given that PrfB3 originated from the functional release factor PrfB1, it is conceivable that PrfB3 exerts its function through binding ribosomes. To check this assumption, the effect of two inhibitors, chloramphenicol and lincomycin, known to hinder chloroplast translation in different ways, was analyzed. In *prfB1*, inhibition of translation stabilizes specific transcripts, which are otherwise unstable (Meurer *et al.*, 2002). However, in *prfB3*, translation inhibition had obviously no effect on RNA abundance, indicating that translational events are not responsible for rapid degradation of 3' processed *petB* RNA (Figure 33). Nevertheless, these experiments do not exclude that PrfB3 is also involved in translation, as it was shown that all spliced *petB* and *petD* precursors that are associated with ribosomes are subjected to translation in maize (Barkan, 1988, 2011). In addition, a maize mutant lacking the monocistronic *petB* transcript is still able to produce cytochrome b_6 at almost normal rates (Barkan *et al.*, 1994).

However, it should be mentioned here that regulation of *petB-petD* transcript maturation and presumably *petB* translation seems to be quite different in maize and Arabidopsis. In contrast with maize, monocistronic *petD* transcripts in Arabidopsis are below the limits of detection in RNA gel blots. This indicates that *petD* translation also takes place on precursor transcripts in

Arabidopsis but presumably more efficiently than in maize (Barkan *et al.*, 1994). Taken together, the data indicate that *petB-petD* intercistronic processing occurs efficiently in the *prfB3* mutants. The resulting *petD* transcripts are rapidly subjected to degradation in both the wild type and *prfB3*, whereas processed *petB* transcripts are degraded only in the mutant. Thus, we strongly suggest that PrfB3 has been recruited to specifically protect *petB* transcripts against 3'→5' exonucleolytic attack by masking the 3'-ends (Figure 39).

It has been proposed that the eubacterial release factor possesses the capability to bind the 23S rRNA already before recognition of the stop codon (Frolova *et al.*, 2000; Korostelev *et al.*, 2010). The RNA-binding activity has presumably been conserved in PrfB3 and ultimately been specified for *petB* transcripts. Indeed, we have shown that PrfB3 predominantly interacts with the *petB* 3' UTR, substantiating the idea that PrfB3 masks the *petB* 3' UTR against exonucleolytic attack (Stoppel *et al.*, 2011).

In addition to PrfB3, several more nuclear-encoded factors required for processing and splicing of the polycistronic *psbB-psbT-psbH-petB-petD* transcript were identified (Barkan, 2011). Thus, increase of the structural complexity of the processing pattern of the *psbB* gene cluster was accompanied by the acquisition of a number of newly evolved nuclear-encoded protein factors. This may allow individual regulation of gene expression despite of their presence in a polycistronic context. PrfB3 is a further example of proteins that originally had a housekeeping function and subsequently have been recruited during evolution for fine-tuning of *petB* RNA stability. PrfB3 represents the first known factor in plants that is involved in regulation of the stability of a single chloroplast RNA without having PPR, TPR, or OPR motifs.

5.2.3 PrfB3 Expression is Highly Responsive to Stress and Environmental Changes

Recently, it was hypothesized that most factors involved in chloroplast RNA maturation and complexity evolved to ensure the functionality of chloroplast genetic information and have no authentic regulatory function (Maier *et al.*, 2008). Although expression of several chloroplast RNA-binding proteins was shown to depend on development, tissues, and environmental conditions, a truly regulatory function has been shown, to the best of our knowledge, only for the PPR protein MCA1, a factor in *C. reinhardtii* (Raynaud *et al.*, 2007; Tillich *et al.*, 2010; Ruwe *et al.*, 2011). It appeared that the abundance of MCA1 limits the amount of *petA* mRNA and accordingly levels of the encoded protein, cytochrome *f* (Raynaud *et al.*, 2007). This and the fact

that the activity of the cytochrome b_6f complex is rate-limiting for the light reaction in photosynthesis (Yamori *et al.*, 2011) prompted us to investigate whether PrfB3 also has a regulatory function in *petB* gene expression.

We have shown that down-regulation of PrfB3 below a threshold of ~25% goes along with a severe reduction in the amount of *petB* RNA and consequently in the abundance of cytochrome b_6 protein levels (Figure 36A). Furthermore, we show that expression of PrfB3 is highly responsive to changes in light quantities and qualities (Figures 37A+B) as well as to the redox status and stress factors like heat and high light (Figure 37C). Similarly, ATAB2 was shown to be involved in the signaling pathway of light-regulated translation of PSI and PSII proteins during early plant development (Barneche *et al.*, 2006). PrfB3 levels rapidly dropped to ~25 to 50% when we applied one stress factor under otherwise constant conditions. The application of the individual stressors for only a limited time period may explain why we did not detect a concomitant reduction of cytochrome b_6 upon stress induction. Presumably, under natural conditions, the response of PrfB3 to combined and more intense stressors may be even more pronounced. We propose that PrfB3 expression is tightly regulated and presumably rate-limiting for levels of *petB* mRNA as well as cytochrome b_6 under changing and/or adverse environmental conditions. For example, PrfB3 could exert its function when a selective reduction or increase in the amount of the cytochrome b_6f complex is required (Schöttler *et al.*, 2007). Physiologically it would also make sense to regulate primarily the rate-limiting step of photosynthetic electron transport. The complex endonucleolytic processing of RNA precursors in chloroplasts presumably evolved not only to allow subsequent adjustment of processed transcript amounts but also to fine-tune translation rates. This regulation also represents an adaptation to the eukaryotic regulatory system.

6   SUMMARY

Chloroplast biogenesis requires constant adjustment of RNA homeostasis under conditions of on-going developmental and environmental changes and its regulation is achieved mainly by post-transcriptional control mechanisms, e.g. mediated by nucleus-encoded ribonucleases.

Bacterial endonuclease RNase E is involved in processing of precursor RNAs and initiation of RNA degradation. It builds up the so-called degradosome complex, which has been thought not to exist in plant chloroplasts. By expression of a tandem affinity purification-tagged version of the plastid RNase E in the *Arabidopsis rne* mutant background in combination with mass spectrometry, we identified the novel vascular plant-specific and co-regulated interaction partner of RNE, designated RHON1. RHON1 is essential for photoautotrophic growth and together with RNE forms a distinct ~800 kDa degradosome-like complex (DLC). Additionally, RHON1 is part of various smaller RNA-containing complexes. RIP-chip and other association studies revealed that the Rho-N motif of RHON1 binds to and supports processing of plastid RNAs. In all respects, such as plastid RNA precursor accumulation, protein pattern, increased number and decreased size of chloroplasts, and defective chloroplast development, the phenotype of *rhon1* knockout mutants resembles that of *rne* lines showing that RNE functions highly depend on the presence of RHON1. Additionally, the phenotypes of *rhon1* and *rne* suggest a link between chloroplast division and DLC-dependent plastid RNA metabolism.

Land plant genomes encode four functional ribosomal peptide chain release factors (Prf) of eubacterial origin, two (PrfA and PrfB homologs) for each endosymbiotic organelle. A novel PrfB-like protein, PrfB3, is localized to the chloroplast stroma in a *petB* RNA-containing complex and found only in higher plants. Notably, PrfB3 is lacking the two most important tripeptide motifs characteristic for all eubacterial and organellar PrfB homologs described so far: the stop codon recognition motif SPF and the catalytic center GGQ for peptidyl-tRNA hydrolysis. Complementation studies, as well as functional and molecular analyses of two allelic mutations in Arabidopsis, both of which lead to a specific deficiency of the cytochrome b_6f complex, revealed that PrfB3 is essentially required for photoautotrophic growth. Plastid transcript, polysome, and translation analyses indicate that PrfB3 has been recruited in vascular plants for stabilization of 3' processed *petB* transcripts. Thus PrfB3 serves as a barrier to exonucleolytic RNA decay, providing an alternative to RNA stem-loop structures. Light- and stress-dependent control of PrfB3 levels likewise allows the plant to adjust cytochrome b_6 levels, which determine overall rates of photosynthesis.

7 ZUSAMMENFASSUNG

Die Chloroplastenbiogenese erfordert eine stetige Anpassung der plastidären Genexpression an wechselnde Umwelt- und Wachstumsbedingungen. Diese wird maßgeblich auf post-transkriptioneller Ebene von kernkodierten Faktoren wie z.B. Ribonukleasen gesteuert.

Die bakterielle Endonuklease RNase E ist an der Prozessierung von Vorläufertranskripten sowie der Initiation des RNA Abbaus beteiligt. Sie ist Hauptbestandteil des Degradosoms, von dem man bislang angenommen hat, dass es in Pflanzen nicht vorkommt. Co-Immuno-präzipitationsanalysen des 'getaggten', plastidären RNE Gens im Arabidopsis *rne* Mutanten-hintergrund und massenspektometrische Bestimmung der dabei aufgereinigten Proteine konnten das bislang unbekannte, pflanzenspezifische und koregulierte RHON1 Protein eindeutig als Interaktionspartner von RNE identifizieren. RHON1 ist essentiell für photoautotrophes Wachstum der Pflanze und bildet mit RNE einen ~800 kDa Degradosom-ähnlichen Komplex (*degradosome-like complex* - DLC). Darüber hinaus finden sich RHON1 Proteine in einer Reihe RNA-enthaltender Subkomplexe. Rip-Chip und andere Assoziationsstudien haben gezeigt, dass das Rho-N Motiv von RHON1 plastidäre Transkripte bindet und ihre Prozessierung begünstigt. Der Phänotyp von *rhon1* Mutanten ähnelt in allen Aspekten dem von *rne*, wie z.B. der Akkumulation von Vorläufertranskripten, der erhöhten Anzahl kleinerer Chloroplasten und der gestörten Chloroplastenentwicklung. Dies zeigt, dass RNE Funktionen stark von dem Vorhandensein von RHON1 abhängig sind. Darüber hinaus lassen die Phänotypen der *rne* und *rhon1* Mutanten die Vermutung aufkommen, dass ein Zusammenhang zwischen Plastidenteilung und DLC-abhängigem plastidärem RNA Metabolismus besteht.

Die Genome von Landpflanzen kodieren vier Translations-Terminationsfaktoren bakteriellen Ursprungs (*peptide chain release factor* - Prf), jeweils zwei Homologe (PrfA und PrfB) für jedes Organell. PrfB3 ist ein PrfB-ähnliches Protein, welches nur in Chloroplasten von höheren Pflanzen vorkommt und einen *petB* RNA enthaltenden Komplex bildet. Bemerkenswerter Weise hat PrfB3 beide für Terminationsfaktoren typischen Tripeptid-Motive verloren: das Stopp-Kodon Erkennungsmotiv SPF und das Motiv GGQ für die Hydrolyse der Peptidyl-tRNA Bindung. Funktionelle und molekulare Analysen zweier allelischer Mutanten in Arabidopsis zeigten, dass PrfB3 essentiell für photoautotrophes Wachstum ist und Mutationen im Gen zu einem spezifischen Verlust des Cytochromkomplexes führen. Transkript-, Polysomen- und Translationsanalysen deuteten darauf hin, dass PrfB3, in Analogie zu RNA Haarnadelstrukturen, 3' prozessierte, Cytochrom b_6 kodierende *petB* Transkripte stabilisiert und somit vor exonukleolytischem Abbau schützt. Die Licht- und Stress-abhängige Kontrolle von PrfB3 Mengen erlauben der Pflanze im Gegenzug die Mengen an Cytochrom b_6 anzupassen, welche wiederum die allgemeine Photosynthese Rate festlegen.

8   LITERATURE

Allen JF (2003) The function of genomes in bioenergetic organelles. Philos. Trans. R. Soc. Lond. B. Biol. Sci. 358: 19-37.

Allen JF (2005) A redox switch hypothesis for the origin of two light reactions in photosynthesis. FEBS Lett. 579: 963-968.

Allison TJ, Wood TC, Briercheck DM, Rastinejad F, Richardson JP, Rule GS (1998) Crystal structure of the RNA-binding domain from transcription termination factor rho. Nat. Struct. Biol. 5: 352-356.

Aravind L, Koonin EV (2001) Prokaryotic homologs of the eukaryotic DNA-end-binding protein Ku, novel domains in the Ku protein and prediction of a prokaryotic double-strand break repair system. Genome Res. 11: 1365-1374.

Arnon DI (1949) Copper enzymes in isolated chloroplasts. Polyphenoloxidase in *Beta vulgaris*. Plant Physiol. 24: 1-15.

Arraiano CM, Andrade JM, Domingues S, Guinote IB, Malecki M, Matos RG, Moreira RN, Pobre V, Reis FP, Saramago M, Silva IJ, Viegas SC (2010) The critical role of RNA processing and degradation in the control of gene expression. FEMS Microbiol. Rev. 34: 883-923.

Asakura Y, Barkan A (2007) A CRM domain protein functions dually in group I and group II intron splicing in land plant chloroplasts. Plant Cell 19: 3864-3875.

Baginsky S, Shteiman-Kotler A, Liveanu V, Yehudai-Resheff S, Bellaoui M, Settlage RE, Shabanowitz J, Hunt DF, Schuster G, Gruissem W (2001) Chloroplast PNPase exists as a homo-multimer enzyme complex that is distinct from the *Escherichia coli* degradosome. RNA 7: 1464-1475.

Barkan A (1988) Proteins encoded by a complex chloroplast transcription unit are each translated from both monocistronic and polycistronic mRNAs. EMBO J. 7: 2637-2644.

Barkan A (1993) Nuclear Mutants of Maize with Defects in Chloroplast Polysome Assembly Have Altered Chloroplast RNA Metabolism. Plant Cell 5: 389-402.

Barkan A, Walker M, Nolasco M, Johnson D (1994). A nuclear mutation in maize blocks the processing and translation of several chloroplast mRNAs and provides evidence for the differential translation of alternative mRNA forms. EMBO J. 13: 3170-3181.

Barkan A (1998) Approaches to investigating nuclear genes that function in chloroplast biogenesis in land plants. Methods Enzymol. 297: 38-57.

Barkan A (2011). Expression of Plastid Genes: Organelle-Specific Elaborations on a Prokaryotic Scaffold. Plant Physiol. 155: 1520-1532.

Barneche F, Winter V, Crèvecoeur M, Rochaix JD (2006) ATAB2 is a novel factor in the signalling pathway of light-controlled synthesis of photosystem proteins. EMBO J. 25: 5907-5918.

Bechtold N, Ellis J, Pelletier G (1993). In planta Agrobacterium mediated gene transfer by infiltration of adult Arabidopsis thaliana plants. C R Acad Sci Paris Life Sci. 316: 1194-1199.

Beligni MV, Mayfield SP (2008) *Arabidopsis thaliana* mutants reveal a role for CSP41a and CSP41b, two ribosome-associated endonucleases, in chloroplast ribosomal RNA metabolism. Plant Mol. Biol. 67: 389-401.

Bellaoui M, Keddie JS, Gruissem W (2003) DCL is a plant-specific protein required for plastid ribosomal RNA processing and embryo development. Plant Mol. Biol. 53: 531-543.

Bernstein JA, Khodursky AB, Lin PH, Lin-Chao S, Cohen SN (2002) Global analysis of mRNA decay and abundance in *Escherichia coli* at single-gene resolution using two-color fluorescent DNA microarrays. Proc. Natl. Acad. Sci. USA 99: 9697-9702.

Bisanz C, Bégot L, Carol P, Perez P, Bligny M, Pesey H, Gallois JL, Lerbs-Mache S, Mache R (2003) The Arabidopsis nuclear DAL gene encodes a chloroplast protein which is required for the maturation of the plastid ribosomal RNAs and is essential for chloroplast differentiation. Plant Mol. Biol. 51: 651-663.

Bollenbach TJ, Tatman DA, Stern DB (2003) CSP41a, a multifunctional RNA-binding protein, initiates mRNA turnover in tobacco chloroplasts. Plant J. 36: 842-852.

Bollenbach TJ, Schuster G, Stern DB (2004) Cooperation of endo- and exoribonucleases in chloroplast mRNA turnover. Prog. Nucleic Acid Res. Mol. Biol. 78: 305-337.

Bollenbach TJ, Lange H, Gutierrez R, Erhardt M, Stern DB, Gagliardi D (2005) RNR1, a 3'-5' exoribonuclease belonging to the RNR superfamily, catalyzes 3' maturation of chloroplast ribosomal RNAs in *Arabidopsis thaliana*. Nucleic Acids Res. 33: 2751-2763.

Bollenbach TJ, Schuster G, Portnoy V, Stern DB (2007) Polyadenylation, processing and degradation of chloroplast RNA. Topics in Current Genetics 19: 175-211.

Bosco CD, Lezhneva L, Biehl A, Leister D, Strotmann H, Wanner G, Meurer J (2004) Inactivation of the chloroplast ATP synthase gamma subunit results in high non-photochemical fluorescence quenching and altered nuclear gene expression in *Arabidopsis thaliana*. J. Biol. Chem. 279: 1060-1069.

Boulouis A, Raynaud C, Bujaldon S, Aznar A, Wollman FA, Choquet Y (2011) The Nucleus-Encoded trans-Acting Factor MCA1 Plays a Critical Role in the Regulation of Cytochrome *f* Synthesis in Chlamydomonas Chloroplasts. Plant Cell 23: 333-349.

Bradford MM (1976) A rapid and sensitive method for the quantitation of microgram quantities of protein utilizing the principle of protein-dye binding. Anal. Biochem. 72: 248-254.

Cai W, Okuda K, Peng L, Shikanai T (2011) PROTON GRADIENT REGULATION 3 recognizes multiple targets with limited similarity and mediates translation and RNA stabilization in plastids. Plant J. 67: 318-327.

Callaghan AJ, Marcaida MJ, Stead JA, McDowall KJ, Scott WG, Luisi BF (2005) Structure of *Escherichia coli* RNase E catalytic domain and implications for RNA turnover. Nature 437: 1187-1191.

Canino G, Bocian E, Barbezier N, Echeverría M, Forner J, Binder S, Marchfelder A (2009) Arabidopsis encodes four tRNase Z enzymes. Plant Phys. 150: 1494-1502.

Carpousis AJ, Van Houwe G, Ehretsmann C, Krisch HM (1994) Copurification of *E. coli* RNase E and PNPase: evidence for a specific association between two enzymes important in RNA processing and degradation. Cell 76: 889-900.

Carpousis AJ (2007) The RNA degradosome of *Escherichia coli*: an mRNA-degrading machine assembled on RNase E. Annu. Rev. Microbiol. 61: 71-87.

Casaregola S, Jacq A, Laoudj D, McGurk G, Margarson S, Tempete M, Norris V, Holland IB (1992) Cloning and analysis of the entire *Escherichia coli* ams gene. ams is identical to hmp1 and encodes a 114 kDa protein that migrates as a 180 kDa protein. J. Mol. Biol. 228: 30-40.

Chen J, Tang WH, Hong MM, Wang ZY (2003) OsBP-73, a rice gene, encodes a novel DNA-binding protein with a SAP-like domain and its genetic interference by double-stranded RNA inhibits rice growth. Plant Mol. Biol. 52: 579-590.

Cho WK, Geimer S, Meurer J (2009) Cluster analysis and comparison of various chloroplast transcriptomes and genes in *Arabidopsis thaliana*. DNA Res. 16: 31-44.

Clough SJ, Bent AF (1998) Floral dip: a simplified method for Agrobacterium-mediated transformation of *Arabidopsis thaliana*. Plant J. 16: 735-743.

Coburn GA, Mackie GA (1996) Overexpression, purification, and properties of *Escherichia coli* ribonuclease II. J. Biol. Chem. 271: 1048-1053.

Coburn GA, Mackie GA (1999) Degradation of mRNA in *Escherichia coli*: an old problem with some new twists. Prog. Nucleic Acid Res. Mol. Biol. 62: 55-108.

Condon C (2010) What is the role of RNase J in mRNA turnover? RNA Biol. 7: 316-321.

Davies BW, Köhrer C, Jacob AI, Simmons LA, Zhu J, Aleman LM, Rajbhandary UL, Walker GC (2010) Role of *Escherichia coli* YbeY, a highly conserved protein, in rRNA processing. Mol. Microbiol. 78: 506-518.

de Boer PA, Crossley RE, Rothfield LI (1989) A division inhibitor and a topological specificity factor coded for by the minicell locus determine proper placement of the division septum in *E. coli*. Cell 56: 641-659.

del Campo EM (2009). Post-transcriptional control of chloroplast gene expression. Gene Regul. Syst. Bio. 3: 31-47.

Dinkins RD, Bandaranayake H, Green BR, Griffiths AJ (1994) A nuclear photosynthetic electron transport mutant of *Arabidopsis thaliana* with altered expression of the chloroplast *petA* gene. Curr. Genet. 25: 282-288.

Dovzhenko A, Dal Bosco C, Meurer J, Koop HU (2003) Efficient regeneration from cotyledon protoplasts in *Arabidopsis thaliana*. Protoplasma 222: 107-111.

Drager RG, Girard-Bascou J, Choquet Y, Kindle KL, Stern DB (1998) In vivo evidence for 5'→3' exoribonuclease degradation of an unstable chloroplast mRNA. Plant J. 13: 85-96.

Even S, Pellegrini O, Zig L, Labas V, Vinh J, Bréchemmier-Baey D, Putzer H (2005) Ribonucleases J1 and J2: two novel endoribonucleases in *B. subtilis* with functional homology to *E. coli* RNase E. Nucleic Acids Res. 33: 2141-2152.

Evguenieva-Hackenberg E (2005) Bacterial ribosomal RNA in pieces. Mol. Microbiol. 57: 318-325.

Feinberg AP, Vogelstein B (1983) A technique for radiolabeling DNA restriction endonuclease fragments to high specific activity. Anal. Biochem. 132: 6-13.

Felder S, Meierhoff K, Sane AP, Meurer J, Driemel C, Plücken H, Klaff P, Stein B, Bechtold N, Westhoff P (2001) The nucleus-encoded HCF107 gene of Arabidopsis provides a link between intercistronic RNA processing and the accumulation of translation-competent *psbH* transcripts in chloroplasts. Plant Cell 13: 2127-2141.

Feldmann KA (1991) T-DNA insertion mutagenesis in Arabidopsis: Mutational spectrum. Plant J. 1: 71-82.

Fisk DG, Walker MB, Barkan A (1999) Molecular cloning of the maize gene CRP1 reveals similarity between regulators of mitochondrial and chloroplast gene expression. EMBO J. 18: 2621-2630.

Frolova LY, Merkulova TI, Kisselev LL (2000) Translation termination in eukaryotes: polypeptide release factor eRF1 is composed of functionally and structurally distinct domains. RNA 6: 381-90.

Gegenheimer P, Apirion D (1981) Processing of procaryotic ribonucleic acid. Microbiol. Rev. 45: 502-541.

Gobert A, Gutmann B, Taschner A, Gössringer M, Holzmann J, Hartmann RK, Rossmanith W, Giegé P (2010) A single Arabidopsis organellar protein has RNase P activity. Nat. Struct. Mol. Biol. 17: 740-744.

Greiner S, Wang X, Herrmann RG, Rauwolf U, Mayer K, Haberer G, Meurer J (2008). The complete nucleotide sequences of the 5 genetically distinct plastid genomes of Oenothera, subsection Oenothera: II. A microevolutionary view using bioinformatics and formal genetic data. Mol. Biol. Evol. 25: 2019-2030.

Grüne H, Westhoff P (1988) Transfer von RNA auf Pall Biodyne A Nylonmembranen und Immobilisierung mittels UV-crosslinking. Pall BioSupport SD 1217 G.

Haeusler RA, Engelke DR (2006) Spatial organization of transcription by RNA polymerase III. Nucleic Acids Res. 34: 4826-4836.

Harris EH, Boynton JE, Gillham NW (1994) Chloroplast ribosomes and protein synthesis. Microbiol. Rev. 58: 700-754.

Hayes R, Kudla J, Schuster G, Gabay L, Maliga P, Gruissem W (1996) Chloroplast mRNA 3'-end processing by a high molecular weight protein complex is regulated by nuclear encoded RNA binding proteins. EMBO J. 15: 1132-1141.

Ito K, Uno M, Nakamura Y (2000) A tripeptide 'anticodon' deciphers stop codons in messenger RNA. Nature 403: 680-684.

Jäger S, Fuhrmann O, Heck C, Hebermehl M, Schiltz E, Rauhut R, Klug G (2001) An mRNA degrading complex in *Rhodobacter capsulatus*. Nucleic Acids Res. 29: 4581-4588.

Jenkins BD, Kulhanek DJ, Barkan A (1997) Nuclear mutations that block group II RNA splicing in maize chloroplasts reveal several intron classes with distinct requirements for splicing factors. Plant Cell 9: 283-296.

Kaberdin VR, Miczak A, Jakobsen JS, Lin-Chao S, McDowall KJ, von Gabain A (1998) The endoribonucleolytic N-terminal half of *Escherichia coli* RNase E is evolutionarily conserved in *Synechocystis sp.* and other bacteria but not the C-terminal half, which is sufficient for degradosome assembly. Proc. Natl. Acad. Sci. USA 95: 11637-11642.

Khandijan EW (1986) UV crosslinking of RNA to nylon membranes enhances hybridization signals. Molec. Biol. Rep. 11: 107-115.

Khyse-Andersen J (1984) Electroblotting of multiple gels: a simple apparatus without buffer tank for rapid transfer of proteins from polyacrylamide gels to nitrocellulose. J. Biochem. Biophys. Met. 10: 203-209.

Kido M, Yamanaka K, Mitani T, Niki H, Ogura T, Hiraga S (1996) RNase E polypeptides lacking a carboxyl-terminal half suppress a mukB mutation in *Escherichia coli*. J. Bacteriol. 178: 3917-3925.

Kisselev LL, Buckingham RH (2000) Translational termination comes of age. Trends Biochem. Sci. 25: 561-566.

Klaff P, Gruissem W (1991) Changes in chloroplast mRNA stability during leaf development. Plant Cell 3: 517-530.

Komatsu T, Kawaide H, Saito C, Yamagami A, Shimada S, Nakazawa M, Matsui M, Nakano A, Tsujimoto M, Natsume M, Abe H, Asami T, Nakano T (2010) The chloroplast protein BPG2 functions in brassinosteroid-mediated post-transcriptional accumulation of chloroplast rRNA. Plant J. 61: 409-422.

Koncz C, Martini N, Szabados L, Hrouda M, Bachmair A, Schell J (1994) Specialized vectors for gene tagging and expression studies. Gelvin SB, Schilperoort RA, eds, Plant Molecular Biology Manual, Vol 2. Kluwer Academic Publishers, Dordrecht, The Netherlands: 1-22.

Korostelev A, Zhu J, Asahara H, Noller HF (2010) Recognition of the amber UAG stop codon by release factor RF1. EMBO J. 29: 2577-2585.

Kroeger TS, Watkins KP, Friso G, van Wijk KJ, Barkan A (2009). A plant-specific RNA-binding domain revealed through analysis of chloroplast group II intron splicing. Proc. Natl. Acad. Sci. USA 106: 4537-4542.

Leal-Klevezas DS, Martínez-Soriano JP, Nazar RN (2000) Cotranscription of 5S rRNA-tRNA(Arg)(ACG) from *Brassica napus* chloroplasts and processing of their intergenic spacer. Gene 253: 303-311.

Leaver CJ (1973) Molecular integrity of chloroplast ribosomal ribonucleic acid. Biochem. J. 135: 237-240.

Lee K, Bernstein JA, Cohen SN (2002) RNase G complementation of rne null mutation identifies functional interrelationships with RNase E in *Escherichia coli*. Mol. Microbiol. 43: 1445-1456.

Lee K, Cohen SN (2003) A *Streptomyces coelicolor* functional orthologue of *Escherichia coli* RNase E shows shuffling of catalytic and PNPase-binding domains. Mol. Microbiol. 48: 349-60.

Lemeille S, Rochaix JD (2010) State transitions at the crossroad of thylakoid signalling pathways. Photosynth. Res. 106: 33-46.

Lisitsky I, Schuster G (1999) Preferential degradation of polyadenylated and polyuridinylated RNAs by the bacterial exoribonuclease polynucleotide phosphorylase. Eur. J. Biochem. 261: 468-474.

Loh PG, Song H (2010) Structural and mechanistic insights into translation termination. Curr. Opin. Struct. Biol. 20: 98-103.

Loiselay C, Gumpel NJ, Girard-Bascou J, Watson AT, Purton S, Wollman FA, Choquet Y (2008) Molecular identification and function of cis- and trans-acting determinants for *petA* transcript stability in *Chlamydomonas reinhardtii* chloroplasts. Mol. Cell. Biol. 28: 5529-5542.

Long EO, Dawid IB (1980) Repeated genes in eukaryotes. Ann. Rev. Biochem. 49: 727-764.

Lu Y, Li C, Wang H, Chen H, Berg H, Xia Y (2011) AtPPR2, an Arabidopsis pentatricopeptide repeat protein, binds to plastid 23S rRNA and plays an important role in the first mitotic division during gametogenesis and in cell proliferation during embryogenesis. Plant J 67: 13-25.

Lurin C, Andrés C, Aubourg S, Bellaoui M, Bitton F, Bruyère C, Caboche M, Debast C, Gualberto J, Hoffmann B, Lecharny A, Le Ret M, Martin-Magniette ML, Mireau H, Peeters N, Renou JP, Szurek B, Taconnat L, Small I (2004) Genome-wide analysis of Arabidopsis pentatricopeptide repeat proteins reveals their essential role in organelle biogenesis. Plant Cell 16: 2089-103.

Maier UG, Bozarth A, Funk HT, Zauner S, Rensing SA, Schmitz-Linneweber C, Börner T, Tillich M (2008). Complex chloroplast RNA metabolism: just debugging the genetic programme? BMC Biol. 36: 1-9.

McMaster GK, Carmichael GG (1977) Analysis of single and double-stranded nucleic acids on polyacrilamid and agarose gels by using glyoxal and acridine orange. Proc Natl Acad Sci USA 74: 4835-4838.

Meierhoff K, Felder S, Nakamura T, Bechtold N, Schuster G (2003) HCF152, an Arabidopsis RNA binding pentatricopeptide repeat protein involved in the processing of chloroplast *psbB-psbT-psbH-petB-petD* RNAs. Plant Cell 15: 1480-1495.

Meurer J, Meierhoff K, Westhoff P (1996a) Isolation of high-chlorophyll-fluorescence mutants of *Arabidopsis thaliana* and their characterisation by spectroscopy, immunoblotting and northern hybridisation. Planta 198: 385-396.

Meurer J, Berger A, Westhoff P (1996b) A nuclear mutant of Arabidopsis with impaired stability on distinct transcripts of the plastid *psbB*, *psbD/C*, *ndhH*, and *ndhC* operons. Plant Cell 8: 1193-1207.

Meurer J, Grevelding C, Westhoff P, Reiss B (1998) The PAC protein affects the maturation of specific chloroplast mRNAs in *Arabidopsis thaliana*. Mol. Gen. Genet. 258: 342-351.

Meurer J, Lezhneva L, Amann K, Gödel M, Bezhani S, Sherameti I, Oelmüller R (2002) A peptide chain release factor 2 affects the stability of UGA-containing transcripts in Arabidopsis chloroplasts. Plant Cell 14: 3255-3269.

Mollier P, Hoffmann B, Debast C, Small I (2002) The gene encoding *Arabidopsis thaliana* mitochondrial ribosomal protein S13 is a recent duplication of the gene encoding plastid S13. Curr. Genet. 40: 405–409.

Monde RA, Schuster G, Stern DB (2000) Processing and degradation of chloroplast mRNA. Biochimie 82: 573-582.

Motohashi R, Yamazaki T, Myouga F, Ito T, Ito K, Satou M, Kobayashi M, Nagata N, Yoshida S, Nagashima A, Tanaka K, Takahashi S, Shinozaki K (2007) Chloroplast ribosome release factor 1 (AtcpRF1) is essential for chloroplast development. Plant Mol. Biol. 64: 481-497.

Mudd EA, Krisch HM, Higgins CF (1990) RNase E, an endoribonuclease, has a general role in the chemical decay of *Escherichia coli* rRNA: evidence that rne and ams are the same genetic locus. Mol. Microbiol. 4: 2127-2135.

Mudd EA, Sullivan S, Gisby MF, Mironov A, Kwon CS, Chung WI, Day A (2008) A 125 kDa RNase E/G-like protein is present in plastids and is essential for chloroplast development and autotrophic growth in Arabidopsis. J. Exp. Bot. 59: 2597-2610.

Murashige T, Skoog F (1962) A revised medium for rapid growth and bioassays with tobacco tissue cultures. Physiol. Plant. 15: 473-497.

Nakamura Y, Ito K, Ehrenberg M (2000) Mimicry grasps reality in translation termination. Cell 101: 349-352.

Nakamura Y, Ito K (2003) Making sense of mimic in translation termination. Trends Biochem. Sci. 28: 99-105.

Nickelsen J (2003) Chloroplast RNA-binding proteins. Curr. Genet. 43: 392-399.

Nishimura K, Ashida H, Ogawa T, Yokota A (2010) A DEAD box protein is required for formation of a hidden break in Arabidopsis chloroplast 23S rRNA. Plant J. 63: 766-777.

Nissen P, Hansen J, Ban N, Moore PB, Steitz TA (2000) The structural basis of ribosome activity in peptide bond synthesis. Science 289: 920-930.

Ossenbühl F, Nickelsen J (2000) Cis- and trans-acting determinants for translation of *psbD* mRNA in *Chlamydomonas reinhardtii*. Mol. Cell. Biol. 20: 8134-8142.

Ossenbühl F, Göhre V, Meurer J, Krieger-Liszkay A, Rochaix JD and Eichacker LA (2004) Efficient assembly of photosystem II in *Chlamydomonas reinhardtii* requires Alb3.1p, a homolog of Arabidopsis ALBINO3. Plant Cell 16: 1790-1800.

Ostheimer GJ, Williams-Carrier R, Belcher S, Osborne E, Gierke J, Barkan A (2003) Group II intron splicing factors derived by diversification of an ancient RNA-binding domain. EMBO J. 22: 3919-3929.

Ow MC, Perwez T, Kushner SR (2003) RNase G of *Escherichia coli* exhibits only limited functional overlap with its essential homologue, RNase E. Mol. Microbiol. 49: 607-622.

Petersen K, Schöttler MA, Karcher D, Thiele W, Bock R (2011) Elimination of a group II intron from a plastid gene causes a mutant phenotype. Nucleic Acids Res. 39: 5181-5192.

Pfalz J, Bayraktar OA, Prikryl J, Barkan A (2009) Site-specific binding of a PPR protein defines and stabilizes 5' and 3' mRNA termini in chloroplasts. EMBO J 28: 2042-2052.

Phinney BS, Thelen JJ (2005) Proteomic characterization of a triton-insoluble fraction from chloroplasts defines a novel group of proteins associated with macromolecular structures. J. Proteome Res. 4: 497-506.

Prikryl J, Watkins KP, Friso G, van Wijk KJ, Barkan A (2008) A member of the Whirly family is a multifunctional RNA- and DNA-binding protein that is essential for chloroplast biogenesis. Nucleic Acids Res. 36: 5152-5165.

Qi Y, Armbruster U, Schmitz-Linneweber C, Delannoy E, de Longevialle AF, Rühle T, Small I, Jahns P, Leister D (2011) Arabidopsis CSP41 proteins form multimeric complexes that bind and stabilize distinct plastid transcripts. J Exp Bot., *in press, doi: 10.1093/jxb/err347*.

Quail PH, Boylan MT, Parks BM, Short TW, Xu Y, Wagner D (1995) Phytochromes: photosensory perception and signal transduction. Science 268: 675-680.

Race HL, Herrmann RG, Martin W (1999) Why have organelles retained genomes? Trends Genet. 15: 364-370.

Raczynska KD, Le Ret M, Rurek M, Bonnard G, Augustyniak H, Gualberto JM (2006) Plant mitochondrial genes can be expressed from mRNAs lacking stop codons. FEBS Lett. 580: 5641-5646.

Raynaud C, Loiselay C, Wostrikoff K, Kuras R, Girard-Bascou J, Wollman FA, Choquet Y (2007) Evidence for regulatory function of nucleus-encoded factors on mRNA stabilization and translation in the chloroplast. Proc. Natl. Acad. Sci. USA 104: 9093-9098.

Reiss B, Klemm M, Kosak H, Schell J (1996) RecA protein stimulates homologous recombination in plants. Proc. Natl. Acad. Sci. USA 93: 3094-3098.

Reith M, Munholland J (1995) Complete nucleotide sequence of the *Porphyra purpurea* chloroplast genome. Plant Mol. Biol. Rep. 13: 333-335.

Rochaix JD (2011a) Assembly of the photosynthetic apparatus. Plant Physiol. 155: 1493-1500.

Rochaix JD (2011b) Regulation of photosynthetic electron transport. Biochim. Biophys. Acta. 1807: 375-383.

Rott R, Zipor G, Portnoy V, Liveanu V, Schuster G (2003) RNA polyadenylation and degradation in cyanobacteria are similar to the chloroplast but different from *Escherichia coli*. J. Biol. Chem. 278: 15771-15777.

Ruwe H, Kupsch C, Teubner M, Schmitz-Linneweber C (2011) The RNA-recognition motif in chloroplasts. J. Plant Physiol. 168: 1361-1371.

Sambrook J, Fritsch EF, Maniatis T (1989) Molecular cloning – a laboratory manual. 2 ed Cold Spring Harbor, New York, USA.

Sane AP, Stein B, Westhoff P (2005) The nuclear gene HCF107 encodes a membrane-associated R-TPR (RNA tetratricopeptide repeat)-containing protein involved in expression of the plastidial *psbH* gene in Arabidopsis. Plant J. 42: 720-730.

Schein A, Sheffy-Levin S, Glaser F, Schuster G (2008) The RNase E/G-type endoribonuclease of higher plants is located in the chloroplast and cleaves RNA similarly to the *E. coli* enzyme. RNA 14: 1057-1068.

Schmitz-Linneweber C, Williams-Carrier R, Barkan A (2005) RNA immunoprecipitation and microarray analysis show a chloroplast Pentatricopeptide repeat protein to be associated with the 5' region of mRNAs whose translation it activates. Plant Cell 17: 2791-2804.

Schmitz-Linneweber C, Small I (2008) Pentatricopeptide repeat proteins: a socket set for organelle gene expression. Trends Plant Sci. 13: 663-670.

Schöttler MA, Flügel C, Thiele W, Bock R (2007) Knock-out of the plastid-encoded PetL subunit results in reduced stability and accelerated leaf age-dependent loss of the cytochrome b_6f complex. J. Biol. Chem. 282: 976-985.

Schreiber U (1986) Detection of rapid induction kinetics with a new type of high-frequency modulated chlorophyll fluorometer. Photosynth. Res. 9: 261-272.

Schreiber U, Schliwa U, Bilger W (1986) Continous recording of photochemical and non-photochemical chlorophyll fluorescence quenching with a new type of modulation fluorometer. Photosynth. Res. 10: 51-62.

Schult K, Meierhoff K, Paradies S, Töller T, Wolff P, Westhoff P (2007) The nuclear-encoded factor HCF173 is involved in the initiation of translation of the *psbA* mRNA in Arabidopsis thaliana. Plant Cell 19: 1329-1346.

Schwenkert S, Umate P, Dal Bosco C, Volz S, Mlçochová L, Zoryan M, Eichacker LA, Ohad I, Herrmann RG, Meurer J (2006) PsbI affects the stability, function, and phosphorylation patterns of photosystem II assemblies in tobacco. J. Biol. Chem. 281: 34227-34238.

Schwenkert S, Legen J, Takami T, Shikanai T, Herrmann RG, Meurer J (2007) Role of the low-molecular-weight subunits PetL, PetG, and PetN in assembly, stability, and dimerization of the cytochrome b_6f complex in tobacco. Plant Physiol. 144: 1924-1935.

Schwenkert S, Netz DJ, Frazzon J, Pierik AJ, Bill E, Gross J, Lill R, Meurer J (2009) Chloroplast HCF101 is a scaffold protein for [4Fe-4S] cluster assembly. Biochem J. 425: 207-214.

Seki M, Narusaka M, Kamiya A, Ishida J, Satou M, Sakurai T, Nakajima M, Enju A, Akiyama K, Oono Y, Muramatsu M, Hayashizaki Y, Kawai J, Carninci P, Itoh M, Ishii Y, Arakawa T, Shibata K, Shinagawa A, Shinozaki K (2002) Functional annotation of a full-length Arabidopsis cDNA collection. Science 296: 141-145.

Sharwood RE, Hotto AM, Bollenbach TJ, Stern DB (2011) Overaccumulation of the chloroplast antisense RNA AS5 is correlated with decreased abundance of 5S rRNA in vivo and inefficient 5S rRNA maturation in vitro. RNA 17: 230-243

Stern DB, Goldschmidt-Clermont M, Hanson MR (2010) Chloroplast RNA metabolism. Annu. Rev. Plant Biol. 61: 125-155.

Stoppel R, Meurer J (2011) The cutting crew - ribonucleases are key players in the control of plastid gene expression. J. Exp. Bot., *in press*.

Stoppel R, Lezhneva L, Schwenkert S, Torabi S, Felder S, Meierhoff K, Westhoff P, Meurer J (2011) Recruitment of a Ribosomal Release Factor for Light- and Stress-Dependent Regulation of *petB* Transcript Stability in *Arabidopsis* Chloroplasts. Plant Cell 23: 2680-2695.

Stoppel R, Manavski N, Schein A, Schuster G, Teubner M, Schmitz-Linneweber C, Meurer J Evidence for a degradosome-like complex in *Arabidopsis* chloroplasts. *submitted*

Strittmatter G, Kössel H (1984) Cotranscription and processing of 23S, 4.5S and 5S rRNA in chloroplasts from *Zea mays*. Nucleic Acids Res. 12: 7633-7647.

Taghbalout A, Rothfield L (2007) RNaseE and the other constituents of the RNA degradosome are components of the bacterial cytoskeleton. Proc. Natl. Acad. Sci. USA 104: 1667-1672.

Taraseviciene L, Miczak A, Apirion D (1991) The gene specifying RNase E (rne) and a gene affecting mRNA stability (ams) are the same gene. Mol. Microbiol. 5: 851-855.

Tillich M, Beick S, Schmitz-Linneweber C (2010) Chloroplast RNA-binding proteins: repair and regulation of chloroplast transcripts. RNA Biol. 7: 172-178.

Turmel M, Otis C, Lemieux C (1999) The complete chloroplast DNA sequence of the green alga *Nephroselmis olivacea*: Insights into the architecture of ancestral chloroplast genomes. Proc. Natl. Acad. Sci. USA 96: 10248-10253.

Vestergaard B, Van LB, Andersen GR, Nyborg J, Buckingham RH, Kjeldgaard M (2001). Bacterial polypeptide release factor RF2 is structurally distinct from eukaryotic eRF1. Mol. Cell 8: 1375-1382.

Walter M, Piepenburg K, Schöttler MA, Petersen K, Kahlau S, Tiller N, Drechsel O, Weingartner M, Kudla J, Bock R (2010) Knockout of the plastid RNase E leads to defective RNA processing and chloroplast ribosome deficiency. Plant J. 64: 851-863.

Westhoff P, Herrmann RG (1988) Complex RNA maturation in chloroplasts: The *psbB* operon from spinach. Eur. J. Biochem. 171: 551-564.

Yamaguchi K, Subramanian AR (2000) The plastid ribosomal proteins. Identification of all the proteins in the 50 S subunit of an organelle ribosome (chloroplast). J. Biol. Chem. 275: 28466-28482.

Yamaguchi K, von Knoblauch K, Subramanian AR (2000) The plastid ribosomal proteins. Identification of all the proteins in the 30 S subunit of an organelle ribosome (chloroplast). J. Biol. Chem. 275: 28455-28465.

Yamori W, Takahashi S, Makino A, Price GD, Badger MR, von Caemmerer S (2011) The roles of ATP synthase and the cytochrome b_6f complexes in limiting chloroplast electron transport and determining photosynthetic capacity. Plant Physiol. 155: 956-962.

Yang J, Schuster G, Stern DB (1996) CSP41, a sequence-specific chloroplast mRNA binding protein, is an endoribonuclease. Plant Cell 8: 1409-1420.

Yehudai-Resheff S, Hirsh M, Schuster G (2001) Polynucleotide phosphorylase functions as both an exonuclease and a poly(A) polymerase in spinach chloroplasts. Mol. Cell. Biol. 21: 5408-5416.

I   ABBREVIATIONS

α	anti
aa	amino acid residue
ATP	adenosine 5'-triphosphate
bp	base pairs
CAPS	cleaved amplified polymorphic sequences
d	days
DLC	degradosome-like complex
DNA	deoxyribonucleic acid
dNTPs	deoxynucleoside triphosphates
EDTA	ethylenediaminetetraacetic acid
EGTA	ethylene glycol tetraacetic acid
EMS	ethyl methanesulfonate
EST	expressed sequence tag
g	gravity force
h	hours
hcf	*high chlorophyll fluorescence*
Hepes	N-[2-Hydroxyethyl]piperazine-N'-[2-ethanesulfonic acid]
kb	kilobases
kDa	kilodalton
min	minutes
MOPS	3-[N-Morpholino]propanesulfonic acid
mRNA	messenger RNA
NPQ	non-photochemical chlorophyll a fluorescence quenching
P700	PSI primary electron donor chlorophyll a
PCR	polymerase chain reaction
PSI	photosystem I

PSII	photosystem II
qP	photochemical chlorophyll a fluorescence quenching
RF	release factor
RNA	ribonucleic acid
rpm	revolutions per minute
rRNA	ribosomal RNA
RT-PCR	reverse transcription PCR
s	seconds
S	Svedberg unit
SDS	sodium dodecyl sulfate
Suc	Sucrose
PAGE	polyacrylamide gel electrophoresis
SSLP	simple sequence length polymorphism
TAP	tandem affinity purification
T-DNA	transferred DNA
Tricine	N-Tris-(hydroxymethyl)-methylglycine
Tris	Tris-(hydroxymethyl)-aminomethane
tRNA	transfer RNA
Tween	polyoxyethylenesorbitan monolaurate
UTR	untranslated region
v/v	volume per volume
WT	wild type
w/v	weight per volume

II   APPENDIX

II. 1   Vector Maps

Figure 40. Gateway pENTR/D-TOPO Vector Used for Generation of Entry Clones for pDEST17.

T1 and T2: transcription termination sequences reducing potential toxicity in *E. coli* by preventing basal expression of the PCR product; attL1 and attL2: bacteriophage λ-derived recombination sequences that allow recombinational cloning of a gene of interest in the entry construct with a Gateway destination vector; TOPO Cloning site: allows rapid, directional cloning of the PCR product. Kanamycin: resistance gene allowing selection of the plasmid in *E. coli*. pUC origin of replication: allows high-copy replication and maintenance in *E. coli*.
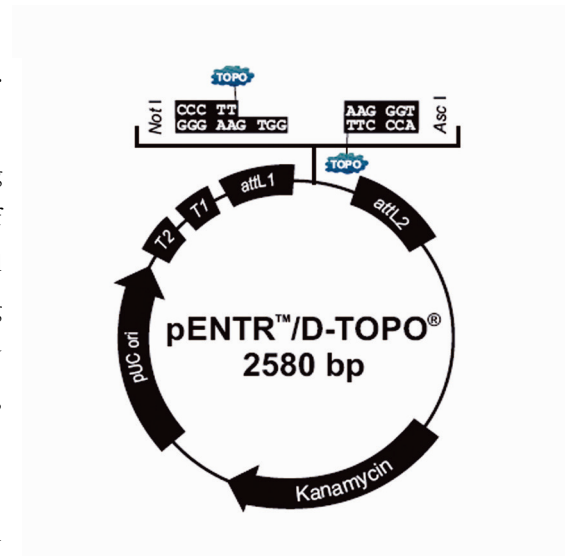
Figure 41. Gateway pDEST17 Vector Used for Overexpression of PAC and PrfB3.

DNA from the entry clone replaces the region between bases 147 and 1830. T7: T7 promoter permitting high-level IPTG-inducible expression of the recombinant protein in *E. coli* strains expressing the T7 RNA polymerase; RBS: Ribosome binding site; 6xHis: N-terminal 6×His tag, permits affinity purification of recombinant fusion protein using a metal-chelating resin such as Ni-NTA; *att*R1 and *att*R2 sites: bacteriophage λ-derived DNA recombination sequences that permit recombinational cloning of the gene of interest from a Gateway entry clone; CmR: Chloramphenicol resistance gene, allows counterselection of the plasmid. *ccd*B: permits negative selection of the plasmid. T7 term: T7 transcription termination region sequence from bacteriophage T7 that permits efficient transcription termination. Ampicillin: resistance gene (β-lactamase) that allows selection of the plasmid in *E. coli*. pBR322 origin of replication (*ori*), permits replication and maintenance in *E. coli*. Rop: ORF that interacts with the pBR322 origin to facilitate low-copy replication in *E. coli*.
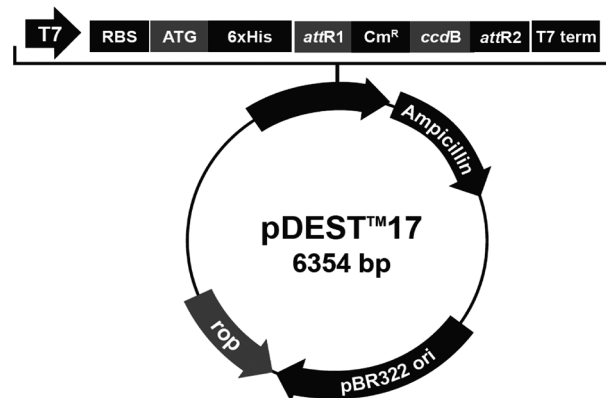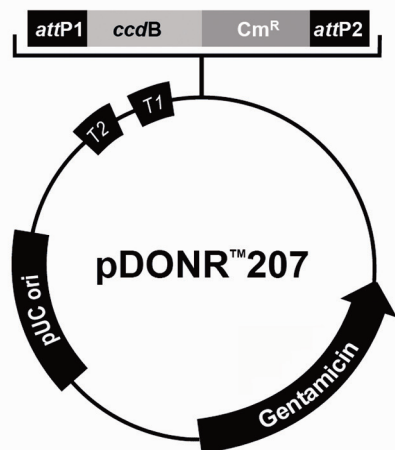
Figure 42. Gateway pDONR207 Vector Used as Entry Vector for TAP-Tag Constructs.

T1 and T2: transcription terminators protecting the cloned gene from expression by vector-encoded promoters, thereby reducing possible toxicity; *att*P1 and *att*P2: bacteriophage λ-derived DNA recombination sequences that allow recombinational cloning of the gene of interest from an *att*B site flanked PCR product; *ccd*B: allows negative selection of the plasmid; CmR: Chloramphenicol resistance gene, allows counterselection of the plasmid; Gentamicin: resistance gene, allows selection of the plasmid in *E. coli;* pUC origin: allows replication and maintenance in *E. coli.*
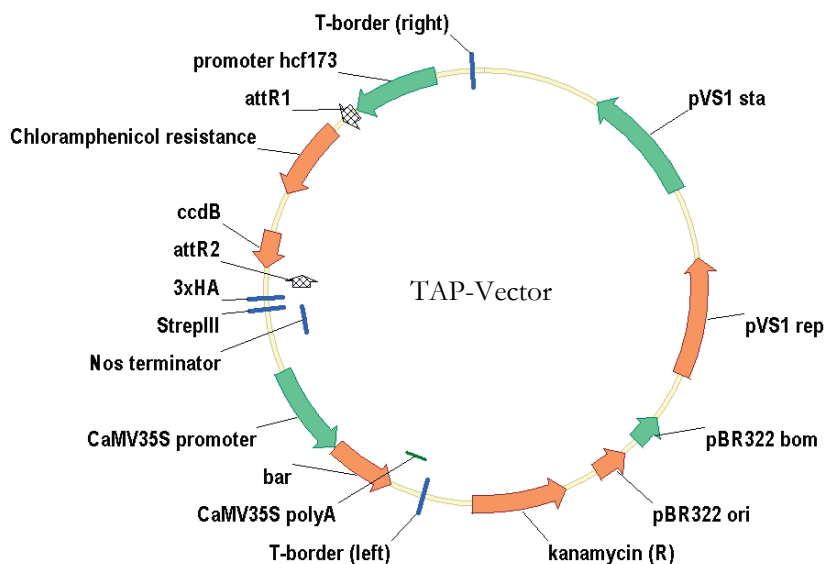

Figure 43. Binary TAP-Vector Used for Complementation and Epitope Tagging of RNE and RHON1.

pVS1 sta: *Agrobacterium* stability region; pVS1 rep: *Agrobacterium* origin of replication; pBR322 bom: site for mobilization from *E. coli* to *Agrobacterium*; pBR322 ori: permits replication and maintenance in *E. Coli*; Kanamycin: resistance gene for selection in *E. coli* and *Agrobacteria*. T-border (left and right): T-DNA right and left border sequences, respectively; *hcf173* promoter: RNA promoter from the nuclear *Arabidopsis* gene *hcf173*; attR1 and attR2: bacteriophage λ-derived recombination sequences that allow recombinational cloning of a gene of interest in the expression construct with a Gateway destination vector; Chloramphenicol resistance: allows counterselection of the plasmid; ccdB: allows negative selection of the plasmid; 3xHA: triple Hemagglutinin tag; StrepIII: double Strep tag separated by a short linker region; Nos terminator: Nopaline synthase terminator; CaMV 35S promoter: RNA promoter from CaMV; bar: Phosphinotricine resistance gene (i.e. Basta), for selection of plant transformants; CaMV35S polyA: polyadenylation signal from CaMV.

Figure 44. Map of the Plant Binary Expression Vector pSEX001-VS.

EcoRI,1: *EcoRI* site at nucleotide position 1; SmaI,542: *SmaI* site at nucleotide position 542; BamHI,547: *BamHI* site at nucleotide position 547; XbaI,552: *XbaI* site at nucleotide position 552; 5578,XhoI: *XhoI* site at nucleotide position 5578; Br and Bl: *Agrobacterium* T-DNA right and left border sequences, respectively; 35S: CaMV 35S RNA promoter; pAA: polyadenylation signal from CaMV; ori: *E. coli* origin of replication; tp-sul: sulfonamide-resistance gene equipped with a chloroplast targeting peptide; Amp: ampicillin-resistance gene; pVS1: *Agrobacterium* origin of replication.
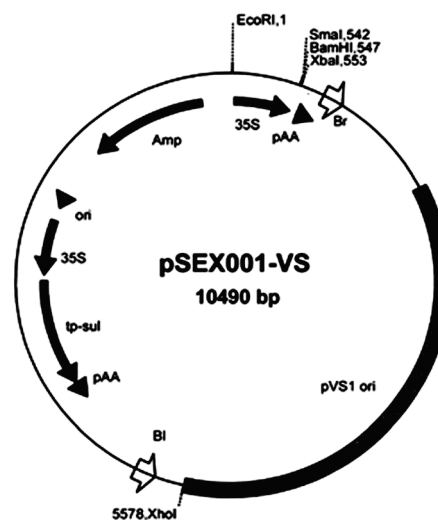
II. 2   Oligonucleotides Used in this Work

Name	Sequence 5' → 3'	Experiment/Figure
A-f	CGTAGTTAACTTTTCGTAACGTTTGG	mapping *rne-2*/7A
A-r	CAAGCTTTTTCACCATACATTGTACTAG	mapping *rne-2*/7A
B-f	GATTGAGCCCCAAAGCATTGGTTG	mapping *rne-2*/7A
B-r	GCAGCTAAAAGATAATGTGTGGTGGAG	mapping *rne-2*/7A
C-f	GGTCACTCAAGCAGTCGAAACTCAAAACTC	mapping *rne-2*/7A
C-r	TCATTGCCGCTTATCGCCTAGCGCTCTC	mapping *rne-2*/7A
D-f	CCAAGTGGATGAAACAACTGC	mapping *rne-2*/7A
D-r	CACGAGCCAAGGTTACCTTG	mapping *rne-2*/7A
E-f	AGAGGCTGATCGGTCTGAAA	mapping *rne-2*/7A
E-r	ATTTTCCATAGGGGGCACTC	mapping *rne-2*/7A
F-f	CCTGAGTGAATGCACACAATG	mapping *rne-2*/7A
F-r	GGTTACACAATGCGTCATGC	mapping *rne-2*/7A
G-f	GGATGAATAGTATCGTCAGG	mapping *rne-2*/7A
G-r	CCTCTGTAGTAGTCTCATTG	mapping *rne-2*/7A
H-f	TGACTACATGGAGATTATGGCC	mapping *rhon1*/12A

Oligonucleotides Used in this Work. continued

Name	Sequence 5' → 3'	Experiment / Figure
H-r	CACGATATGATCAAGCTTTAACG	mapping *rhon1*/12A
I-f	TTACTTTTTGCCTCTTGTCATTG	mapping *rhon1*/12A
I-r	GGCTTTCTCGAAATCTGTCC	mapping *rhon1*/12A
J-f	GATCAGACGCAAGACCGTTA	mapping *rhon1*/12A
J-r	AATCACTTGTTGGTTACCTC	mapping *rhon1*/12A
K-f	GTTCCAATCCGTGTTGGAGCAGATG	mapping *rhon1*/12A
K-r	CAAGACTCCAGAGCCATATCCTATTGCCG	mapping *rhon1*/12A
L-f	TTCAGAGGCAGATCAATTTGCACGCGGG	mapping *rhon1*/12A
L-r	TGCGCCTGCCTTCTGTGCATCAAAGTGC	mapping *rhon1*/12A
M-f	GGAGTCTTGTTATGACTGGCAATCGG	mapping *rhon1*/12A
M-r	CCCATCAAGCCCATGAAGATTATTGGCC	mapping *rhon1*/12A
P1	CATGTCTCAGATCATCTAGCTG	PCR/7B+C,10B
P2	GCGTGGACCGCTTGCTGCAACT	PCR
P3	GTCCTGCACAACTGATAGTG	PCR
P4	GCAGATGAAGGTGTGGAAGGAG	RT-PCR/7C
P5	CACCAAAGAACCTCCATTGG	RT-PCR/7C
P6	GCAGACCATCTAAGTCTTTCTGC	PCR/7B,10B
P7	TCAGTGACAACGTCGAGCAC	PCR/7A,12B+E
P8	TGTGTTACCAAGATAAGCCAGAG	PCR/12B+E
P9	ACTTCTATTGGGGACAGATTTCAGACG	PCR/12B+E
rrn16S-f	TAAGCATCGGCTAACTCTGTGCC	probe/20B,24
rrn16S-r	TACAGCACTGCACGGGTCGATAC	probe/20B,24
rrn23S-f	GAAAGGCTTACGGTGGATAC	probe/20B,23
rrn23S-r5'	ATCGGTCACCCAGGAGTATT	probe/24
rrn23S-f3'	AGGCGTGCAAAGGTTTCCT	probe/24
rrn23S-r	GGTGGGCTTACTACTTAGAT	probe/20B,23

Oligonucleotides Used in this Work. continued

Name	Sequence 5' → 3'	Experiment / Figure
rrn4.5S-f	ACGAGCCGTTTATCATTACGATAGGTGTC	probe/20B,24
rrn4.5S-r	CCGGTCTGTTAGGATGCCTCAG	probe/20B,24
rrn5S-f	GGCGTAGAGGAACAACACCAATCC	probe/20B,24
rrn5S-f	AGCTATTTTTCCGCAGGACCTCC	probe/20B,24
rbcL-f	CTAGAGGATCTGCGAATCCCTCC	probe/20B,21B,23
rbcL-r	CTAGTATTTGCGGTGAATCCCCC	probe/20B,21B,23
ycf1-f	GCCTCTGCATTTAGCATTGGGTAG	probe/20B
ycf1-f	TGTTTAGTCCCACCCGTTTCTGAG	probe/20B
rbcL	Meurer *et al.*, 1996b	probe/21C
accD	Meurer *et al.*, 1996b	probe/21C
psaI/*ycf4*/*cemA*	Meurer *et al.*, 1996b	probe/21C
petA	Meurer *et al.*, 1996b	probe/21C
RHON1-AttB1-entry-f	GGGGACAAGTTTGTACAAAAAAGCAGGCTGAAGTCTGTTCATGGCGATG	cloning *rhon1*^TAP/12C
RHON1-AttB1-entry-r	GGGGACCACTTTGTACAAGAAAGCTGGGTCGCTGGAATCACTACCAAGCAAC	cloning *rhon1*^TAP/12C
RNE-AttB1-entry-f	GGGGACAAGTTTGTACAAAAAAGCAGGCTCTCAATACCATGGATGTTACTG	cloning *rne*^TAP/10A
RNE-AttB1-entry-r	GGGGACCACTTTGTACAAGAAAGCTGGGTCTCGCCTTTGTTTACCACTGGTC	cloning *rne*^TAP/10A
RHON1-phos-f	TCTGCTCCTGAAGTCTGTTCATGGCGATG	cDNA *RHON1*
RHON1-phos-r	AGCAAGGTTCAGCTGGAATCACTACCGC	cDNA *RHON1*
PrfB3-P-f	P-ATGGCGGCAAAGATTATTGGTGGATGCTGC	Complementation/27A
PrfB3-Xba-r	TACCTCTAGATTAAGCCTAAATCGCATCAATTGATC	Complementation/27A
PrfB3-f	GATCTCCAGGCGCAAAATCTCAG	*prfB3-1* PCR/27B+D
PrfB3-r	GTGGTATGATATCAACAGTCGCTG	*prfB3-1* PCR/27B+D
LBb1	GCGTGGACCGCTTGCTGCAACT	*prfB3-1* PCR/27B
B3-Ex1-f	CAGGAAGAGAACATCATCTCG	*prfB3-2* RT-PCR/27C

Oligonucleotides Used in this Work. continued

Name	Sequence 5' → 3'	Experiment / Figure
B3-Ex4-r	TGCACACCTCGCTCACCTAAGAG	*prfB3-2* RT-PCR/27C
*psbB*5'	CGCGGATCCTGGTTGGGCTGGTTC	probe A/31
*psbB*3'	CGCGGATCCAGTTACACCTACTTG	probe A/31
*psbH*5'	CGCGGATCCGGATCTATGCTAAG	probe B/31
*psbH*3'	CGCGGATCCGGAAATATACAATC	probe B/31
*petB*5'	probe pSoP1351; Westhoff and Herrmann, 1988	probe C/31
petB-intron-f	TACTTCGTCGGATATTCATTCGAG	probe D/31
petB-intron-r	TGAGATAGGTAAACCAAGGTTACTC	probe D/31
petB-f	TGGTTCGAAGAACGTCTTGAGATTCAGGCG	probe E/31 probe *petB*/32,33
petB-r	CCGACCATCGATGAACTGATCGGATTAACCAACC	probe E/31 probe *petB*/32,33
petB-petD	probe pSoP850; Westhoff and Herrmann, 1988	probe F/31
*petD*5'-1	GCGGATCCGGTGAAGGAACGATG	probe G/31
*petD*5'-2	CGTCTAGACCATAATCCATTATCT	probe G/31
petD-intron-f	GTGTCTTTGTTCCAACCACTGTGTAAGCC	probe H/31 probe *petD*/32,33
petD-intron-r	CAGGTAAATGCTCAACACCCACGTAAGC	probe H/31 probe *petD*/32,33
petD-f	ACCCGCATGGCCCAACGACCTTTTA	probe I/31
petD-r	GGGTACGGTTAATAATCCCGCTGGTACTGAAACC	probe I/31
AtprfB3-Sal-f	AGCGTCGACGCTCCGGTGAAATAAAATGGCGGC	GFP cloning/26A
AtprfB3-Sal-r	CGCGTCGACCGTTTTGGCCTAGCCTTTCTGCCC	GFP cloning/26A
psaA-f	CCAATTTCTAAACGCTGGAGTAGATCC	quantitative RT-PCR
psaA-r	CATGACCAATACCCCAGTTGGTCCTATAC	quantitative RT-PCR
petB-f	CTCCTTTGGTAGTTCGACCG	quantitative RT-PCR
petB-r	CCAACCAAAGTTAGCTTCAGTC	quantitative RT-PCR
petD-f	GGATATTTCCCTTCAACTCCAC	quantitative RT-PCR

Oligonucleotides Used in this Work. continued

Name	Sequence 5' → 3'	Experiment / Figure
PrfB3-Topo17-f	CACCATGGATGACATGGACAC	cloning for overexpression
PrfB3-Topo17-r	GCCTAAATCGCATCAATTGATC	cloning for overexpression
PAC-Topo17-f	CACCGCTACGAAGAAGCTGAC	cloning for overexpression
PAC-Topo17-f	CTGCCTACCACTTCAAGTTGAG	cloning for overexpression

Oligonucleotides Used in this Work. continued

Name	Sequence 5' → 3'	Experiment / Figure

III   ACKNOWLEDGEMENTS

IV   PUBLICATIONS

Parts of this work have already been published or are submitted for publication.

- **Stoppel R**, Manavski N, Schein A, Schuster G, Teubner M, Schmitz-Linneweber C, Meurer J Evidence for a degradosome-like complex in *Arabidopsis* chloroplasts. *submitted*

- **Stoppel R** and Meurer J (2011) Review article: The Cutting Crew - Ribonucleases are Key Players in the Control of Plastid Gene Expression. ***J Exp Bot***, *in press*

- **Stoppel R**, Lezhneva L, Schwenkert S, Torabi S, Felder S, Meierhoff K, Westhoff P, Meurer J (2011) Recruitment of a ribosomal release factor for light- and stress-dependent regulation of *petB* transcript stability in *Arabidopsis* chloroplasts. ***Plant Cell*** 23: 2680-2695.
  Highlighted by Nancy A. Eckardt (2011), *Plant Cell* 23: 2474; including author profile.

- Mrácek J, Greiner S, Cho WK, Rauwolf U, Braun M, Umate P, Altstätter J, **Stoppel R**, Mlcochová L, Silber MV, Volz SM, White S, Selmeier R, Rudd S, Herrmann RG, Meurer J (2006) Construction, database integration, and application of an *Oenothera* EST library. ***Genomics*** 88: 372-380.

VI   EIDESSTATTLICHE VERSICHERUNG

Ich versichere hiermit an Eides statt, dass die vorgelegte Dissertation von mir selbständig und ohne unerlaubte Hilfe angefertigt ist.

München, den ....

                                                               Rhea Stoppel

VII   ERKLÄRUNG

Hiermit erkläre ich, dass die Dissertation nicht ganz oder in wesentlichen Teilen einer anderen Prüfungskommission vorgelegt worden ist und dass ich zuvor nicht versucht habe, anderweitig eine Dissertation einzureichen oder mich einer Doktorprüfung zu unterziehen.

München, den ....

                                                               Rhea Stoppel